HETEROGENEOUS RESERVOIR CHARACTERIZATION UTILIZING EFFICIENT GEOLOGY PRESERVING RESERVOIR PARAMETERIZATION THROUGH HIGHER ORDER SINGULAR VALUE DECOMPOSITION (HOSVD)

A Dissertation

by

SARDAR AFRA

Submitted to the Office of Graduate and Professional Studies of
Texas A&M University
in partial fulfillment of the requirements for the degree of

DOCTOR OF PHILOSOPHY

Chair of Committee,	Shankar P. Bhattacharyya
Co-Chair of Committee,	Eduardo Gildin
Committee Members,	Laszlo B. Kish
	Scott L. Miller
Head of Department,	Chanan Singh

May 2015

Major Subject: Electrical Engineering

ABSTRACT

Petroleum reservoir parameter inference is a challenging problem to many of the reservoir simulation workflows, especially when it comes to real reservoirs with high degree of complexity and non-linearity, and high dimensionality. In fact, the process of estimating a large number of unknowns in an inverse problem lead to a very costly computational effort. Moreover, it is very important to perform geologically consistent reservoir parameter adjustments as data is being assimilated in the history matching process, i.e., the process of adjusting the parameters of reservoir system in order to match the output of the reservoir model with the previous reservoir production data. As a matter of fact, it is of great interest to approximate reservoir petrophysical properties like permeability and porosity while reparameterizing these parameters through reduced-order models. As we will show, petroleum reservoir models are commonly described by in general complex, nonlinear, and large-scale, i.e., large number of states and unknown parameters. Thus, having a practical approach to reduce the number of reservoir parameters in order to reconstruct the reservoir model with a lower dimensionality is of high interest. Furthermore, de-correlating system parameters in all history matching and reservoir characterization problems keeping the geological description intact is paramount to control the ill-posedness of the system.

In the first part of the present work, we will introduce the advantages of a novel parameterization method by means of higher order singular value decomposition analysis (HOSVD). We will show that HOSVD outperforms classical parameterization techniques with respect to computational and implementation cost. It also, provides more reliable and accurate predictions in the petroleum reservoir history

matching problem due to its capability to preserve geological features of the reservoir parameter like permeability. The promising power of HOSVD is investigated through several synthetic and real petroleum reservoir benchmarks and all results are compared to that of classic SVD. In addition to the parameterization problem, we also addressed the ability of HOSVD in producing accurate production data comparing to those of original reservoir system. To generate the results of the present work, we employ a commercial reservoir simulator known as ECLIPSE.

In the second part of the work, we will address the inverse modeling, i.e., the reservoir history matching problem. We employed the ensemble Kalman filter (EnKF) which is an ensemble-based characterization approach to solve the inverse problem. We also, integrate our new parameterization technique into the EnKF algorithm to study the suitability of HOSVD based parameterization for reducing the dimensionality of parameter space and for estimating geologically consistence permeability distributions. The results of the present work illustrates the characteristics of the proposed parameterization method by several numerical examples in the second part including synthetic and real reservoir benchmarks. Moreover, the HOSVD advantages are discussed by comparing its performance to the classic SVD (PCA) parameterization approach.

To Arezoo

ACKNOWLEDGEMENTS

"In the middle of difficulty lies opportunity." *Albert Einstein*

I would have never been able to finish this dissertation without the guidance of my advisers and committee members, help from friends, and support from my wife and family. I would like to gratefully thank my advisers, Dr. Eduardo Gildin and Dr. Shankar P. Bhattacharyya. My deepest gratitude to Dr. Gildin for his fantastic guidance, patience, and kind caring during the course of my study and research. He taught me how to build and develop my ideas and more important to believe in my abilities and skills. He let me to experience a fabulous research time in a great and professional academic atmosphere for which I am thankful. I would like to extend my sincerest appreciation to Dr. Bhattacharyya for his understanding, help and support throughout my research. It was my privilege to work under his supervision. He helped me to pass the hardest time I had during my work and is the reason that I could continue my education. I also would like to thank my committee members, Dr. Laszlo B. Kish and Dr. Scott L. Miller for their precious advice.

I would like to dedicate my dissertation to my lovely wife, Arezoo. Without her endless support and love, I would have never finished this work. She is my one love which every minute I spent with her is a wonderful dream comes true.

I would also like to thank my parents, Mohammad and Pari. They were always supporting and encouraging me with their love and best wishes. I would not be half the man I am without them. My deepest appreciation to my parents in law, Mr. and Mrs. Emrani as well. They gave me my one love Arezoo. Last but not the least, I would like to thank my sister and brother, Tara and Salar for their support and love.

NOMENCLATURE

V	vector
$\mathbf{U}$	matix
$\mathcal{T}$	tensor
A	cross sectional area normal to flow, $[ft^2]$
$\diamond$	the Kronecker product between two matrices
ϕ	porous medium rock porosity, fraction
B	oil formation volume factor, $[\frac{bbl}{STB}]$
c_R	reservoir rock compressibility, $[psi^{-1}]$
c_o	oil compressibility, $[psi^{-1}]$
c_w	water compressibility, $[psi^{-1}]$
μ	viscosity, $[cp]$
$\mathbf{K}$	permeability, $[Darcy]$
c_o	oil compressibility, $[psi^{-1}]$
p	pressure, $[psia]$
∇p	pressure gradient, $[\frac{psia}{ft}]$
q	production rate or flow rate, $[\frac{bbl}{day}]$
t	time, $[days]$
γ	specific gravity, $[\frac{psia}{ft}]$
ρ	density, $[\frac{lb}{ft^3}]$
h	thickness, $[ft]$
r_e	Peaceman effective radius, $[ft]$
r_w	well radius, $[ft]$
s	skin factor

TABLE OF CONTENTS

LIST OF FIGURES

FIGURE Page

LIST OF TABLES

TABLE Page

1. INTRODUCTION AND LITERATURE REVIEW

There is an increasing global demand for energy for upcoming decades based on a recent research study by ExxonMobil Corporation [39, 40]. Moreover, oil, gas and coal are significant source of the energy that is delivered for global consumption (Fig. 1.1). On the other hand, owing to the fact that oil and natural gas are non-

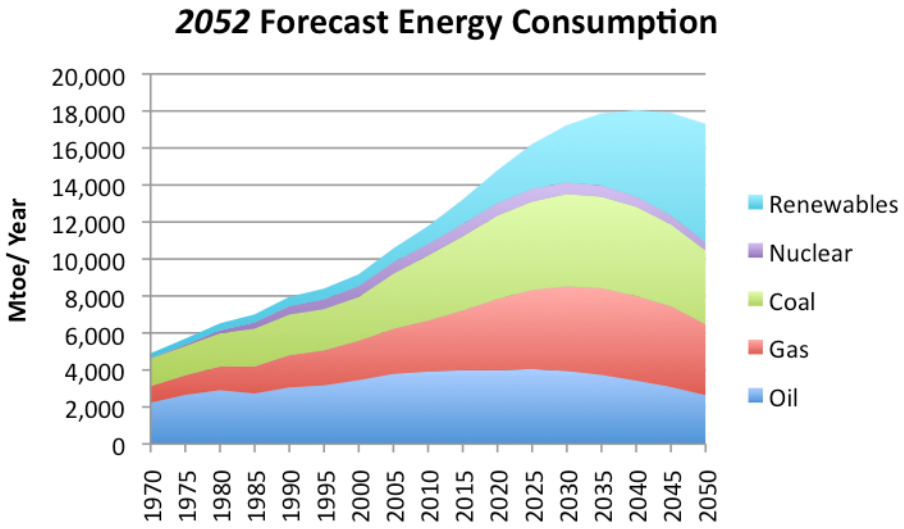

Figure 1.1: World energy consumption. From [40]

renewable resources, it will become more challenging to keep current production rate in order to fulfill this increasing global demand for energy. In fact, the majority of current oil and gas fields are produced for a long time, e.g., their production rates is decreasing each year now on, and there is a low chance of discovering new large fields. Therefore, it is of high interest to optimize the production costs while maximizing oil recovery in order to fill the gap between global demand for energy and decreasing resources [39].

Closed-loop control has been introduced in the upstream side of the exploration and production (E&P) field life-cycle of the Oil and Gas industry in the form of closed loop reservoir management (CLRM) [68, 81]. The upstream sector is comprised of the fossil fuel reservoirs together with the network of wells and the near surface infrastructure [77]. The central idea of the CLRM paradigm is to optimize reservoir production (e.g., hydrocarbons) by delaying water production and minimizing fluid injection during the reservoir life-cycle. This can be accomplished by setting up a model-based optimization and parameter estimators for proper account of uncertainties. To this end, CLRM has been shown to significantly impact the amount of hydrocarbons extracted and, in turn, the volume of global reserves by increasing the recovery factor of conventional reservoirs.

Real-time closed loop control is routinely applied in the downstream sector (refineries) of the hydrocarbon production [13, 8, 110]. Nonlinear plants can be controlled using model-based control and identified dynamical systems [80, 128, 3]. Although the behavior of these nonlinear systems are complex on their own right, the solution time for the control evaluation and their practical implementation is usually small (milliseconds). However, the deployment of the CLRM concept to realistic reservoirs has been minimal. In reservoir management, the time scales are not as severe as in the upstream examples, yet the problems that one faces in controlling petroleum systems are more complex in the sense that one deals with highly non-linear and uncertain models, which are described mathematically, by large-scale dynamical systems - millions of state-variables are very often needed and massive computational machinery are required for simulation and optimization. Furthermore, porous media properties such as conductivity or permeability contains many small scales and uncertainties. For example, in fractured media, the small scales can be much smaller compared to the field scales. For this reason, it is computationally

expensive to solve forward problems directly, and, in particular, it is prohibitively expensive to solve many such forward problems as in the case of uncertainty quantification and controller design.

In this work, we will focus on developing model reduction strategies that can be incorporated into the parameter estimation processes amenable for reservoir control [20, 23, 25, 69]. In the petroleum industry, parameter estimation is often called history matching. The central issue in history matching is to construct a reservoir model to predict accurately future reservoir production utilizing observation data. Several parameters describe a reservoir model which each of those parameters may convey a huge amount of data. Some parameters are specified per grid block like permeability and porosity and others for the entire model or a particular layer such as relative permeability and capillary pressure. History matching is a highly underdetermined, nonlinear and ill-posed problem owing to insufficiency and complexity of observed data from reservoir [104]. This means there is a possibility of obtaining reservoir models that match observed measurements but then provide incorrect predictions. Many workflows in uncertainty quantification and history matching rely on massive computations, and the availability of computing resources is still seen as a limiting factor. Considering that large-scale computer-based simulation provided the only feasible method for producing quantitative predictive information about complex behavior, novel ways to reduce the computational burden related to simulations need to be developed.

A number of studies have been conducted to reduce computational efforts in reservoir simulation and history matching [67, 51, 22, 1, 129]. The methodologies basically worked in two fronts: reducing the number of states using model reduction techniques, and reducing the number of unknown parameters in a process known as parameterization [119]. Among all of these methods, a common approach that

is applied to history matching is proper orthogonal decomposition (POD) [132, 7], which in different areas, is also known as principal component analysis (PCA) and Karhunen- Loève Decomposition (KL). In the standard PCA (POD), it is necessary to carry out an eigen-decomposition of the random field covariance matrix which is expensive for large models. Furthermore due to the vectorization of the snapshots data in the POD computation, many features may be lost in the reduced space [11, 86, 90]. In this dissertation, we introduce the multi-linear algebra based approach, namely the high-order singular valued decomposition (HOSVD) [86, 90, 130], to reduce dimensionality representation of reservoir properties, such as permeability, taking into account an ensemble of models. We treat property ensembles as a high-dimensional tensor, and by means of tensor algebra (HOSVD) we show that the reduced models preserve better geometric features keeping them more intact during the reduced basis computations. This is of great importance in the case of reservoirs as the properties in consideration have geological meaning.

Developing efficient and accurate history matching workflows is a daunting task to be performed using grid-based simulation due to the large-scale nature of the reservoir models and the several calls of the simulator. This is due to the fact that large number of gridblocks is needed to accurately represent the continuous solution of the underlying partial differential equations of multi phase flow in porous media, leading to large number of uncertain parameters representing the geological description of the reservoir [27].

Having a reliable and accurate reservoir model is of high interest in reservoir engineering field. However, obtaining such a model requires a fine detailed description of the reservoir which results in a large scale underdetermined inverse problem. Thus, it is crucial to reduce the dimensionality of the actual model for the sake of computational time and cost. The objectives of this dissertation is to provide a novel

reservoir parameterization method through introducing higher order singular value decomposition (HOSVD) algorithm in order to obtain a reservoir model of lower dimension [65, 58, 35]. In other words, we employ HOSVD capability to reduce dimensionality representation of reservoir properties, such as permeability, taking into account an ensemble of models. We treat property ensembles as a high-dimensional tensor, and by means of tensor algebra (HOSVD) we show that the reduced models preserve better geometric features keeping them more intact during the reduced basis computations [2, 60].

To this end, model-order reduction techniques have been used to mitigate the high cost of performing these simulations by means of two different thrusts: (1) parameterization of the geological description, e.g., permeability and porosities, in few parameters to be estimated; and (2) reduction on the number of states, i.e., pressures and saturations to be computed in each simulation call. Although there is not a consensus in which direction one should follow to efficiently and accurately represent the geological model, both thrusts share a common framework: subspace projection. In what follows, a brief introduction to model reduction by projection is given. It should be pointed out that for the exposition given below we will assume two-phase immiscible (oil-water) flow [67, 51, 68].

This dissertation is organized as follows. Section 2 describes tensor algebra in details and provides most important definitions and theorem regarding the application of multilinear algebra in reservoir simulation problems. We will also, introduce higher order singular value decomposition (HOSVD) method as a parameterization algorithm (dimensionality reduction method) and also best rank–1 and rank–$(R_1, R_2, \cdots, R_N)$ approximation of a tensor will be explained. Section 3, briefly establishes the reservoir simulation framework and explain permeability parameterization problem in reservoir simulation and history matching. Moreover, a two phase

reservoir simulation example is provided to show how the performance of our in-house reservoir simulator. eager reader could refer to [54, 24, 18, 17] for more detail on reservoir simulation and optimization. Furthermore, we present an introductory discussion on ensemble Kalman filter (EnKF) as a strong parameter estimation method [34]. Section 4 discusses permeability field parameterization using higher order singular value decomposition. In fact, it provides the results based on geostatistical permeability realization including a description for permeability field parameterization and dimensionality reduction using HOSVD. We also include results of efficient geology preserving reservoir parameterization through HOSVD and summarize important points on HOSVD based parameterization as well as providing results for a real benchmark reservoir model known as SPE 10 in order to show the performance of the proposed parameterization method and in comparison to other common parameterization methods such as classic SVD. In section 5 we integrate the EnKF parameter estimation method with HOSVD based parameterization in order to investigate the performance of the new parameterization method in a real inverse problem, i.e., history matching problem. In fact, the last Section describes reservoir parameter distribution inference through HOSVD parameterization for a SPE 10 benchmark. Finally, section 6 summarizes the present work and provides some interesting area for further investigation and as future research studies.

2. INTRODUCTION TO TENSOR ALGEBRA

This section briefly presents basic material on tensor algebra which are necessary to understand the fundamental ideas and tools of the present work. As a matter of fact, we need to establish the basic concept of multilinear algebra in order to introduce the higher order tensor decomposition concept in a proper manner. We start with definitions and theorems of tensor algebra and continue with briefly explaining tensor operations and matrix representation. Finally, we conclude this section by reviewing classic singular value decomposition (SVD) and illustrate the higher order singular value decomposition (HOSVD) method as the main tool in model reduction for parameterization purposes in the present work. Many of these definitions and theorems proof can be found in the following papers and book [4, 15, 21, 42, 85].

2.1 Basic Definitions

In multilinear algebra, *tensor* is a multi-dimensional array. In fact, *tensor* is a higher order matrix (array) with a dimension more than 2. A more theoretically precise definition of a high order tensor is as follows:

Definition 2.1.1: Assume P Euclidean vector spaces $A_1, A_2, \cdots, A_P$ all with finite dimensions $J_1, J_2, \cdots, J_P$. Given P vectors $B_i \in A_i$ and any arbitrary vector Y_i for all $i \in 1, 2, \cdots, P$, we define a *multilinear map* on $A_1 \times A_2 \times \cdots \times A_P$ as follows:

$$\big(B_1 \diamond B_2 \diamond \cdots \diamond B_P\big)\big(Y_1, Y_2, \cdots, Y_P\big) = \langle B_1, Y_1\rangle_{A_1} \langle B_2, Y_2\rangle_{A_2} \cdots \langle B_P, Y_P\rangle_{A_P}. \quad (2.1)$$

wherein $\langle B_i, Y_i\rangle_{A_i}$ indicates the scalar product in A_i.

Definition 2.1.2: The *tensor product space* over $A_1, A_2, \cdots, A_P$ is referred to as the space created by all the elements of the stated multilinear map. And each

member of the tensor product space is called a *tensor*.

2.2 Tensor Products, Orthogonality and Norm

To better understand the concept of higher order singular value decomposition (HOSVD) method, a few basic operations within the tensor product space are defined in this section.

Definition 2.2.1: The inner product of two arbitrary tensors $\mathcal{P} \in \mathbb{C}^{I_1 \times I_2 \times \cdots \times I_N}$ and $\mathcal{Q} \in \mathbb{C}^{J_1 \times J_2 \times \cdots \times J_M}$, is defined element wise as :

$$\big(\langle \mathcal{P}, \mathcal{Q} \rangle_{n,m}\big)_{i_1 i_2 \cdots i_{n-1} i_{n+1} i_N j_1 j_2 \cdots j_{m-1} j_{m+1} j_M} \equiv \sum_{i_n, j_m} p_{i_1 i_2 \cdots i_n \cdots i_N} \cdot q_{j_1 j_2 \cdots j_n \cdots j_M}. \tag{2.2}$$

Definition 2.2.2: The outer product of two arbitrary tensors $\mathcal{P} \in \mathbb{C}^{I_1 \times I_2 \times \cdots \times I_N}$ and $\mathcal{Q} \in \mathbb{C}^{J_1 \times J_2 \times \cdots \times J_M}$, is expressed element wise as :

$$\big(\mathcal{P} * \mathcal{Q}\big)_{i_1 i_2 \cdots i_n j_1 j_2 \cdots j_N} \equiv p_{i_1 i_2 \cdots i_n} \cdot q_{j_1 j_2 \cdots j_M}. \tag{2.3}$$

Definition 2.2.3: Multiplication of a tensor $\mathcal{T} \in \mathbb{C}^{I_1 \times I_2 \times \cdots \times I_N}$ by a matrix $U \in \mathbb{C}^{J \times I_n}$ which is called *mode-n product* results in a tensor of size $I_1 \times I_2 \times \cdots \times I_{n-1} \times J \times I_{n+1} \times \cdots \times I_N$ and defined as follows:

$$\Big(\mathcal{T} \times_n U\Big)_{i_1 i_2 \cdots i_{n-1} j i_{n+1} \cdots i_N} = \sum_{i_n} t_{i_1 i_2 \cdots i_N} u_{j i_n}. \tag{2.4}$$

Definition 2.2.4: The scalar product of two arbitrary tensors $\mathcal{P}, \mathcal{Q} \in \mathbb{C}^{I_1 \times I_2 \times \cdots \times I_N}$ is defined as:

$$\langle \mathcal{P}, \mathcal{Q} \rangle \equiv \sum_{i_1} \sum_{i_2} \cdots \sum_{i_N} q^*_{i_1 i_2 \cdots i_N} \cdot p_{i_1 i_2 \cdots i_N}. \tag{2.5}$$

Note that the tensor scalar product is generalized version of the classic scalar

product of two vectors.

Definition 2.2.5: If the scalar product of two tensors is zero, then they are mutually *orthogonal*.

Definition 2.2.6: The Frobenius norm of a tensor is defined as follow:

$$\|\mathcal{T}\| \equiv \sqrt{\langle \mathcal{T}, \mathcal{T} \rangle}. \tag{2.6}$$

Definition 2.2.7: Mathematically, the number of dimensions of *tensor* $\mathcal{T} \in R^{I_1 \times I_2 \cdots \times I_N}$ is referred to as the *order (modes)* of a tensor.

Definition 2.2.8: A *slice* of a tensor is obtained by varying two indices while fixing all others. Figure 2.1, shows *lateral*, *frontal* and *horizontal* slices of a three-way tensor.

Definition 2.2.9: The dimension of the vector space spanned by $n - mode$ vectors of a tensor is its *n–rank*.

The other significant difference between matrices and tensors is that the different *n–rank* of a tensor might not be same. Thus, one way to define rank of a tensor is to count the number of *rank*–1 terms which one could decompose that specific tensor. Moreover, it would be mentioned that a tensor has rank 1 if it could be written as the outer product of N vectors[43, 45]. Therefore, the following definition resulted for the rank of an arbitrary tensor

Definition 2.2.10: The minimum number of *rank*–1 tensors that linearly combined to construct a high order tensor is the *rank* of that tensor.

2.3 Unfolding Higher Order Tensor

The unfolded form of a tensor are generated by stacking all *mode–n* slices next to each other into a matrix [43, 45, 44].

Definition 2.3.1: Given tensor $\mathcal{T} \in \mathbb{C}^{P_1 \times P_2 \times \cdots \times P_P}$, the *mode–n* realization of

tensor $\mathcal{T}$ includes tensor element $t_{p_1,p_2,\cdots,p_P}$ with corresponding index of (p_p, q) which:

$$q = 1 + \sum_{n=1,n\neq P}^{P} \big(i_n - 1\big)Q_n \tag{2.7}$$

wherein

$$Q_n = \prod_{m=1,m\neq P}^{P} P_m \tag{2.8}$$

In other words, based on the previous illustration of tensor order and considering definition 2.3.1, *mode–n* realization of a tensor are easily defined as column vectors of unfolded tensor $\mathcal{T}$ in the mode n denoted by $T_{(n)}$. For instance, *mode–*1 matrix resulted from unfolding a matrix (second-order tensor) is equivalent to the original matrix and its *mode–*2 unfolded matrix is actually its transposed form. Thus, an N-th order tensor has N unfolded matrices. Example 2.3.1 perfectly illustrate the concept of unfolding realization of a tensor. We generated a simple tensor in order to make process easy to follow.

Example: Assume tensor $\mathcal{T} \in \mathbb{R}^{4\times3\times2}$ contains the two frontal slices as follows:

$$\mathcal{T}(:,:,1) = \begin{pmatrix} 0.1 & 0.2 & 0.3 \\ 0.4 & 0.5 & 0.6 \\ 0.7 & 0.8 & 0.9 \\ 1.0 & 1.1 & 1.2 \end{pmatrix} \quad \mathcal{T}(:,:,2) = \begin{pmatrix} 2.1 & 2.2 & 2.3 \\ 2.4 & 2.5 & 2.6 \\ 2.7 & 2.8 & 2.9 \\ 3.0 & 3.1 & 3.2 \end{pmatrix}$$

Now, unfolded realizations would be as follows:

$$\mathcal{T}_{(1)} = \begin{pmatrix} 0.1 & 0.2 & 0.3 & 2.1 & 2.2 & 2.3 \\ 0.4 & 0.5 & 0.6 & 2.4 & 2.5 & 2.6 \\ 0.7 & 0.8 & 0.9 & 2.7 & 2.8 & 2.9 \\ 1.0 & 1.1 & 1.2 & 3.0 & 3.1 & 3.2 \end{pmatrix} \quad \mathcal{T}_{(2)} = \begin{pmatrix} 0.1 & 0.4 & 0.7 & 1.0 & 2.1 & 2.4 & 2.7 & 3.0 \\ 0.2 & 0.5 & 0.8 & 1.1 & 2.2 & 2.5 & 2.8 & 3.1 \\ 0.3 & 0.6 & 0.9 & 1.2 & 2.3 & 2.6 & 2.9 & 3.2 \end{pmatrix}$$

$$\mathcal{T}_{(3)} = \begin{pmatrix} 0.1 & 0.2 & 0.3 & 0.4 & \cdots & 0.8 & 0.9 & 1.2 \\ 2.1 & 2.2 & 2.3 & 2.4 & \cdots & 2.8 & 2.9 & 3.2 \end{pmatrix}$$

Figure 2.1 visualizes the unfolding process of a $(J_1 \times J_2 \times J_3)$–tensor and depicts all corresponding unfolded realizations.

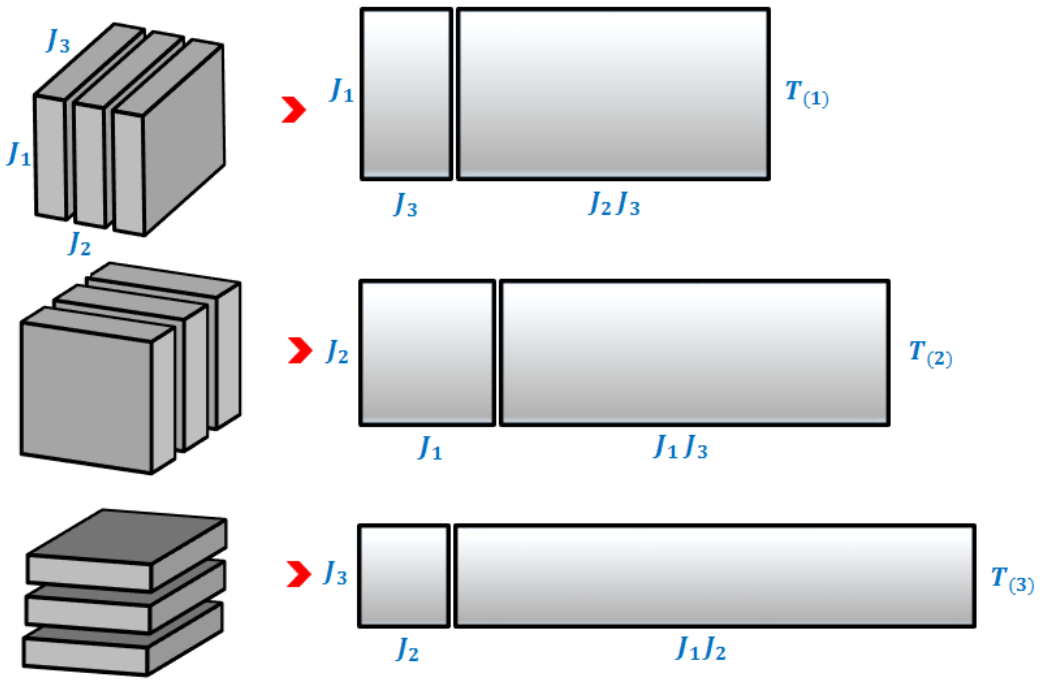

Figure 2.1: Visualization of unfolding an arbitrary three-way tensor $\mathcal{T}$. Adapted from [41].

Definition 2.3.2: The Kronecker product of two matrices $\mathbf{U} \in \mathbb{R}^{M\times N}$ and $\mathbf{V} \in \mathbb{R}^{P\times Q}$ is defined as follows:

$$\mathbf{U} \diamond \mathbf{V} \equiv \begin{pmatrix} u_{11}\cdot\mathbf{V} & u_{12}\cdot\mathbf{V} & \cdots & u_{1N}\cdot\mathbf{V} \\ u_{21}\cdot\mathbf{V} & u_{22}\cdot\mathbf{V} & \cdots & u_{2N}\cdot\mathbf{V} \\ \vdots & \vdots & \ddots & \vdots \\ u_{M1}\cdot\mathbf{V} & u_{M2}\cdot\mathbf{V} & \cdots & u_{MN}\cdot\mathbf{V} \end{pmatrix} \tag{2.9}$$

The first part of this section summarized all basic concepts and definitions in regard with tensor algebra and specifically higher order tensors. Also, some important tensor operators are described in this section. In the next part, we will introduce higher order singular value decomposition for higher order tensors and will review some interesting properties of this decomposition as well. Eager reader can refer to [121, 126, 127, 101, 89, 41] for more details on tensor algebra.

2.4 Higher Order Singular Value Decomposition (HOSVD)

This subsection briefly presents multilinear singular value decomposition (SVD) basics and introduces concepts of SVD for higher order tensors. The multilinear singular value decomposition, also known as Higher Order Singular Value Decomposition (HOSVD), is the main tool in the present work and is utilized to introduced a novel parameterization and model reduction method with applications in petroleum reservoir simulation and characterization. This section is arranged as follows. Subsection 3.1 introduces higher order singular value decomposition along with its pivotal properties. In subsection 3.2 the HOSVD computation algorithm is explained in details. Subsections 3.3 states the problem of finding best rank–1 approximation of a tensor proceeds by a generalization of this problem in subsection 3.4 on calculating best rank–$(R_1, R_2, \cdots, R_N)$ approximation of a tensor.

2.4.1 Definition and Properties

This subsection provides matrix singular value decomposition and proceeds to multi linear singular value decomposition. In fact, the HOSVD concept is established utilizing that of classic SVD[85, 70, 46, 44, 45, 43, 38].

Theorem 3.1: For all matrix $\mathbf{A} \in \mathbb{C}^{N_1 \times N_2}$, the following matrix decomposition holds

$$\mathbf{A} = \mathbf{U}\mathbf{S}\mathbf{V}^H = \mathbf{S} \times_1 \mathbf{U} \times_2 \mathbf{V}^H \tag{2.10}$$

now let $\mathbf{U}^1$ denotes $\mathbf{U}$ and $\mathbf{U}^2$ denotes $\mathbf{V}^H$, then

$$\mathbf{A} = \mathbf{S} \times_1 \mathbf{U}^1 \times_2 \mathbf{U}^2 \tag{2.11}$$

Moreover, the following statements hold as well

- $\mathbf{U}^1 = \left(U_1^1 U_2^1 \cdots U_{N_1}^1\right)$ is a unitary matrix of size $N_1 \times N_1$.
- $\mathbf{U}^2 = \left(U_1^2 U_2^2 \cdots U_{N_2}^2\right)$ is a unitary matrix of size $N_2 \times N_2$.
- $\mathbf{S}$ is a pseudo-diagonal and ordered matrix of size $N_1 \times N_2$. In other words, the matrix $\mathbf{S}$ contains all singular values of matrix $\mathbf{A}$ in a descending order.

Figure 2.2 shows matrix SVD visualization.

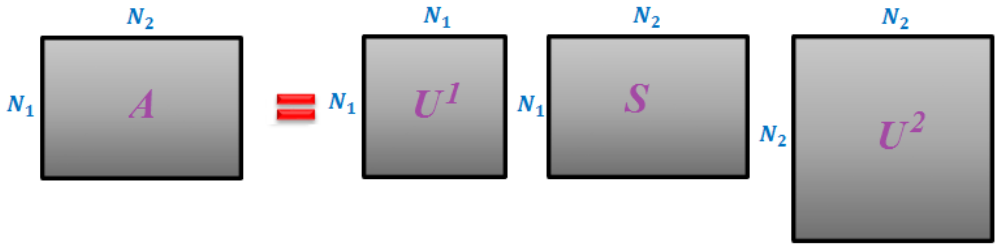

Figure 2.2: Visualization matrix SVD.

Given theorem 3.1 and definitions presented in section 2, one could represent a $(J_1 \times J_2 \times \cdots \times J_M)$–order tensor in the same fashion as classic singular value decomposition for matrices provided in theorem 3.2 as follows.

Theorem 3.2: For all tensor $\mathcal{T} \in \mathbb{C}^{N_1 \times N_2 \times \cdots \times N_M}$, the following can be expressed as tensor decomposition

$$\mathcal{T} = \mathcal{C} \times_1 \mathbf{U^1} \times_2 \mathbf{U}^2 \times \cdots \times_M \mathbf{U}^M \tag{2.12}$$

Also, the following statements hold as well

- $\mathbf{U}^m = \left(U_1^1 U_2^1 \cdots U_{N_m}^m\right)$ is a unitary matrix of size $N_m \times N_m$.
- $\mathcal{C}$ is a tensor of size $N_1 \times N_2 \times \cdots \times N_M$, referred to as *core tensor* which represents coefficients matrix in classic matrix SVD and contains sub-tensors that are all orthogonal and ordered tensor. Sub-tensor $\mathcal{C}_{n_m=\alpha}$ can be acquired by fixing index m to α. Here, *all orthogonality* means that for all m, α and β, sub-tensors $\mathcal{C}_{n_m=\alpha}$ and $\mathcal{C}_{n_m=\beta}$ are orthogonal with $\alpha \neq \beta$. Furthermore, the following holds for the m–mode singular values of tensor $\mathcal{T}$, $\|\mathcal{T}_{n_m=j}\|$, denoted by σ_j^m

$$\|\mathcal{T}_{n_m=1}\| \geq \|\mathcal{T}_{n_m=2}\| \geq \cdots \geq \|\mathcal{T}_{n_m=N_m}\| \geq 0. \tag{2.13}$$

In other words, once *horizontal slices* of tensor $\mathcal{T}$ are jointly orthogonal in terms of tensor inner product, then the sub-tensors are *all orthogonal*. Reader must note that core tensor $\mathcal{C}$, unlike the classic matrix SVD, is not pseudo-diagonal which means it is a full tensor that satisfy the all orthogonality condition. U^ms are the bases (factor) matrices (which are orthogonal) and can be thought of as the principal components in each mode as well. Also, one could derive a matrix representation form of HOSVD

as follow:

$$\mathcal{T} = U^m \cdot C_m \cdot \left(U^{m+1} \diamond U^{m+2} \diamond \cdots \diamond U^M \diamond U^1 \diamond U^2 \diamond \cdots \diamond U^{m-1}\right). \tag{2.14}$$

in which $\diamond$ denotes Kronecker product of two matrices. Due to the *orthogonality* property, HOSVD is essentially unique. The Frobenius norms of $(M-1)$th–order of the sub-tensors act as the same way as singular values in classic matrix SVD. Figure 2.3 visualizes higher order singular value decomposition of a three-way tensor. Moreover, the following holds for the tensor HOSVD product in theorem 3.2

$$\|\mathcal{T}\|^2 = \|\mathcal{C}\|^2. \tag{2.15}$$

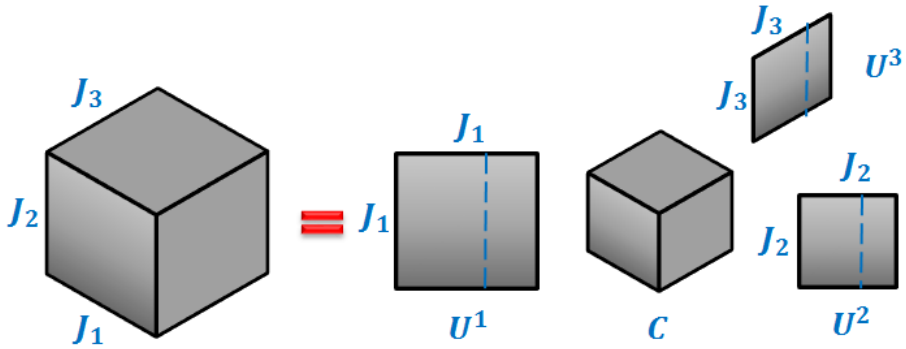

Figure 2.3: Visualization matrix HOSVD for a three-way tensor. Adapted from [41].

2.4.2 HOSVD Computation Algorithm

In the present subsection, an iterative algorithm is derived for computing higher order singular value decomposition of a high dimension tensor. Considering theorem 3.2 and the m–mode product commutative property, one can simply rewrite equation

2.12 as follows

$$\mathcal{C} = \mathcal{T} \times_1 \mathbf{U^1}^H \times_2 \mathbf{U^2}^H \times \cdots \times_M \mathbf{U^M}^H. \tag{2.16}$$

Now, by assuming the unfolded representation of a tensor from equation 2.14 and Kronecker product one can easily relate the link between classic matrix SVD and HOSVD of a tensor. First of all, since $\mathcal{C}$ is all orthogonal and ordered so as is $\mathcal{C}_m$ with Frobenius norms equivalent to σ_j^m with respect to its jointly orthogonal rows. Second, one should note that the Kronecker product, $U^{m+1} \diamond U^{m+2} \diamond \cdots \diamond U^M \diamond U^1 \diamond U^2 \diamond \cdots \diamond U^{m-1}$, is orthogonal due to orthogonality property of all $\mathbf{U}^m$s. Thus, if one define matrix $\mathbf{\Sigma}^m$ and a column wise orthogonal matrix $\mathbf{V^m}$ as in equations 2.12 and 2.12 respectively

$$\mathbf{\Sigma}^m = \begin{pmatrix} \sigma_1^m & 0 & \cdots & 0 \\ 0 & \sigma_2^m & \cdots & \vdots \\ \vdots & \vdots & \ddots & 0 \\ 0 & 0 & \cdots & \sigma_{J_m}^m. \end{pmatrix} \tag{2.17}$$

$$\mathbf{V^m} = \Big(\mathbf{U}^{m+1} \diamond \mathbf{U}^{m+2} \diamond \cdots \diamond \mathbf{U}^M \diamond \mathbf{U}^1 \diamond \mathbf{U}^2 \diamond \cdots \diamond \mathbf{U}^{m-1}\Big)\hat{\mathcal{C}}_m^H. \tag{2.18}$$

Wherein, $\hat{\mathcal{C}}_m^H$ is normalized replicate of $\mathcal{C}_m^H$. Then the result, equation 2.12, is matrix SVD of unfolded form of tensor $\mathcal{T}$.

$$\mathcal{T}_m = \mathbf{U}^m \mathbf{\Sigma}^m {\mathbf{V}^m}^H. \tag{2.19}$$

As a mater of fact, the m-mode singular matrix U^m can simply be found by calculating the left singular matrix of unfolded form of $\mathcal{T}$. Thus, computing HOSVD is equivalent to reapplying SVD, M times. Eventually, using the equation 2.14, one could simply compute the core tensor $\mathcal{C}$. All steps are summarized in algorithm 2.1 as follows.

Algorithm 2.1 Higher Order SVD Computation Procedure [41]

procedure HOSVD
  Input: m–order tensor $\mathcal{T}$
  Output: *core tensor* $\mathcal{C}$ and basis $\mathbf{U^1}, \mathbf{U^2}, \cdots, \mathbf{U^M}$
  for $m = 1$ **to** M **do**
    Calculate $\mathcal{T}_m$ ▷ unfolded versions of tensor $\mathcal{T}$
    Apply classic SVD to $\mathcal{T}_m$ ▷ unfolded versions of tensor $\mathcal{T}$
  end for
  $\mathcal{C} \leftarrow \mathcal{T} \times_1 \mathbf{U^{1H}} \times_2 \mathbf{U^{2H}} \times \cdots \times_M \mathbf{U^{MH}}$ ▷ compute *core tensor*
  return: *core tensor* $\mathcal{C}$ and basis $\mathbf{U^1}, \mathbf{U^2}, \cdots, \mathbf{U^M}$
end procedure.

A number of various research studies have been conducted in order to apply HOSVD in different fields of science and engineering like signal processing [91] , face recognition [131], data and chemical analysis [71], among others. The application of HOSVD to flow problems has been minimal due to the lack of fast and reliable tools for the decomposition computations. In recent years, however, new tools and algorithms have been developed that show promising results in large-scale multilinear algebra computations [9, 123].

In terms of computation of the HOSVD terms, one can use the so-called Alternating Least Squares (ALS) Method [87], [91] and [9]. Making the analogy of the approximation of a matrix by one of lower rank using SVD, one can come up with a truncated HOSVD in similar fashion. Indeed, in order to reduce the order of a given tensor, one can select only those basis that conserve more energy in each mode, which always are corresponded to the larger singular values in SVD. Thus, the problem of finding the larger *mode-n* singular values of a tensor turns into the problem of finding the best lower rank approximation of a tensor which is a optimization problem. Unlike the regular SVD, this problem does not have a closed form solution. A very common approach to obtain a truncated HOSVD is to use the alternating

least squares (ALS) method.

2.4.3 Best Rank–1 Approximation

As mentioned in the previous subsection, the goal here is to approximate a higher order tensor by one of the lower rank in an efficient fashion with respect to an optimal least square scenario. There are two different way to do so: (1) estimating a tensor using a *rank*–1 tensor referred to as *rank*–1 approximation; (2) by specification of *mode–m* ranks at the beginning and providing a *rank*–$(R_1, R_2, \cdots, R_M)$ tensor approximation. Furthermore, unlike the classic matrix SVD, approximating a tensor with one of the lower rank might not results in a globally optimum solution. However, by selecting a good initial guess the algorithm may yields in the best *rank*–1 or *rank*–$(R_1, R_2, \cdots, R_M)$ tensor approximation locally. Therefore, the following two subsections are organized to provide essential materials on finding best *rank*–1 and *rank*–$(R_1, R_2, \cdots, R_M)$ tensor approximations using higher order power method and alternative least square method respectively.

The problem is to find a scalar γ and normal vectors $\mathbf{U^1}, \mathbf{U^2}, \cdots, \mathbf{U^M}$ so that the following statement holds

$$\underset{\hat{\mathcal{T}}}{minimize}\ f(\hat{\mathcal{T}}) \equiv \|\mathcal{T} - \hat{\mathcal{T}}\|_F^2. \tag{2.20}$$

wherein, $\hat{\mathcal{T}} \equiv \gamma.\mathbf{U^1} * \mathbf{U^2} * \cdots * \mathbf{U^M}$ is a *rank*–1 tensor that minimizes the objective function in equation 2.20 which is a straightforward least square loss function. The stated optimization problem can be solved utilizing Lagrange multipliers method. Eager reader can refer to [41, 45] for details on the solution of this optimization problem. Here, we only summarized the algorithm called *higher order power method* or HOPM, that we employed to find Lagrange multipliers and corresponding derivatives. The Lagrange multipliers corresponding to the problem stated in equation

2.20 are as follows

$$\mathcal{T} \times_1 \mathbf{U^{1}}^H \times \cdots \times_{m-1} \mathbf{U^{m-1}}^H \times_{m+1} \mathbf{U^{m+1}}^H \cdots \times_M \mathbf{U^{M}}^H = \gamma.\mathbf{U^{m}}, \tag{2.21}$$

$$\mathcal{T} \times_1 \mathbf{U^{1}}^H \times \times_2 \mathbf{U^{2}}^H \times \cdots \times_M \mathbf{U^{M}}^H \times = \gamma, \tag{2.22}$$

$$\|\mathbf{U^{m}}\| = 1. \tag{2.23}$$

Now, we may employ Alternating Least Square (ALS) method in order to find local minimum of objective function in an iterative single step algorithm. In fact, we can obtain optimum Lagrange multiplier γ and the normalized vector $\mathbf{U^{m}}$ in each iteration step independently as we fix all other vectors. The procedure continues until convergence. Algorithm 2.2 sums up the steps of higher order power method.

Algorithm 2.2 Higher Order Power Method (HOPM) [41]

procedure HOPM
  Input: m–order tensor $\mathcal{T}$
  Output: vectors $\mathbf{U^{1}}, \mathbf{U^{2}}, \cdots, \mathbf{U^{M}}$
  initiate $\mathbf{U_0^{1}}, \mathbf{U_0^{2}}, \cdots, \mathbf{U_0^{M}}$ ▷ left singular vectors of $\mathcal{T}_m$
  while not converge **do**
    $\hat{\mathbf{U}}_i^m = \mathcal{T} \times_1 \mathbf{U}_{i-1}^1 \times \cdots \times_{m-1} \mathbf{U}_{i-1}^{m-1} \times_{m+1} \mathbf{U}_{i-1}^{m+1} \cdots \times_M \mathbf{U}_{i-1}^M$;
    $\gamma_i^m = \|\hat{\mathbf{U}}_i^m\|$;
    $\mathbf{U}_i^m = \hat{\mathbf{U}}_i^m / \gamma_i^m$;
  end while
end procedure.

2.4.4 Best Rank–$(R_1, R_2, \cdots, R_N)$ Approximation

This subsection describe an extension to the best *rank*–1 approximation of a tensor to a case that we are interested in estimating a given higher order tensor with one of lower rank. As a matter of fact, we want to find the best *rank*–$(R_1, R_2, \cdots, R_M)$

approximation of a assumed tensor which means reducing each tensor mode to a specific rank R_m. Thus, making the analogy of the approximation of a matrix by one of lower rank using SVD, one can come up with a truncated HOSVD is similar fashion. Indeed, in order to reduce the order of a given tensor, one could select only those basis that conserve more energy in each mode, which always are corresponded to the larger singular values in SVD. Mathematically, given the tensor $\mathcal{T} \in R^{J_1 \times J_2 \cdots \times J_M}$, we seek to find

$$\min_{\hat{\mathcal{T}}} \|\mathcal{T} - \hat{\mathcal{T}}\|_F^2. \tag{2.24}$$

wherein, $\hat{\mathcal{T}} \in R^{J_1 \times J_2 \cdots \times J_M}$ is the approximated tensor of the order of $(r_1, r_2, \cdots r_M)$ which $r_i < J_i$. Therefore, the problem of finding the larger *mode–m* singular values of a tensor turns into the problem of finding the best lower rank approximation of a tensor which is a optimization problem. Unlike the classic SVD, this problem does not have a closed form solution. A very common approach to obtain a truncated HOSVD is to employ the alternating least squares (ALS) method, proposed by Kroonenberg and de Leeuv [87] which is referred to as *higher order orthogonal iteration method* (HOOI). Input of the algorithm is a tensor $\mathcal{T}$ of rank $(J_1 \times J_2 \cdots \times J_M)$ and its output is an approximated lower rank tensor $\hat{\mathcal{T}} \in R^{J_1 \times J_2 \cdots \times J_M}$ with a reduced rank of $(r_1, r_2, \cdots r_M)$. The purpose is to find the best reduced rank approximation through computing left singular matrices of the input tensor in a iterative manner until algorithm converged. The approach contains three steps. First step is initializing the factor matrices by applying HOSVD to the input. In second step, which is the iteration part of algorithm, left singular matrices corresponding to each mode are estimated independently and separately. In other words, least mean square min-

imization leads to maximizing function f over U^m, which are orthonormal:

$$f = \|\mathcal{U}_i^m \times_m \mathbf{U}^{m^H}\|_F^2. \tag{2.25}$$

wherein,

$$\mathcal{U}_i^m \equiv \mathcal{T} \times_1 \mathbf{U}^{\mathbf{1}^H} \times \cdots \times_{m-1} \mathbf{U}^{\mathbf{m-1}^H} \times_{m+1} \mathbf{U}^{\mathbf{m+1}^H} \cdots \times_M \mathbf{U}^{\mathbf{M}^H}. \tag{2.26}$$

Thus, in each iteration one factor matrix is optimally estimated and other matrices considered as constant. Last step of algorithms is to reconstruct the estimated lower rank tensor after convergence. Algorithm 3.2 summarizes all steps of higher order orthogonal iteration method (HOOI) through an alternating least square method. Figures 2.4 and 2.5 show test experiments to compare the classic SVD and HOSVD in terms of compression for face recognition applications [115]. All images are taken from AT&T Laboratories Cambridge [19]. Eager readers would also refer to [87], [91] and [9] for more details on ALS and some other refined algorithms on truncation HOSVD.

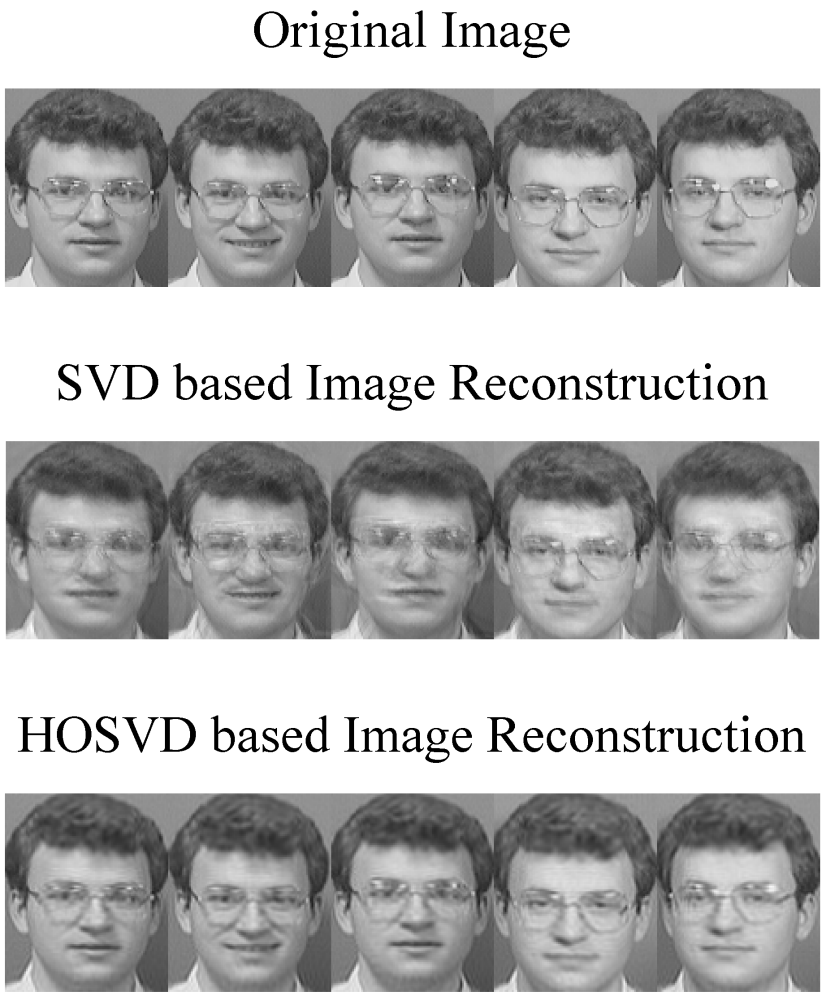

Figure 2.4: Comparison Compressed face images in different expressions and viewpoints using SVD and HOSVD.

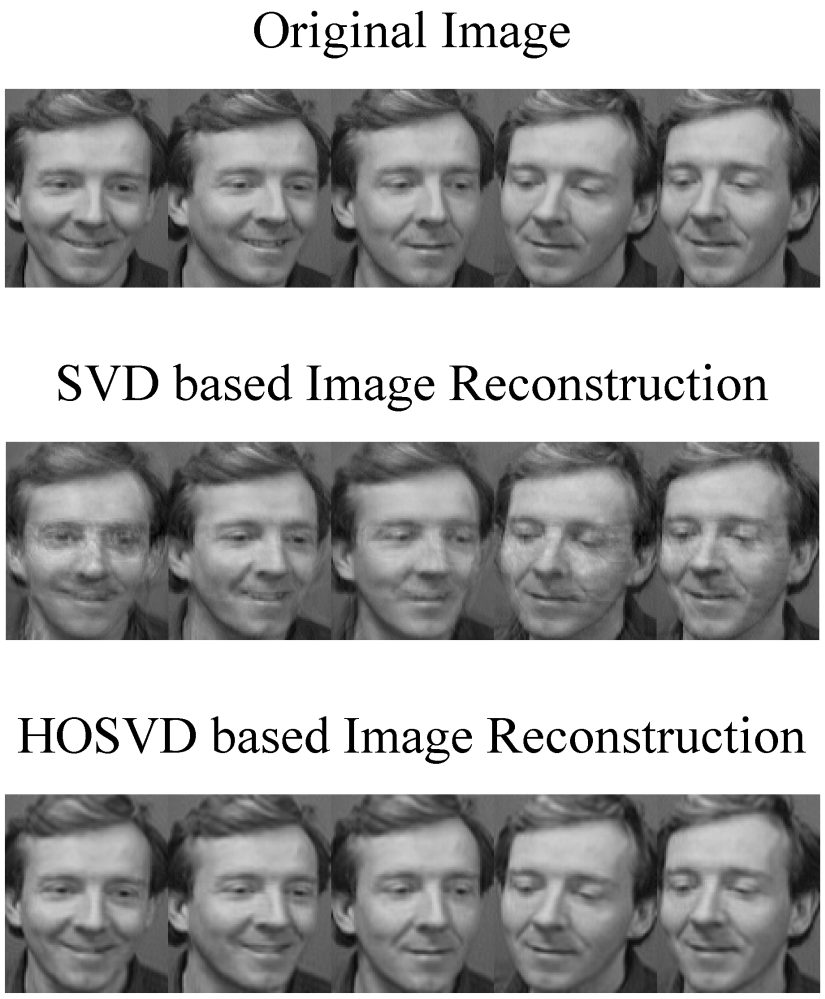

Figure 2.5: Comparison Compressed face images in different expressions and viewpoints using SVD and HOSVD.

Algorithm 2.3 Higher Order Orthogonal Iteration (HOOI) [41]

procedure HOOI
  Input: m–order tensor $\mathcal{T}$
  Output: *core tensor* $\mathcal{C}$ and matrices $\mathbf{U^1}, \mathbf{U^2}, \cdots, \mathbf{U^M}$
  initiate $\mathbf{U_0^1}, \mathbf{U_0^2}, \cdots, \mathbf{U_0^M}$ ▷ left singular matrices of $\mathcal{T}_m$
  while not converge **do**
    $\hat{\mathbf{U}}_i^m = \mathcal{T} \times_1 \mathbf{U}_{i-1}^1 \times \cdots \times_{m-1} \mathbf{U}_{i-1}^{m-1} \times_{m+1} \mathbf{U}_{i-1}^{m+1} \cdots \times_M \mathbf{U}_{i-1}^M$;
    $\underset{\mathbf{U}^m \in \mathbb{R}^{J_m \times R_m}}{\textbf{maximize}}\ f \equiv \|\mathcal{U}_i^m \times_m \mathbf{U}^{m^H}\|$;
    $\gamma_i^m = f\Big(\big(\mathbf{U}_i^m\big)_{max}\Big)$;
    $\mathbf{U}_i^m = \big(\mathbf{U}_i^m\big)_{max}$;
  end while
end procedure.

3. POROUS MEDIA FLOW MODELING

Constructing mathematical model for a petroleum reservoir needs thorough understanding of reservoir components including reservoir rock and fluid (oil, water, and gas) and geological description of the environment. Reservoir rock properties including permeability and porosity are of high interest. Furthermore, reservoir fluid properties such as fluid densities, viscosity and formation volume factors depend on fluid pressure and relative permeability and capillary pressure are tied to saturation of fluids within the reservoir. This section briefly presents essential reservoir simulation basics and backgrounds on permeability parameterization as well as ensemble Kalman Filter (EnKF) algorithm for reservoir history matching, which are necessary to understand the motivations and results of the present work[69, 23, 24].

3.1 Petroleum Reservoirs

Hydrocarbons, i.e., oil and natural gas, were formed as a result of subsiding animals and plants in presence of high temperature and pressure buried at a depth between 3000 - 15000 ft for millions of years. A reservoir rock, *porous medium*, is the one which contain oil or natural gas in its pores, i.e., void spaces inside the rock, and it has some specific physical characteristics in order to be able to hold and flow the petroleum fluid within the rock. Two of the primary variables related to the fluid dynamics in porous media are the porosity, ϕ, and permeability, $\mathbf{K}$. The *porosity* accounts for the amount of void spaces in the porous media that can store the hydrocarbon fluids. In other words, *porosity* is the ratio of void pore volume to the total rock volume and is stated as a percentage. As a matter of fact, porosity is

a measure for expressing rock storage capacity and is defined as follows:

$$\phi = \frac{pore\ volume}{bulk\ volume}. \tag{3.1}$$

On the other hand, if the void spaces are not connected, the fluid cannot be moved from one region to the other. The ability to transmit the fluid within the rock is refer to as *permeability* and depends on whether the pores are connected within the rock or not and how well they are actually interconnected. In other words, permeability accounts for how easier is to transfer fluid inside the reservoir. Henry Philibert Gaspard Darcy [36, 113] was the first scientist who found out about this characteristic during his studies of water flow through filter beds, and proposed the following mathematical definition for single phase, three dimensional fluid flow called *Darcy's law*:

$$q = -\frac{k}{\mu}\Big(\nabla p - \gamma \nabla Z\Big). \tag{3.2}$$

wherein, q is Darcy's flux, k is the intrinsic permeability of the medium, ∇p is pressure gradient and μ is viscosity of fluid. ∇Z is elevation gradient as well. Next subsections describe in details single and multi-phase flow equations using Darcy's law. Usually, the hydrocarbons can be produced by drilling a producing well and by pressure differential the fluid can reach the surface. However, only $5 - 10\%$ of the recoverable hydrocarbons can be retrieved in this manner. Therefore, one usually drill an injection well, and inject some form of fluid to push out the remaining oil/gas. This is called secondary production and often known as water flooding in the case of water injection. Figure 3.1 depicts a very simplified schematic of a real production system in an oilfield.

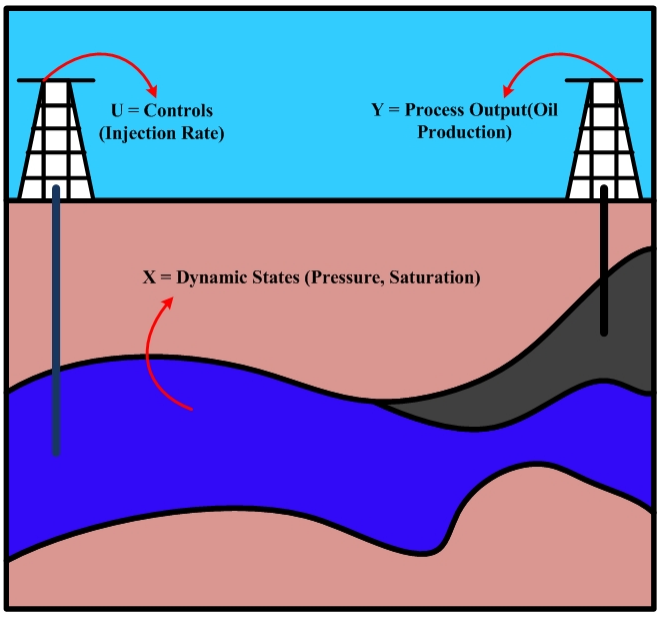

Figure 3.1: schematic of a real production system, Edited from [118]

3.2 Reservoir Fluid Flow Modeling

In order to demonstrate the main concepts developed here, we will pose the reservoir simulation problem as a dynamical system. Thus, we will first consider the flow equation in its mathematical form and show how one can arrive at the system description. We start by describing it via a single phase flow diffusion in a media. Reservoir engineers need to acquire more accurate information about the performance of a assumed petroleum reservoir in order to to estimate its future production precisely at various operating conditions. Having such a reliable reservoir model helps to understand the behavior of the reservoir and its properties including the properties of reservoir rock and fluid within the reservoir. Also, providing a precise reservoir model improve the reservoir management plans by minimizing the development cost and maximizing the future production of the reservoir[61, 122, 108, 6, 106, 30].

3.2.1 Mass Conservation for Fluid Flow in Porous Media

For developing fluid flow equation we need to derive mass continuity or mass conservation law equation first. Then, combining material balance equation, state equations, and Darcy's law we will come up with the diffusion equation for fluid flow in porous media[36, 88, 10, 113]. We assume reservoir fluid flows through porous media with a constant volume V in the direction x from point $x - \frac{\delta x}{2}$ to $x + \frac{\delta x}{2}$ in δt and consider a perpendicular cross section to the fluid flow with area xy as well. The goal is to derive material balance equation for the center of an arbitrary cubical volume in figure 3.2. Material balance states that the difference between inflow mass and outflow mass is accumulated mass in porous media. Therefore, considering mass flux of fluid in direction x which is ρu_x the following holds for inflow mass flux across the xy area in direction x in δt

$$\left(\rho u_x\right)_{x-\frac{\delta x}{2},y,z}\delta y\delta z\delta t, \tag{3.3}$$

and for outflow mass flux as follows

$$\left(\rho u_x\right)_{x+\frac{\delta x}{2},y,z}\delta y\delta z\delta t. \tag{3.4}$$

and the same correlations for direction y

$$\left(\rho u_y\right)_{x,y-\frac{\delta y}{2},z}\delta x\delta z\delta t, \tag{3.5}$$

$$\left(\rho u_y\right)_{x,y+\frac{\delta y}{2},z}\delta x\delta z\delta t. \tag{3.6}$$

and z direction as well

$$\left(\rho u_z\right)_{x,y,z-\frac{\delta z}{2}}\delta x\delta y\delta t, \tag{3.7}$$

$$\left(\rho u_z\right)_{x,y,z+\frac{\delta z}{2}} \delta x \delta y \delta t. \tag{3.8}$$

where, ρ is reservoir fluid density. Also, we have the following from material balance

$$Flux_{inflow} - Flux_{outflow} = Accumulation = Mass_{after} - Mass_{before}. \tag{3.9}$$

Now, combining these correlations together using material balance we get

$$\begin{aligned}
&\Big(\left(\rho u_x\right)_{x-\frac{\delta x}{2},y,z} - \left(\rho u_x\right)_{x+\frac{\delta x}{2},y,z}\Big)\delta y \delta z \delta t \\
&\quad + \Big(\left(\rho u_y\right)_{x,y-\frac{\delta y}{2},z} - \left(\rho u_y\right)_{x,y+\frac{\delta y}{2},z}\Big)\delta x \delta z \delta t \\
&\quad + \Big(\left(\rho u_z\right)_{x,y,z-\frac{\delta z}{2}} - \left(\rho u_z\right)_{x,y,z+\frac{\delta z}{2}}\Big)\delta x \delta y \delta t \\
&\quad = m(t+\delta t) - m(t).
\end{aligned} \tag{3.10}$$

wherein, $m(t)$ is accumulated mass inside the rock. We can write the following for accumulation

$$m = \rho \phi \delta x \delta y \delta z. \tag{3.11}$$

Assuming that cross sectional area is constant and equal for all directions and divide both sides by $\delta x \delta y \delta z \delta t$ we may rewrite the equation 3.10 as follows

$$\begin{aligned}
&\frac{\left(\rho u_x\right)_{x-\frac{\delta x}{2},y,z} - \left(\rho u_x\right)_{x+\frac{\delta x}{2},y,z}}{\delta x} \\
&\quad + \frac{\left(\rho u_y\right)_{x,y-\frac{\delta y}{2},z} - \left(\rho u_y\right)_{x,y+\frac{\delta y}{2},z}}{\delta y} \\
&\quad + \frac{\left(\rho u_z\right)_{x,y,z-\frac{\delta z}{2}} - \left(\rho u_z\right)_{x,y,z+\frac{\delta z}{2}}}{\delta z} \\
&\quad = \frac{\rho \phi_{t+\delta t} - \rho \phi_t}{\delta t}.
\end{aligned} \tag{3.12}$$

now, getting the limit of both side, we arrive at

$$\begin{aligned}
&\lim_{\delta x \to 0} \frac{\left(\rho u_x\right)_{x-\frac{\delta x}{2},y,z} - \left(\rho u_x\right)_{x+\frac{\delta x}{2},y,z}}{\delta x} \\
&+ \lim_{\delta y \to 0} \frac{\left(\rho u_y\right)_{x,y-\frac{\delta y}{2},z} - \left(\rho u_y\right)_{x,y+\frac{\delta y}{2},z}}{\delta y} \\
&+ \lim_{\delta z \to 0} \frac{\left(\rho u_z\right)_{x,y,z-\frac{\delta z}{2}} - \left(\rho u_z\right)_{x,y,z+\frac{\delta z}{2}}}{\delta z} \\
&= \lim_{\delta t \to 0} \frac{\rho\phi_{t+\delta t} - \rho\phi_t}{\delta t}.
\end{aligned} \tag{3.13}$$

and finally we get the *conservation mass* equation for single phase fluid flow as follows

$$\frac{\partial(\rho\phi)}{\partial t} = -\nabla.(\rho\mathbf{u}) + q. \tag{3.14}$$

wherein, q is sink or source flow, usually from well, and $\mathbf{u}$ is Darcy's velocity.

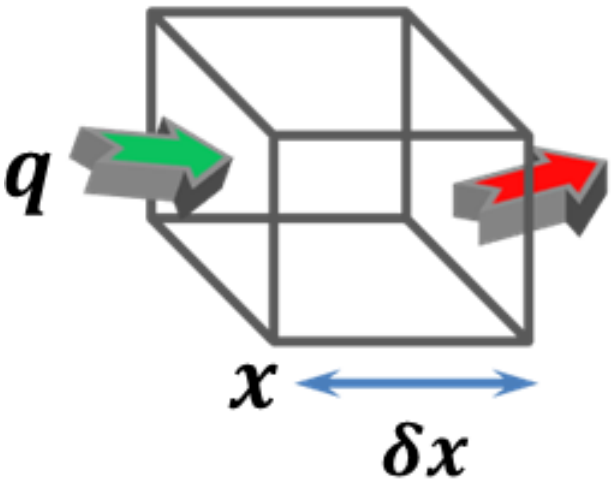

Figure 3.2: Mass conservation law for 1D fluid flow.

3.2.2 Diffusion Equation

Understanding the nature and behavior of any dynamic system requires to develop a mathematical description that express the physics of the system precisely in a mathematical manner. In studying reservoir fluid flow, governing equations of transient fluid flow through the porous medium is a set of time dependent partial differential equations referred to as *diffusion equation*[36, 92, 124]. As discussed previously, in order to obtain the *diffusion equation*, we combine mass conservation, state equation, and Darcy's law. We may rewrite Darcy velocity in 3D dimension as follows

$$\mathbf{u} = -\frac{1}{\mu}\mathbf{k}\Big(\nabla p - \rho g \nabla Z\Big). \tag{3.15}$$

wherein, $\mathbf{k}$ is reservoir rock *absolute permeability* tensor, $\gamma = \rho g$ is *specific gravity*, and ∇Z is elevation gradient. Now, if we substitute equation 3.15 in the mass conservation equation 3.14, we arrive at the general equation for *single phase* flow in porous media as follows

$$\frac{\partial\big(\phi\rho\big)}{\partial t} + q = \nabla.\Big(\frac{\rho}{\mu}\mathbf{k}\big(\nabla p + \gamma\nabla z\big)\Big). \tag{3.16}$$

3.3 Numerical Solution to Diffusion Equation

As one can see, the *diffusion equation* is a time dependent partial differential equation (PDE) which is first order in time and second order in space. Due to their complex and nonlinear nature such equations are very hard, if not impossible, to solve analytically. Thus, one has to employ numerical methods such as finite difference and finite element in order to find a solution to these equations. Here, in this work, in order to simulate the reservoir behavior, and therefore solve the diffusion equation, we utilize the *finite difference* method[54, 109, 16, 32].

The main idea of *finite difference* method is to solve PDE by estimating spatial derivatives using a finite grid network and through truncating higher order terms in a Taylor series expansion. In reservoir simulation, we are interested in approximating pressure and saturation of fluids inside the porous media. Performing *finite difference* properly yields a linear system of algebraic equations which can be solved by matrix computations. Since, the PDEs are time and space dependent, so we need to apply *finite difference* twice to tackle the problem. First, we perform *finite difference* to PDEs in space for estimating spatial derivatives which yields a system of ordinary differential equations (ODE). Second, we apply it to the resulted ODE system in order to approximate time derivatives and this last one results in a system of nonlinear equations. Also, the reader notes that due to employing grid network, the solution is not continuous and is known only at grid points. Next two sessions will describe the discretization process and performing *finite difference* in order to solve diffusion equation for single and two phase flow system respectively[125, 112, 122, 133, 103].

3.4 Numerical Solution to Single Phase Flow System

The purpose of this subsection is to provide a brief introduction to utilizing finite difference method in solving a single phase fluid flow equation. As mentioned before, there are two types of discretization, one in space and the other in time.

In finite difference method, one may estimates derivatives in a partial differential equation using a linear combination of values of function at mesh grid points. Thus, for a given function f first order derivatives are defined as follows

$$\frac{\partial f}{\partial x} = \lim_{\Delta x \to 0} \frac{f(x + \Delta x) - f(x)}{\Delta x} \tag{3.17}$$

and one can choose to expand the Taylor series to the right or to the left for function

f at points $x_i = i\Delta x$ as follows

$$f(x_i + \Delta x) = f(x_i) + \Delta x\Big(\frac{\partial f(x_i)}{\partial x}\Big) + \frac{(\Delta x)^2}{2}\Big(\frac{\partial^2 f(x_i)}{(\partial x)^2}\Big) + \cdots , \tag{3.18}$$

$$f(x_i - \Delta x) = f(x_i) - \Delta x\Big(\frac{\partial f(x_i)}{\partial x}\Big) + \frac{(\Delta x)^2}{2}\Big(\frac{\partial^2 f(x_i)}{(\partial x)^2}\Big) - \cdots . \tag{3.19}$$

These two equations are referred as forward and backward finite differences. To this end, substitution equations 3.18 and 3.19 into equation 3.17 and letting $f(x_i+\Delta x) = f_{i+1}$ and $f(x_i - \Delta x) = f_{i-1}$, we arrive to an approximation for first order derivatives of function $f(x)$ called central differences as follows

$$\Big(\frac{\partial f(x)}{\partial x}\Big)_i = \frac{f_{i+1} - f_{i-1}}{2\Delta x} \tag{3.20}$$

These discretization in space can be shown to yield good approximation for the PDE. The reader can see [54, 36] for an account of accuracy and convergence of these methods. We also have a time derivative term in the diffusion equation so we need to apply a time discretization as well in order to convert PDE to a system of nonlinear equations. We have to note that time and space derivatives are decoupled which means we can discretize these terms independently. So, for the single phase fluid flow PDE equation after discretization in space and time, we have

$$\begin{aligned} &- \Big(T_{i\pm1/2,j,k} + T_{i,j\pm1/2,k} + T_{i,j,k\pm1/2}\Big)p_{i,j,k} \\ &+ T_{i\pm1/2,j,k}p_{i\pm1,j,k} + T_{i,j\pm1/2,k}p_{i,j\pm1,k} \\ &+ T_{i,j,k\pm1/2}p_{i,j,k\pm1} + q_{i,j,k} = C_{i,j,k}V_{i,j,k}\frac{dp_{i,j,k}}{dt}. \end{aligned} \tag{3.21}$$

wherein,

$$C_i = \frac{\phi c_t}{B}, \tag{3.22}$$

and

$$T_{i\pm\frac{1}{2},j,k} = 0.001127\,\frac{k_x \Delta y \Delta z}{\Delta x}\frac{1}{B_0\mu_0}, \tag{3.23}$$

$$T_{i,j\pm\frac{1}{2},k} = 0.001127\,\frac{k_y \Delta x \Delta z}{\Delta y}\frac{1}{B_0\mu_0}, \tag{3.24}$$

$$T_{i,j,k\pm\frac{1}{2}} = 0.001127\,\frac{k_z \Delta x \Delta y}{\Delta z}\frac{1}{B_0\mu_0}. \tag{3.25}$$

NOTE 1: The terms $0.001127\,\frac{k_x \Delta y \Delta z}{\Delta x}\frac{1}{B_0\mu_0}$ are the transmissibilities, $T_{i\pm\frac{1}{2},j,k}$, and are required at the gridblock boundaries. The transmissibility is a measure of how easy fluid can transfer through the porous medium. The transmissibility is proportional to geometry and permeability. In fact, the transmissibility links flow to the pressure difference between two adjacent gridblocks. The reader notes that all gridblocks assigned properties can vary with respect to heterogeneity in actual reservoir. For instance, each gridblock may have different thickness or permeability and porosity. Moreover, the permeability can vary in different directions. Now, in order to compute transmissibility at gridblock boundaries, we need to utilize harmonic average between gridblock properties [54].

NOTE 2: The subscribed term $\pm\frac{1}{2}$ refer to interface connection between plus or minus direction of the grid. The first part of transmissibility term, which is called geometric transmissibility, is constant. The second term contain fluid properties and change over time with changes in pressure, thus, this term would be updated in every time step. Finally, coefficient 0.001127 is conversion factor, translating units to the field units in petroleum engineering [54].

NOTE 3: In order to compute the properties at the faces , i.e., gridblocks

boundaries, we first calculate the volumetric average pressure at the grid interface (interfaces perpendicular to x, y, and z direction). Then, in order to find fluid properties we use the look up table, that is provided, for formation volume factor and viscosity u against pressure. In addition, we interpolate to calculate the new values of FVF and viscosity. One could instead compute everything in the center of grids and then calculate harmonic average to get the results [54]. Moreover, the coefficient C_i in accumulation term can be written as follows:

$$C_i = \frac{\phi^0 c_R}{B_i^{n+1}} + \frac{\phi^n c_f}{B^0}. \tag{3.26}$$

Additionally, gravity term has to be included in the LHS by

$$\overrightarrow{\nabla}\Phi = \overrightarrow{\nabla}p - \gamma\overrightarrow{\nabla}Z. \tag{3.27}$$

Now, taking all of these into account and adding gravity effects, the diffusion equation becomes

$$\begin{aligned}
&-\Big(T_{i\pm\frac{1}{2}} + T_{j\pm\frac{1}{2}} + T_{k\pm\frac{1}{2}}\Big)p_{i,j,k}^{n+1} \\
&\qquad + T_{i\pm\frac{1}{2}}p_{i\pm1}^{n+1} + T_{j\pm\frac{1}{2}}p_{j\pm1}^{n+1} + T_{k\pm1/2}p_{k\pm1} + \cdots \\
&\qquad - \Big(T_{i\pm\frac{1}{2}}\gamma_{i\pm\frac{1}{2}} + T_{j\pm\frac{1}{2}}\gamma_{j\pm\frac{1}{2}} + T_{k\pm\frac{1}{2}}\gamma_{k\pm\frac{1}{2}}\Big)Z_{i,j,k} \\
&\qquad + T_{i\pm\frac{1}{2}}\gamma_{i\pm\frac{1}{2}}Z_{i\pm1} + T_{j\pm\frac{1}{2}}\gamma_{j\pm\frac{1}{2}}Z_{j\pm1} \\
&\qquad + T_{k\pm\frac{1}{2}}\gamma_{k\pm\frac{1}{2}}Z_{k\pm1} + q_{i,j,k} = RHS.
\end{aligned} \tag{3.28}$$

Wherein, for the sake of simplicity we just write the subscripts that change in each

grid. For the right hand side (RHS) discretization results in following:

$$\frac{\left(\frac{\phi^0 c_R}{B_i^{n+1}} + \frac{\phi^n c_f}{B^0}\right) V_i}{\Delta t}\left(p_i^{n+1} - p_i^n\right). \tag{3.29}$$

Term $q_{i,j,k}$ can be pressure or rate control. By using Peaceman equation [8], one can write

$$q = J_w\left(p - p_{wf}\right), \tag{3.30}$$

where J_w is a productivity index that depends on pressure.

(3.31)

Now, we may apply time discretization to complete the discretization step. We have choices to evaluate each term, at either time step n or $n+1$. This leads to the two different approach for finding the pressure that will be explained in the next session.

3.4.1 Lagging Coefficient Method

This method simplifies the calculation by assuming all coefficient terms except pressure are interpreted at time n (not $n+1$). Considering this assumption, the only unknown term in the set of flow equations is *pressure* at the next time step $(n+1)$ and the pressure solution can be obtained by any linear system solver, such as Gaussian elimination method or iterative techniques. To illustrate the method, the flow equation from the previous subsection can be re-written with lagging coefficient assumption as

Transmissibility Matrix

$$
\begin{aligned}
-\Big(T^n_{i\pm\frac{1}{2}} + T^n_{j\pm\frac{1}{2}} + T^n_{k\pm\frac{1}{2}}\Big)p^{n+1}_{i,j,k} \\
+ T^n_{i\pm\frac{1}{2}}p^{n+1}_{i\pm1} + T^n_{j\pm\frac{1}{2}}p^{n+1}_{j\pm1} + T^n_{k\pm\frac{1}{2}}p_{k\pm1} + \cdots \\
- \Big(T^n_{i\pm\frac{1}{2}}\gamma^n_{i\pm\frac{1}{2}} + T^n_{j\pm\frac{1}{2}}\gamma^n_{j\pm\frac{1}{2}} + T^n_{k\pm\frac{1}{2}}\gamma^n_{k\pm\frac{1}{2}}\Big)Z_{i,j,k} \\
+ T^n_{i\pm\frac{1}{2}}\gamma^n_{i\pm\frac{1}{2}}Z_{i\pm1} + T^n_{j\pm\frac{1}{2}}\gamma^n_{j\pm\frac{1}{2}}Z_{j\pm1} \\
+ T^n_{k\pm\frac{1}{2}}\gamma_{k\pm\frac{1}{2}}Z^n_{k\pm1} = RHS. \qquad (3.32)
\end{aligned}
$$

Accumulation Term

$$
\frac{\Big(\frac{\phi^0 c_R}{B^{n+1}_i} + \frac{\phi^n c_f}{B^0}\Big)V_i}{\Delta t}\big(p^{n+1}_i - p^n_i\big). \qquad (3.33)
$$

Sink/Source Term

$$
q = J^n_w\big(p^{n+1}_i - p_{wf}\big). \qquad (3.34)
$$

$$
(3.35)
$$

The set of equation can be formulated in matrix form as

$$
\Big[T\Big]_{N\times N}\Big[P^{n+1}_N\Big]_{N\times1} - \Big[G\Big]_{N\times1}\Big[Z\Big] = \Big[B\Big]_{N\times N}\Big[P^n\Big]_{N\times1} + \Big[Q\Big]_{N\times1} \qquad (3.36)
$$

Here, the transmissibility matrix structure is heptadiagonal (7 bands) and is depicted in figure 3.3. The accumulation matrix, on the other hand, is diagonal. One could simply check that any change in ordering may results in a changes in the transmissibility matrix.

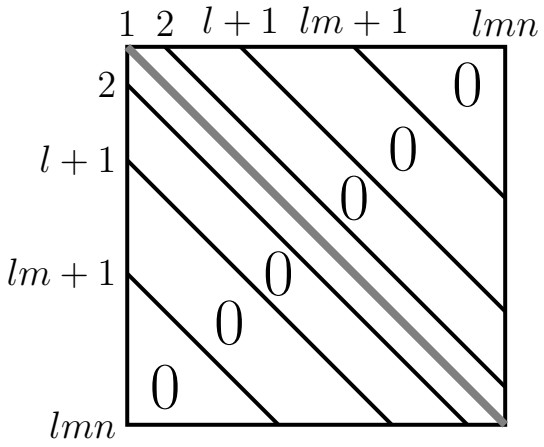

Figure 3.3: Transmissibility matrix trend for single phase flow.

3.4.2 Fully Implicit Method

This method will evaluate all terms at the $n+1$ time level, which means the system of equations become more complex and cannot be solved directly like the lagging coefficient method. After discretization, the fully implicit version of the diffusion equation 3.16 can be stated as follows

$$R(p^n, p^{n-1}, Q^n) = \mathbf{T}^n p^n - \mathbf{A}^n \left(p^n - p^{n-1}\right) - Q^n = 0. \tag{3.37}$$

wherein, $R(.)$ is the residual vector and is desired to be zero. $\mathbf{T}$ is heptagonal transmissibility matrix and $\mathbf{A}$ is a block diagonal accumulation matrix. Matrix Q denotes the sink/source terms. All of these matrices depend on p and are updated at each iteration of every time step. The equation 3.37 is in fact, a nonlinear set of algebraic equations and could be solved by applying the *Newton Raphson (NR)* iteration until the norm of residual term gets close to zero in following equation

$$J\delta = -R. \tag{3.38}$$

where, J is the Jacobian matrix defined by $J_{ij} = \partial R_i / \partial p_j$ and $\delta_i = p_i^{n,k} - p_i^{n,k-1}$ that k and $k+1$ specify NR iteration step. The eager reader may refer to [24, 8] for more details on the fully implicit method. The steps of *NR method* is summarized in algorithm 4.1 as follows

Algorithm 3.1 Fully Implicit Method, Newton Raphson Iteration

1: **Construct** *Residual* matrix $[R]$
2: **Construct** *Jacobian* matrix $[J]$
3: **Calculate** delta matrix by $[D] = [J] \ - [R]$
4: **Update** new pressure from delta matrix
5: **while** $\|R\| \leq 0.1$ **do**
6: **Recalculate** matrix $[R]$
7: **end while**

To illustrate the algorithm machinery , we write all the matrices for the 1D case. The generalization to the three dimensional case follow easily from analogy.

$$
\begin{aligned}
& T_{i-\frac{1}{2}}^{n+1}\left(p_{i-1}^{n+1} - p_i^{n+1}\right) + T_{i+\frac{1}{2}}^{n+1}\left(p_{i+1}^{n+1} - p_i^{n+1}\right) + T_{i-\frac{1}{2}}^{n+1}\gamma_{i-\frac{1}{2}}^{n+1}\left(Z_{i-1} - Z_i\right) + \cdots \\
& \quad + T_{i+\frac{1}{2}}^{n+1}\gamma_{i+\frac{1}{2}}^{n+1}\left(Z_{i+1} - Z_i\right) - \frac{\left(\frac{\phi^0 c_R}{B_i^{n+1}} + \frac{\phi^n c_f}{B^0}\right)V_i}{\Delta t}\left(p_i^{n+1} - p_i^n\right) - \cdots \\
& \quad - \frac{G_w}{B^n \mu^n}\left(p_i^{n+1} - p_{wf}\right) = 0
\end{aligned} \tag{3.39}
$$

and from the residual matrix we can compute *Jacobian* as follows:

$$\frac{\delta R_i}{\delta p_{i-1}^{n+1}} = T_{i-\frac{1}{2}}^{n+1} + \big(p_{i-1}^{n+1} - p_i^{n+1}\big)\frac{\delta T_{i-\frac{1}{2}}^{n+1}}{\delta p_{i-1}^{n+1}} + \big(Z_{i-1} - Z_i\big)\bigg(T_{i-\frac{1}{2}}^{n+1}\frac{\gamma_{i-\frac{1}{2}}^{n+1}}{\delta p_{i-1}^{n+1}} - \gamma_{i-\frac{1}{2}}^{n+1}\frac{T_{i-\frac{1}{2}}^{n+1}}{\delta p_{i-1}^{n+1}}\bigg), \tag{3.40}$$

$$\frac{\delta R_i}{\delta p_{i+1}^{n+1}} = T_{i+\frac{1}{2}}^{n+1} + \big(p_{i+1}^{n+1} - p_i^{n+1}\big)\frac{\delta T_{i+\frac{1}{2}}^{n+1}}{\delta p_{i+1}^{n+1}} + \big(Z_{i+1} - Z_i\big)\bigg(T_{i+\frac{1}{2}}^{n+1}\frac{\gamma_{i+\frac{1}{2}}^{n+1}}{\delta p_{i+1}^{n+1}} - \gamma_{i+\frac{1}{2}}^{n+1}\frac{T_{i+\frac{1}{2}}^{n+1}}{\delta p_{i+1}^{n+1}}\bigg), \tag{3.41}$$

$$\begin{aligned}\frac{\delta R_i}{\delta p_i^{n+1}} = &-T_{i-\frac{1}{2}}^{n+1} + \big(p_{i-1}^{n+1} - p_i^{n+1}\big)\frac{\delta T_{i-\frac{1}{2}}^{n+1}}{\delta p_i^{n+1}} + \big(p_{i+1}^{n+1} - p_i^{n+1}\big)\frac{\delta T_{i+\frac{1}{2}}^{n+1}}{\delta p_i^{n+1}} + \\ &- \frac{\Big(\frac{\phi^0 c_R}{B_i^{n+1}} + \frac{\phi^n c_f}{B^0}\Big)V_i}{\Delta t} - \big(p_i^{n+1} - p_i^n\big)\frac{V_i}{\Delta t}c_r\phi^0\frac{\delta\big(\frac{1}{B^{n+1}}\big)}{\delta p_i^{n+1}} - G_w/B\mu + \\ &+ \big(Z_{i-1} - Z_i\big)\bigg(T_{i-\frac{1}{2}}^{n+1}\frac{\gamma_{i-\frac{1}{2}}^{n+1}}{\delta p_i^{n+1}} - \gamma_{i-\frac{1}{2}}^{n+1}\frac{T_{i-\frac{1}{2}}^{n+1}}{\delta p_i^{n+1}}\bigg) + \\ &+ \big(Z_{i+1} - Z_i\big)\bigg(T_{i+\frac{1}{2}}^{n+1}\frac{\gamma_{i+\frac{1}{2}}^{n+1}}{\delta p_i^{n+1}} - \gamma_{i+\frac{1}{2}}^{n+1}\frac{T_{i+\frac{1}{2}}^{n+1}}{\delta p_i^{n+1}}\bigg).\end{aligned} \tag{3.42}$$

3.5 Numerical Solution to two Phase Flow System

Similarly, as we have done for the case of single-phase flow in previous subsection, we can generalize the algorithms for two-phase flow system. The general PDE equation for two-phase flow considering here, oil-water, is

$$\frac{\partial\big(\phi\rho_l S_l\big)}{\partial t} + q_l = \nabla.\Big(\frac{\rho_l k_{rl}\mathbf{k}}{\mu_l}\big(\nabla p_l - \gamma_l\nabla Z\big)\Big),\ l = o, w. \tag{3.43}$$

Where $S_o + S_w = 1$. Here, we ignore capillary pressure defined as ($P_c = P_o - P_w$). To this end, we are looking for grid's pressures and saturations of each phase as the solution in order to account for the flow dynamics into the porous media. We can transform above equation into the standard condition[8] and to get the following

equation

$$\frac{\partial}{\partial t}\Big(\frac{\phi S_l}{B_l}\Big) + \frac{q_l}{B_l} = \nabla.\Big(\frac{\rho_l K K_{rl}}{\mu_l B_l}\big(\nabla p_l - \gamma_l \nabla Z\big)\Big). \tag{3.44}$$

As pointed out before, we need to discretize this equation in space and time. First we discretize second derivatives in the left hand side using *finite difference approximation*(discretization in space) and then discretize first order time derivatives in the right hand side (discretization in time). This will be shown next.

3.5.1 Space Discretization

For one cell (block-centered method), we can discretize the following in x-direction like this

$$\begin{aligned}\frac{\partial}{\partial x}\left(\frac{\mathbf{k}k_{rl}}{\mu_l B_l}\Big(\frac{\partial p}{\partial x}\Big)\right) &= \frac{\partial}{\partial x}\left(\frac{\mathbf{k}k_{rl}}{\mu_l B_l}\frac{p_{i+\frac{1}{2},jk} - p_{i-\frac{1}{2},jk}}{\Delta x}\right)\\ &= \frac{1}{\Delta x^2}\left(\frac{\mathbf{k}k_{rl}}{\mu_l B_l}\right)_{i+\frac{1}{2},jk}\big(p_{i+1,jk} - p_{ijk}\big)\\ &+ \frac{1}{\Delta x^2}\left(\frac{\mathbf{k}k_{rl}}{\mu_l B_l}\right)_{i-\frac{1}{2},jk}\big(p_{i-1,jk} - p_{ijk}\big).\end{aligned} \tag{3.45}$$

and a similar discretization in y-dimension

$$\begin{aligned}\frac{\partial}{\partial y}\left(\frac{\mathbf{k}k_{rl}}{\mu_l B_l}\Big(\frac{\partial p}{\partial y}\Big)\right) &= \frac{\partial}{\partial y}\left(\frac{\mathbf{k}k_{rl}}{\mu_l B_l}\frac{p_{ij+\frac{1}{2}k} - p_{ij-\frac{1}{2}k}}{\Delta y}\right)\\ &= \frac{1}{\Delta y^2}\left(\frac{\mathbf{k}k_{rl}}{\mu_l B_l}\right)_{ij+\frac{1}{2}k}\big(p_{ij+1k} - p_{ijk}\big)\\ &+ \frac{1}{\Delta y^2}\left(\frac{\mathbf{k}k_{rl}}{\mu_l B_l}\right)_{ij-\frac{1}{2}k}\big(p_{ij-1k} - p_{ijk}\big).\end{aligned} \tag{3.46}$$

for z-direction gravity term came in

$$\begin{aligned}\frac{\partial}{\partial z}\left(\frac{\mathbf{k}k_{rl}}{\mu_l B_l}\left(\frac{\partial p}{\partial z}-\gamma_l \Delta Z\right)\right) &= \frac{\partial}{\partial z}\left(\frac{\mathbf{k}k_{rl}}{\mu_l B_l}\left(\frac{p_{ij,k+\frac{1}{2}}-p_{ij,k-\frac{1}{2}}}{\Delta z}-\gamma_l \Delta Z\right)\right)\\ &= \frac{1}{\Delta z^2}\left(\frac{\mathbf{k}k_{rl}}{\mu_l B_l}\right)_{ij,k+\frac{1}{2}}\left(p_{ij,k+1}-p_{ijk}\right)\\ &+ \frac{1}{\Delta y^2}\left(\frac{\mathbf{k}k_{rl}}{\mu_l B_l}\right)_{ij,k-\frac{1}{2}}\left(p_{ij,k-1}-p_{ijk}\right)\\ &- \gamma_l\left(\left(\frac{\mathbf{k}k_{rl}}{\mu_l B_l}\right)_{ij,k-\frac{1}{2}}-\left(\frac{\mathbf{k}k_{rl}}{\mu_l B_l}\right)_{ij,k-\frac{1}{2}}\right). \end{aligned} \tag{3.47}$$

3.5.2 Discretization in Time

For the left-hand side, we discretize in time to get the following for both oil and water.

water

$$\begin{aligned}\frac{\partial}{\partial t}\left(\frac{\phi S_w}{B_w}\right) &= \phi S_w \frac{\partial}{\partial t}\left(\frac{1}{B_w}\right)+\frac{S_w}{B_w}\frac{\partial \phi}{\partial t}+\frac{\phi}{B_w}\frac{\partial S_w}{\partial t}\\ &= \frac{\phi S_w}{B_w}\left(c_w+c_r\right)\frac{\partial p}{\partial t}+\frac{\phi}{B_w}\frac{\partial S_w}{\partial t}\\ &= \frac{\phi S_w}{B_w}\left(c_w+c_r\right)\frac{p_{ijk}^{n+1}-p_{ijk}^{n}}{\Delta t}+\frac{\phi}{B_w}\frac{S_{w,ijk}^{n+1}-S_{w,ijk}^{n}}{\Delta t}. \end{aligned} \tag{3.48}$$

oil

$$\begin{aligned}\frac{\partial}{\partial t}\left(\frac{\phi S_o}{B_o}\right) &= \frac{\partial}{\partial t}\left(\frac{\phi}{B_o}-\frac{\phi S_w}{B_o}\right)\\ &= \phi\frac{\partial}{\partial t}\left(\frac{1}{B_o}\right)+\frac{1}{B_o}\frac{\partial \phi}{\partial t}-\phi S_w\frac{\partial}{\partial t}\left(\frac{1}{B_o}\right)-\frac{S_w}{B_o}\frac{\partial \phi}{\partial t}-\frac{\phi}{B_o}\frac{\partial S_w}{\partial t}\\ &= \frac{\phi}{B_o}\left(c_o+c_r\right)\frac{\partial p}{\partial t}-\frac{\phi S_w}{B_o}\left(c_o+c_r\right)\frac{\partial p}{\partial t}-\frac{\phi}{B_o}\frac{\partial S_w}{\partial t}\\ &= \frac{\phi\left(1-S_w\right)}{B_o}\left(c_o+c_r\right)\frac{p_{ijk}^{n+1}-p_{ijk}^{n}}{\Delta t}-\frac{\phi}{B_o}\frac{S_{w,ijk}^{n+1}-S_{w,ijk}^{n}}{\Delta t}. \end{aligned} \tag{3.49}$$

Based on volume integration within the cell, $\Delta V = \Delta x \Delta y \Delta z$, we arrive at the following for water and oil.

water

$$\begin{aligned}
&\frac{\phi S_w \Delta V}{B_w}\big(c_w + c_r\big)\frac{p_{ijk}^{n+1} - p_{ijk}^{n}}{\Delta t} + \frac{\phi \Delta V}{B_w}\frac{S_{w,ijk}^{n+1} - S_{w,ijk}^{n}}{\Delta t} \\
&\qquad = \frac{\Delta y \Delta z}{\Delta x}\left(\frac{\mathbf{k}k_{rw}}{\mu_w B_w}\right)_{i\pm\frac{1}{2}jk}\big(p_{i\pm1jk} - p_{ijk}\big) \\
&\qquad + \frac{\Delta x \Delta z}{\Delta y}\left(\frac{\mathbf{k}k_{rw}}{\mu_w B_w}\right)_{ij\pm\frac{1}{2}k}\big(p_{ij\pm1k} - p_{ijk}\big) \\
&\qquad + \frac{\Delta x \Delta y}{\Delta z}\left(\frac{\mathbf{k}k_{rw}}{\mu_w B_w}\right)_{ijk\pm\frac{1}{2}}\big(p_{ijk\pm1} - p_{ijk}\big) \\
&\qquad - \gamma_w \Delta x \Delta y\left(\left(\frac{\mathbf{k}k_{rw}}{\mu_w B_w}\right)_{ijk+\frac{1}{2}} - \left(\frac{\mathbf{k}k_{rw}}{\mu_w B_w}\right)_{ijk-\frac{1}{2}}\right) - \frac{q_w}{B_w}.
\end{aligned} \tag{3.50}$$

oil

$$\begin{aligned}
&\frac{\phi\big(1 - S_w\big)\Delta V}{B_o}\big(c_o + c_r\big)\frac{p_{ijk}^{n+1} - p_{ijk}^{n}}{\Delta t} - \frac{\phi \Delta V}{B_o}\frac{S_{w,ijk}^{n+1} - S_{w,ijk}^{n}}{\Delta t} \\
&\qquad = \frac{\Delta y \Delta z}{\Delta x}\left(\frac{\mathbf{k}k_{ro}}{\mu_o B_o}\right)_{i\pm\frac{1}{2}jk}\big(p_{i\pm1jk} - p_{ijk}\big) \\
&\qquad + \frac{\Delta x \Delta z}{\Delta y}\left(\frac{\mathbf{k}k_{ro}}{\mu_o B_o}\right)_{ij\pm\frac{1}{2}k}\big(p_{ij\pm1k} - p_{ijk}\big) \\
&\qquad + \frac{\Delta x \Delta y}{\Delta z}\left(\frac{\mathbf{k}k_{ro}}{\mu_o B_o}\right)_{ijk\pm\frac{1}{2}}\big(p_{ijk\pm1} - p_{ijk}\big) \\
&\qquad - \gamma_o \Delta x \Delta y\left(\left(\frac{\mathbf{k}k_{ro}}{\mu_o B_o}\right)_{ijk+\frac{1}{2}} - \left(\frac{\mathbf{k}k_{ro}}{\mu_o B_o}\right)_{ijk-\frac{1}{2}}\right) - \frac{q_o}{B_o}.
\end{aligned} \tag{3.51}$$

Now if we define the transmissibility as follows

$$T_{l,i+\frac{1}{2}jk} = \frac{\Delta y \Delta z}{\Delta x}\left(\frac{\mathbf{k}k_{rl}}{\mu_l B_l}\right)_{i+\frac{1}{2}jk} = \frac{2\Delta y \Delta z}{\Delta x}\frac{\mathbf{k}_{i+\frac{1}{2}jk}k_{ijk}}{\mathbf{k}_{i+\frac{1}{2}jk} + k_{ijk}}\left(\frac{k_{rl}}{\mu_l B_l}\right)_{i+\frac{1}{2}jk}. \tag{3.52}$$

and according to Peaceman Equation, we have

$$q_l = WI\big(P_{ijk} - P_{wf}\big) = \frac{2\pi \mathbf{k} k_{rl,ijk}\Delta z}{\mu_l\big(\ln\frac{r_o}{r_w} + s\big)}\big(P_{ijk} - P_{wf}\big). \tag{3.53}$$

where $r_o = 0.14\sqrt{\Delta x^2 + \Delta y^2}$. Therefore, the flow equation becomes

water

$$\begin{aligned}
&\left(\frac{\phi S_w \Delta V}{B_w \Delta t}\big(c_w + c_r\big) + T_{w,i\pm\frac{1}{2}} + T_{w,j\pm\frac{1}{2}} + T_{w,k\pm\frac{1}{2}} + \frac{WI_w}{B_w}\right)p_{ijk}^{n+1} + \\
&\qquad + \frac{\phi\Delta V}{B_w\Delta t}S_{w,ijk}^{n+1} - T_{w,i\pm\frac{1}{2}}p_{i+1}^{n+1} - T_{w,j\pm\frac{1}{2}}p_{j+1}^{n+1} - T_{w,k\pm\frac{1}{2}}p_{k+1} \\
&\qquad = \frac{WI_w}{B_w}p_{wf} - \gamma_w\Delta x\Delta y\left(\Big(\frac{\mathbf{k}k_{rw}}{\mu_w B_w}\Big)_{k+\frac{1}{2}} - \Big(\frac{\mathbf{k}k_{rw}}{\mu_w B_w}\Big)_{k-\frac{1}{2}}\right) + \\
&\qquad + \frac{\phi S_w\Delta V}{B_w\Delta t}\big(c_w + c_r\big)p_{ijk}^{n} + \frac{\phi\Delta V}{B_w\Delta t}S_{w,ijk}^{n}.
\end{aligned} \tag{3.54}$$

oil

$$\begin{aligned}
&\left(\frac{\phi\big(1 - S_w\big)\Delta V}{B_o\Delta t}\big(c_o + c_r\big) + T_{o,i\pm\frac{1}{2}} + T_{o,j\pm\frac{1}{2}} + T_{o,k\pm\frac{1}{2}} + \frac{WI_o}{B_o}\right)p_{ijk}^{n+1} \\
&\qquad + \frac{\phi\Delta V}{B_o\Delta t}S_{w,ijk}^{n+1} - T_{o,i\pm\frac{1}{2}}p_{i+1}^{n+1} - T_{o,j\pm\frac{1}{2}}p_{j+1}^{n+1} - T_{o,k\pm\frac{1}{2}}p_{k+1} \\
&\qquad = \frac{WI_o}{B_o}p_{wf} - \gamma_o\Delta x\Delta y\left(\Big(\frac{\mathbf{k}k_{ro}}{\mu_o B_o}\Big)_{k+\frac{1}{2}} - \Big(\frac{\mathbf{k}k_{ro}}{\mu_o B_o}\Big)_{k-\frac{1}{2}}\right) \\
&\qquad + \frac{\phi S_w\Delta V}{B_o\Delta t}\big(c_o + c_r\big)p_{ijk}^{n} + \frac{\phi\Delta V}{B_o\Delta t}S_{w,ijk}^{n}.
\end{aligned} \tag{3.55}$$

3.5.3 Lagging Coefficient Method

Similarly to the single-phase flow system, this method simplifies the calculation by assuming all coefficient terms except pressures and saturations are interpreted at time n (not $n+1$). Considering this assumption, the only unknown term in set of flow equation is *pressure* and *saturation* at the next time step $(n+1)$ and the

pressure solution can be obtained using preconditioned PCG, GMRES or preconditioned BiCGSTAB. To illustrate the method, the flow equation from the previous subsection can be re-written with lagging coefficient assumption as

water

$$\begin{aligned}\left(\frac{\phi^n {S_w}^n \Delta V}{{B_w}^n \Delta t}\left(c_w + c_r\right) + T^n_{w,i\pm\frac{1}{2}} + T^n_{w,j\pm\frac{1}{2}} + T^n_{w,k\pm\frac{1}{2}} + \frac{{WI_w}^n}{{B_w}^n}\right) p^{n+1}_{ijk} \\ + \frac{\phi^n \Delta V}{{B_w}^n \Delta t} S^{n+1}_{w,ijk} - T^n_{w,i\pm\frac{1}{2}} p^{n+1}_{i+1} - T^n_{w,j\pm\frac{1}{2}} p^{n+1}_{j+1} - T^n_{w,k\pm\frac{1}{2}} p_{k+1} \\ = \frac{{WI_w}^n}{{B_w}^n} p_{wf} - \gamma_w \Delta x \Delta y \left(\left(\frac{\mathbf{k} k^n_{rw}}{\mu^n_w {B_w}^n}\right)_{k+\frac{1}{2}} - \left(\frac{\mathbf{k} k^n_{rw}}{\mu^n_w {B_w}^n}\right)_{k-\frac{1}{2}} \right) \\ + \frac{\phi^n S_w \Delta V}{{B_w}^n \Delta t}\left(c_w + c_r\right) p^n_{ijk} + \frac{\phi^n \Delta V}{{B_w}^n \Delta t} S^n_{w,ijk}. \end{aligned} \tag{3.56}$$

oil

$$\begin{aligned}\left(\frac{\phi^n \left(1 - S^n_w\right) \Delta V}{B^n_o \Delta t}\left(c_o + c_r\right) + T^n_{o,i\pm\frac{1}{2}} + T^n_{o,j\pm\frac{1}{2}} + T^n_{o,k\pm\frac{1}{2}} + \frac{WI^n_o}{B^n_o}\right) p^{n+1}_{ijk} \\ + \frac{\phi^n \Delta V}{B^n_o \Delta t} S^{n+1}_{w,ijk} - T^n_{o,i\pm\frac{1}{2}} p^{n+1}_{i+1} - T^n_{o,j\pm\frac{1}{2}} p^{n+1}_{j+1} - T^n_{o,k\pm\frac{1}{2}} p_{k+1} \\ = \frac{WI^n_o}{B^n_o} p_{wf} - \gamma_o \Delta x \Delta y \left(\left(\frac{\mathbf{k} k^n_{ro}}{\mu^n_o B^n_o}\right)_{k+\frac{1}{2}} - \left(\frac{\mathbf{k} k^n_{ro}}{\mu^n_o B^n_o}\right)_{k-\frac{1}{2}} \right) \\ + \frac{\phi^n S^n_w \Delta V}{B^n_o \Delta t}\left(c_o + c_r\right) p^n_{ijk} + \frac{\phi^n \Delta V}{B^n_o \Delta t} S^n_{w,ijk}. \end{aligned} \tag{3.57}$$

3.5.4 Fully Implicit Method

Similarly to the single-phase case, this method evaluates all terms at $n+1$ time level which means the system of equations become more complex and cannot be solved directly like the lagging coefficient method.

water

$$
\begin{aligned}
R_w(p^{n+1}, S_w^{n+1}) = \\
&\left(\frac{\phi^{n+1} {S_w}^{n+1} \Delta V}{{B_w}^{n+1} \Delta t}\big(c_w + c_r\big) + T^{n+1}_{w,i\pm\frac{1}{2}} + T^{n+1}_{w,j\pm\frac{1}{2}} + T^{n+1}_{w,k\pm\frac{1}{2}} + \frac{{WI_w}^{n+1}}{{B_w}^{n+1}}\right) p^{n+1}_{ijk} \\
&+ \frac{\phi^{n+1}\Delta V}{{B_w}^{n+1}\Delta t} S^{n+1}_{w,ijk} - T^{n+1}_{w,i\pm\frac{1}{2}} p^{n+1}_{i+1} - T^{n+1}_{w,j\pm\frac{1}{2}} p^{n+1}_{j+1} - T^{n+1}_{w,k\pm\frac{1}{2}} p_{k-1} \\
&- \frac{{WI_w}^{n+1}}{{B_w}^{n+1}} p_{wf} + \gamma_w \Delta x \Delta y \left(\left(\frac{\mathbf{k} k^{n+1}_{rw}}{\mu_w^{n+1} {B_w}^{n+1}} \right)_{k+\frac{1}{2}} - \left(\frac{\mathbf{k} k^{n+1}_{rw}}{\mu_w^{n+1} {B_w}^{n+1}} \right)_{k-\frac{1}{2}} \right) \\
&- \frac{\phi^{n+1} S_w^{n+1} \Delta V}{{B_w}^{n+1}\Delta t}\big(c_w + c_r\big) p^n_{ijk} - \frac{\phi^{n+1}\Delta V}{{B_w}^{n+1}\Delta t} S^n_{w,ijk}.
\end{aligned} \tag{3.58}
$$

oil

$$
\begin{aligned}
R_o(p^{n+1}, S_w^{n+1}) = \\
&\left(\frac{\phi^{n+1}\big(1 - S_w^{n+1}\big)\Delta V}{B_o^{n+1}\Delta t}\big(c_o + c_r\big) + T^{n+1}_{o,i\pm\frac{1}{2}} + T^{n+1}_{o,j\pm\frac{1}{2}} + T^{n+1}_{o,k\pm\frac{1}{2}} + \frac{WI_o^{n+1}}{B_o^{n+1}}\right) p^{n+1}_{ijk} \\
&+ \frac{\phi^{n+1}\Delta V}{B_o^{n+1}\Delta t} S^{n+1}_{w,ijk} - T^{n+1}_{o,i\pm\frac{1}{2}} p^{n+1}_{i+1} - T^{n+1}_{o,j\pm\frac{1}{2}} p^{n+1}_{j+1} - T^{n+1}_{o,k\pm\frac{1}{2}} p_{k-1} \\
&- \frac{WI_o^{n+1}}{B_o^{n+1}} p_{wf} + \gamma_o \Delta x \Delta y \left(\left(\frac{\mathbf{k} k^{n+1}_{ro}}{\mu_o^{n+1} B_o^{n+1}} \right)_{k+\frac{1}{2}} - \left(\frac{\mathbf{k} k^{n+1}_{ro}}{\mu_o^{n+1} B_o^{n+1}} \right)_{k-\frac{1}{2}} \right) \\
&- \frac{\phi^{n+1} S_w^{n+1} \Delta V}{B_o^{n+1}\Delta t}\big(c_o + c_r\big) p^n_{ijk} - \frac{\phi^{n+1}\Delta V}{B_o^{n+1}\Delta t} S^n_{w,ijk}.
\end{aligned} \tag{3.59}
$$

Similarly to the single-phase case, we can write residual vector as follows

$$
R = \big[R_o^T, R_w^T\big]^T. \tag{3.60}
$$

thus the Jacobian is as follows

$$
J = \frac{\partial R}{\partial x} = \begin{bmatrix} \frac{\partial R_o}{\partial p_o} & \frac{\partial R_o}{\partial S_w} \\ \frac{\partial R_w}{\partial p_o} & \frac{\partial R_w}{\partial S_w} \end{bmatrix}. \tag{3.61}
$$

wherein, x is system state vector and is defined as $x = \left(p_o^T, S_w^T\right)^T$. Algorithm 4.2 summarizes the formulation and procedure for two phase flow equation problem.

Algorithm 3.2 Fully Implicit Method, Newton Raphson Iteration–Two Phase

1: **Construct** *Residual* vector $[R]$
2: **Construct** *Jacobian* matrix $[J]$
3: **Solve** $R = -J\delta$ ▷ using preconditioned PCG, GMRES or BiCGSTAB
4: **Update** new pressure from delta matrix
5: **while** $\|R\| \leq 0.1$ **do**
6: **Recalculate** matrix $[R]$
7: **end while**

3.6 Two Phase Flow Reservoir Simulation Example

In this subsection, we provide a simple two phase flow reservoir simulation example to show the performance of our in-house reservoir simulator. Considering the two dimensional (2D) two-phase flow of slightly compressible oil reservoir as depicted in figure 3.4, the reservoir consists of 15×15 grid blocks. The permeability distributions for a 2D model is shown in figure 3.5. We assume an isotropic heterogeneous permeability distribution, i.e., $K_x = K_y = K_z$. There is one producer which is in operation with a constant bottom-hole pressure (BHP) of 2900 psi and one water injector which has a constant rate of injection of $300 bbl/day$. The producer is located at grid block (15,15) and the injector is at $(1, 1)$. The well radius is 0.35 ft. Oil viscosity curve is shown in figure 3.6. The reservoir properties are given in the table 3.1.

The following figures are a set of outputs of the developed reservoir simulator, and consists of reservoir pressure and water saturation distributions (maps) in the reservoir. These, basically are the reservoir responses to the input in a water flood-

ing scenario. This information help us to understand better the performance of a reservoir and more importantly, to predict the future production of a particular development scenario. Furthermore, employing such a reservoir simulator could help to optimize and to implement any production and reservoir management plan by minimizing the project costs and maximizing oil and/or gas production. It also, improves the oil recovery enhancement plans which maximize the oil production and increase the life of a given reservoir.

Pressure and water saturation distribution maps are shown in figures 3.7 and 3.8, respectively. Water saturation distribution map implies how the saturation of water change from injector grid to producer gridblock in the course of the waterflooding period, which is 365 days in this case. Pressure distribution map shows how the pressure of a grid block changes during the simulation and also provide pressure trends from injector grid to producing well. Oil production rate and total oil production during the course of simulation are depicted in figures 3.9 and 3.10, respectively. Once a producing well starts to produce water, this is known as breakthrough. It is obvious from theses figures that at the beginning of the simulation, oil production rates increases until it reach its maximum at 300 bbl/day and stay constant until breakthrough happens; after, pressure decreases until reservoir depletes. Depletion happens due to drop in average reservoir pressure as a result of oil production. Figures 3.11 and 3.12 show water production rate and total water production curves. In fact, these curves indicate breakthrough time and the amount of produced water during the simulation. Figure 3.13 present the water cut curve which is the ratio of produced water to the total amount of produced fluids in a producing well. Finally, figure 3.14 shows injector bottomhole pressure curve. Bottomhole pressure is the pressure at the downhole that water can be injected into the reservoir. Having lower bottomhole pressure is of high interest in industry due to the design of surface

equipment.

From the numerical experiments, it can be seen that changing time step results in getting different errors which means the larger time step results in the more difference between lagging coefficient and fully implicit. The lagging coefficient method's performance seems to become worse than fully implicit at larger time steps(see Figs. 3.15 and 3.16). This is because of the assumption of evaluating properties at previous time step $n-1$. Therefore, for larger time steps, the old properties have to be used for a longer time comparing to smaller time steps. However, this difference is not clearly shown in the visualization by pressure map. Also, from the figures one could see that wherever (in each grid block) the permeability is low the pressure map stays high.

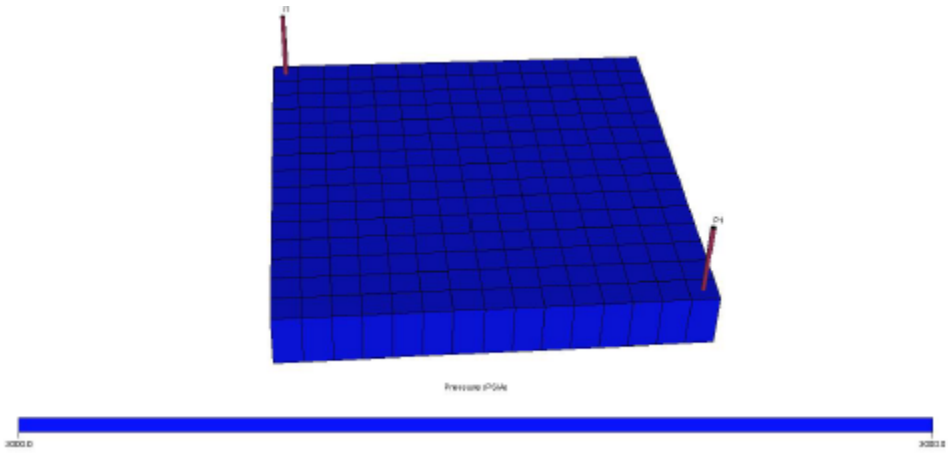

Figure 3.4: Reservoir configuration in two phase reservoir simulation example. The injector is in $(1,1)$ grid block and the producing well is placed at $(15,15)$ grid block.

Table 3.1: Reservoir and fluid properties.

Property		Quantity	Unit
Model Properties	Simulation	Two-phase oil and water	N/A
	Simulation Time	6×360	day
	Grid blocks	15×15	ft
	Grid block size	10×10	ft
	Reservoir depth	4000	ft
	Porosity	0.2	md
	Rock compressibility	$3.0E-6$	psi^{-1}
	Reservoir geometry	2D	N/A
	Number of injectors	1	N/A
	Number of producers	1	N/A
Oil Properties	Viscosity	Figure 3.6	cp
	Compressibility	$3.0E-6$	psi^{-1}
	Oil density	62.4	$\frac{lb}{ft^3}$
Water Properties	Viscosity	1	cp
	Compressibility	$3.0E-6$	psi^{-1}
	Water density	62.4	$\frac{lb}{ft^3}$
Initial Conditions	Pressure	3000	psi
	Water saturation	0.2	N/A

3.7 Model Reduction Method

In this subsection, we briefly introduce the concept of model reduction and parameterization applied to the reservoir simulation problem. By proper selection of input (control) and outputs (measurements), the two-phase flow equations can be recast into a large (e.g., millions of state variables) nonlinear dynamical system given

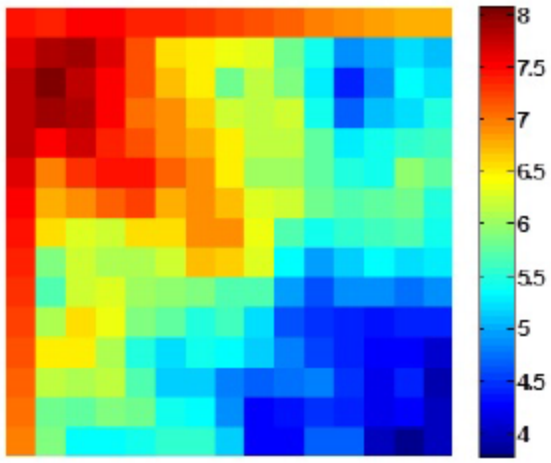

Figure 3.5: Permeability distribution map (configuration) in two-phase reservoir simulation example. For this example we utilize a heterogeneous permeability distribution generated by SGSIM.

by

$$\begin{cases} \mathbf{F}\left(\dot{\mathbf{x}}(t), \mathbf{x}(t), \mathbf{u}(t)\right) = \mathbf{0} \\ \mathbf{y}(t) = (\mathbf{H}(\mathbf{x}(t), \mathbf{u}(t)) \end{cases} \tag{3.62}$$

where $\mathbf{F}$ is called the state equation, $\mathbf{H}$ the output equation, $\mathbf{x}$ is a n-dimensional state vector, $\mathbf{u}$ is a b-dimensional input (or control) vector, $\mathbf{y}$ in a p-dimensional output (or measurements) vector, and t represents the time span. In this case, the control variables and measurements are usually flow rates and bottom-hole pressures at particular wells. In order to reduce the number of variables and parameters, one can apply model reduction techniques to 3.62. In this work, projection techniques will be used [5]. The idea is to construct the projector $\mathbf{P} = \mathbf{V}\mathbf{W}^T$ where $\mathbf{V}, \mathbf{W}^T \in \mathbb{R}^{n \times r}$ with $\mathbf{W^T V} = \mathbf{I_r}$, such that the reduced-order model can be obtained by projecting the state-space equations into a much smaller subspace by

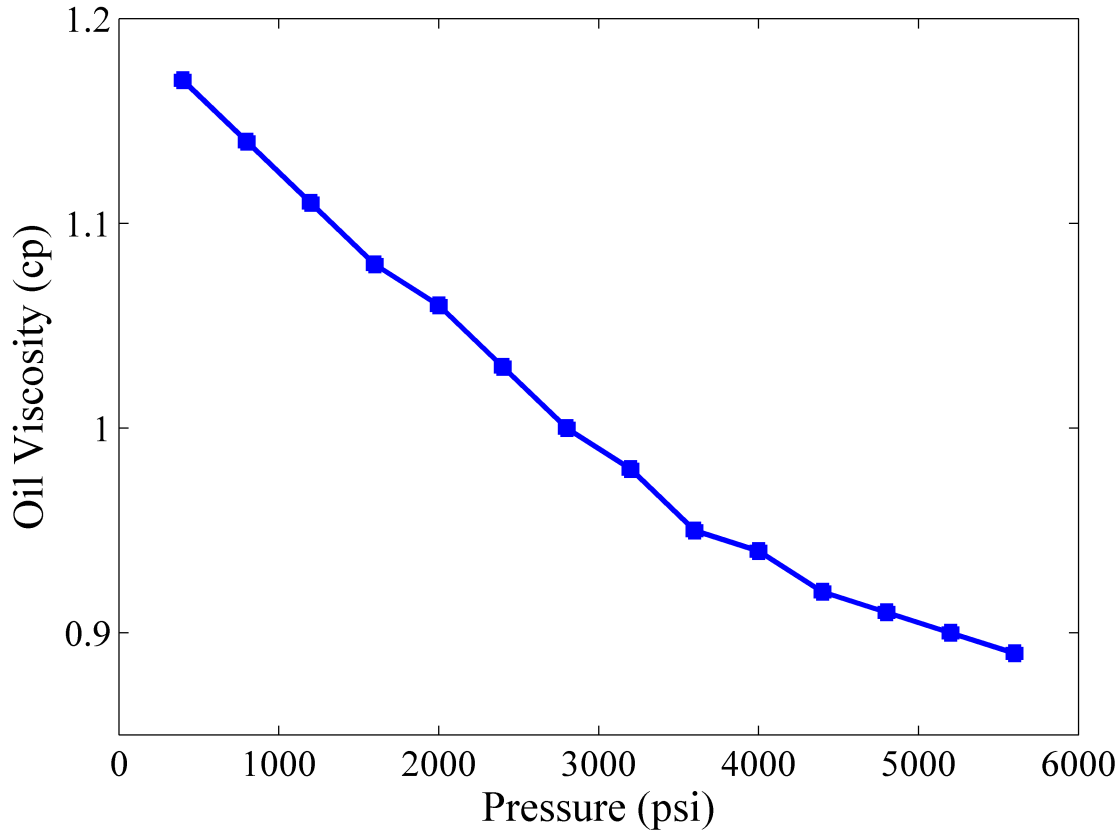

Figure 3.6: Oil viscosity curve against pressure for the two-phase reservoir simulation example.

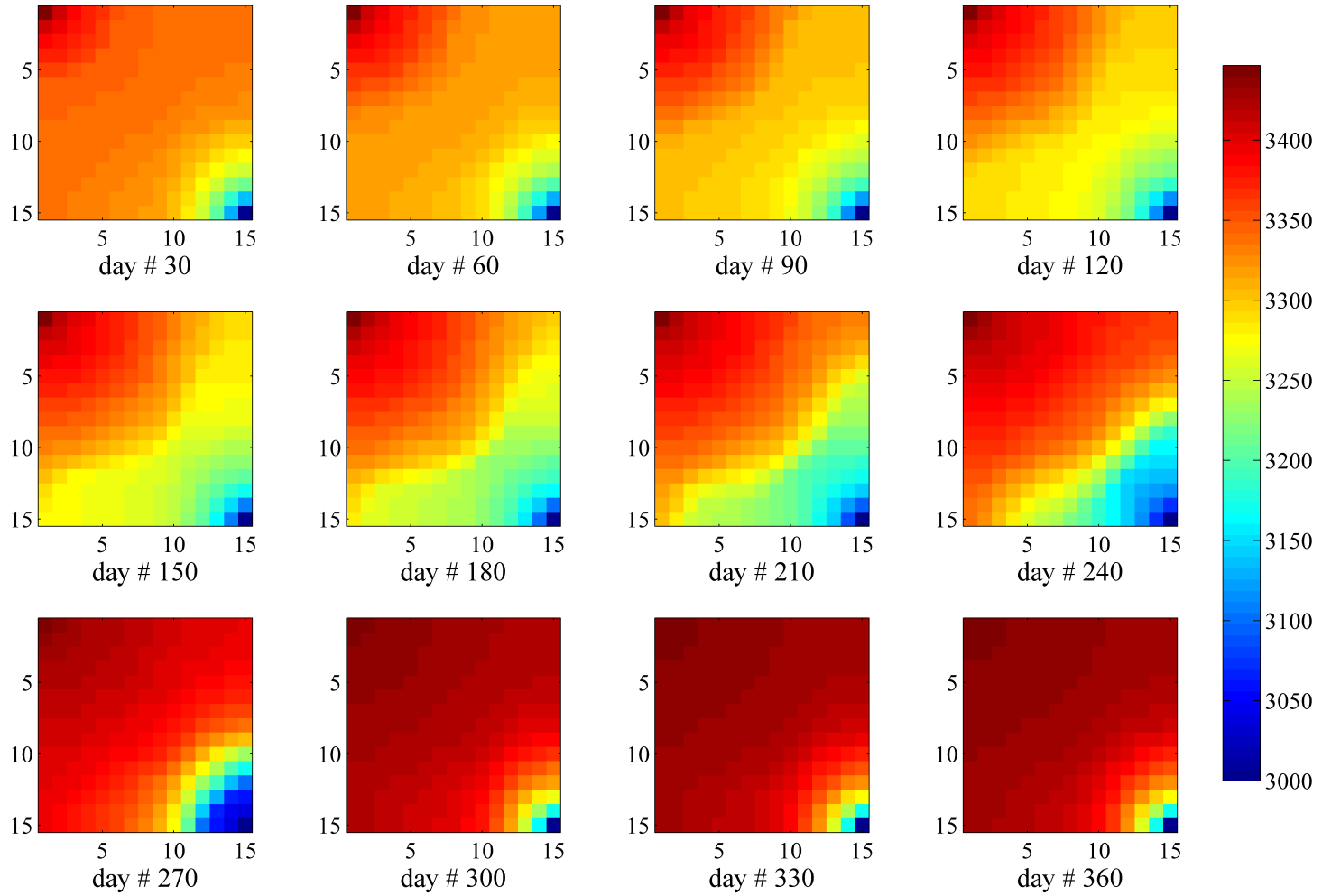

Figure 3.7: Oil pressure distributions at different time steps for synthetic two-phase reservoir simulation example.

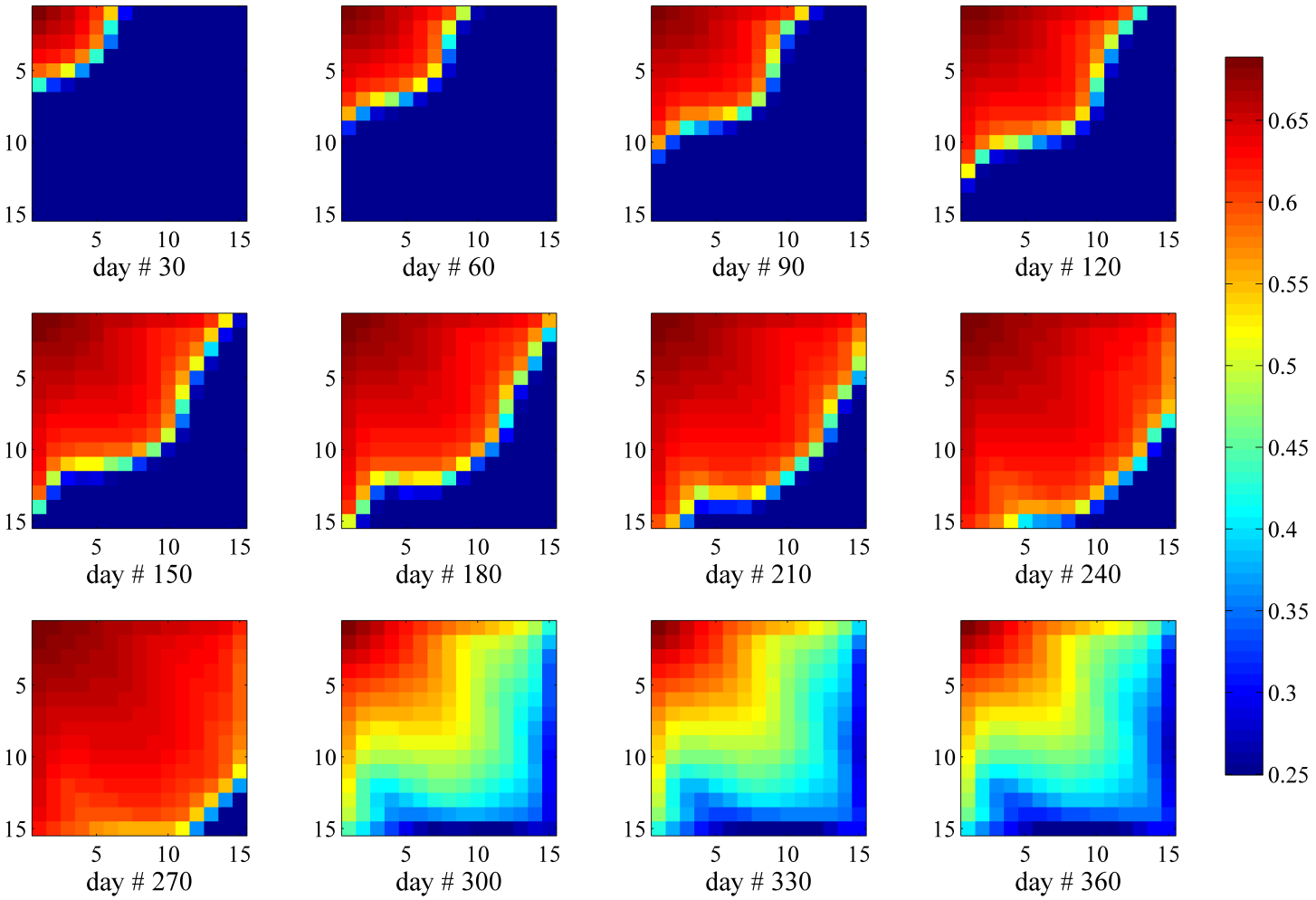

Figure 3.8: Water saturation distributions at different time steps for synthetic two-phase reservoir simulation example.

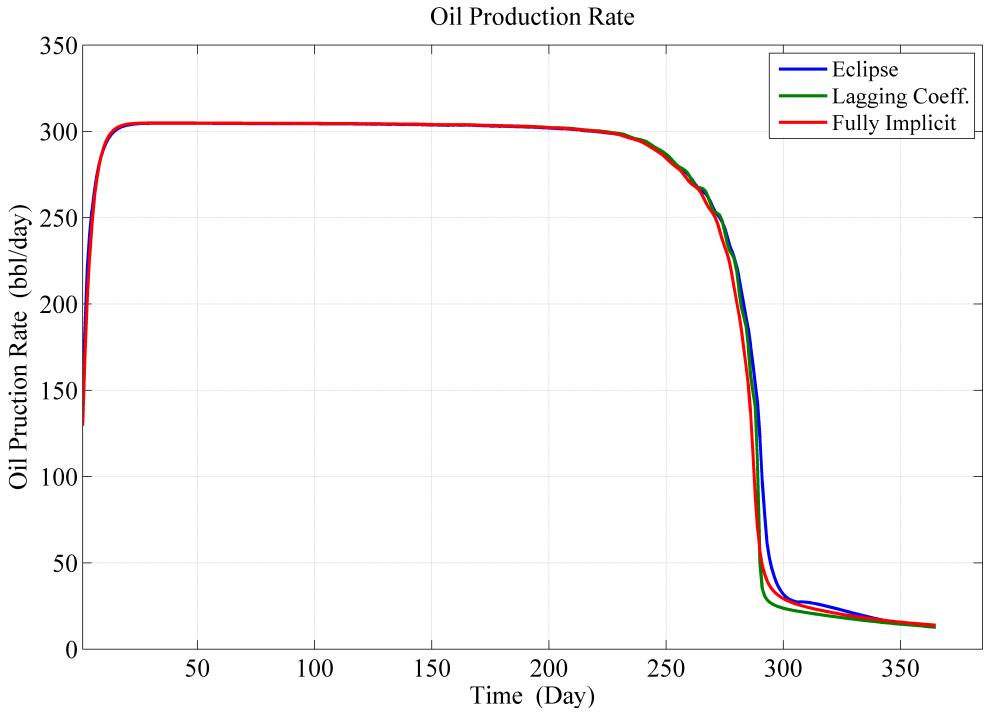

Figure 3.9: Oil production rates. Comparison between the results of lagging coefficient, fully implicit and ECLIPSE.

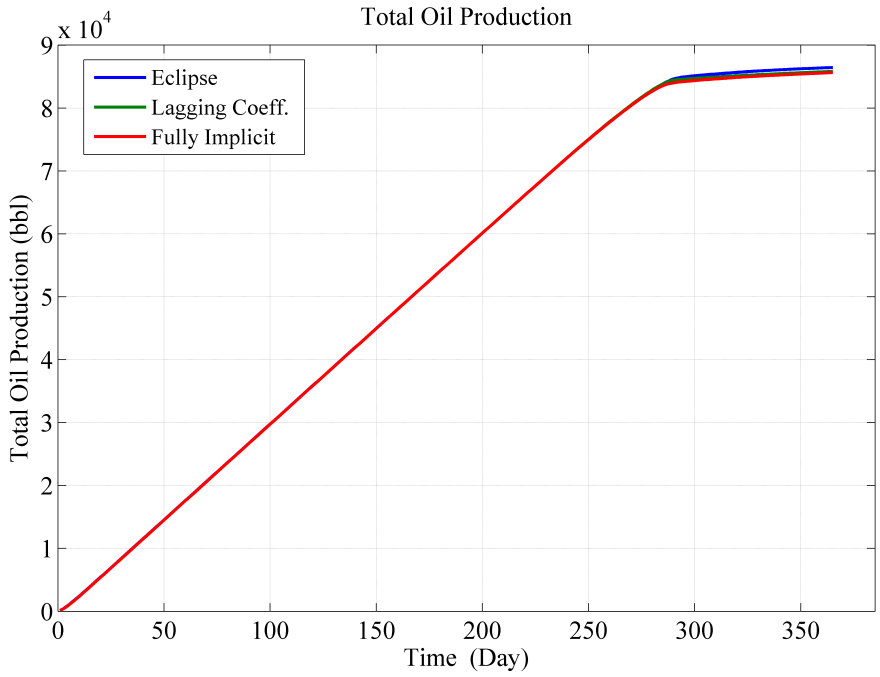

Figure 3.10: Total oil production rates. Comparison between the results of lagging coefficient, fully implicit and ECLIPSE.

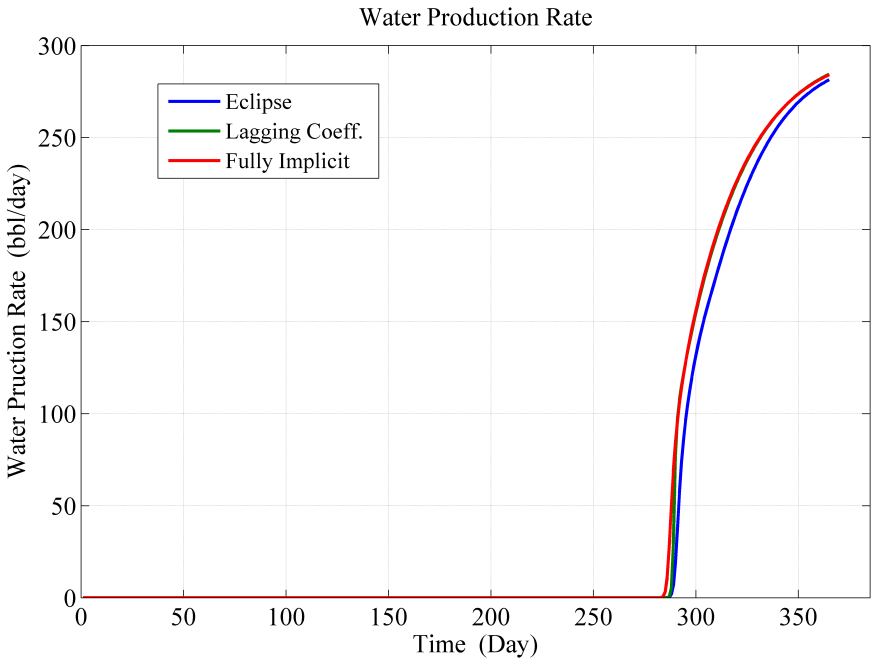

Figure 3.11: Water production rates. Comparison between the results of lagging coefficient, fully implicit and ECLIPSE.

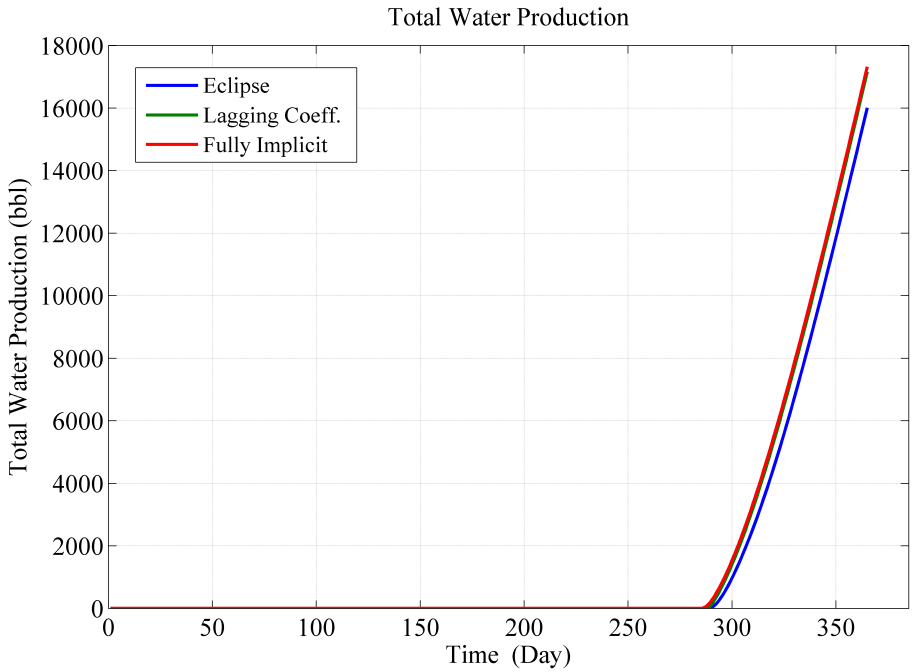

Figure 3.12: Total water production rates. Comparison between the results of lagging coefficient, fully implicit and ECLIPSE.

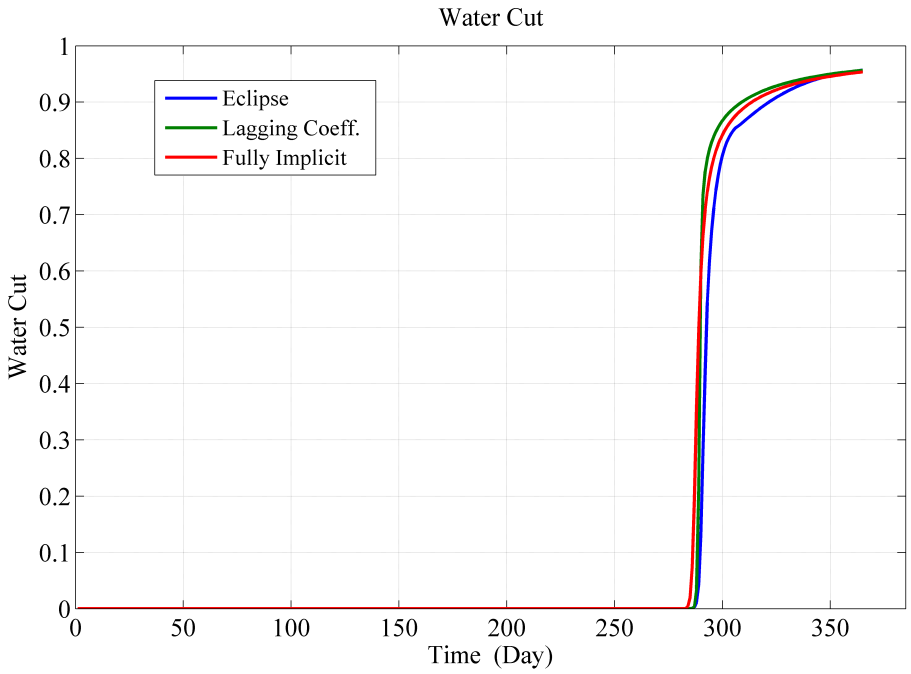

Figure 3.13: Water cut curves. Comparison between the results of lagging coefficient, fully implicit and ECLIPSE.

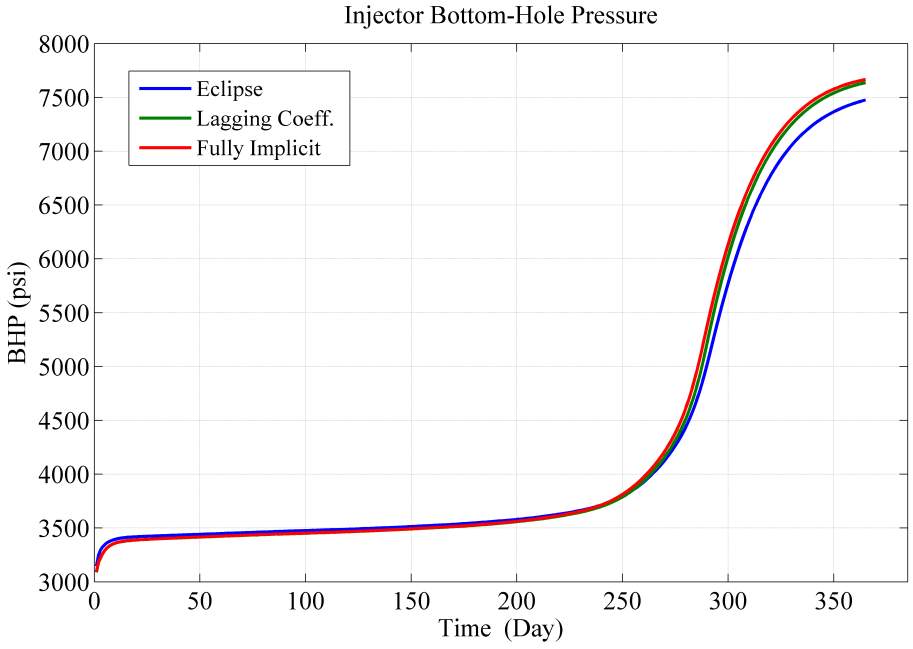

Figure 3.14: Injection Bottomhole pressure (BHP) curves. Comparison between the results of lagging coefficient, fully implicit and ECLIPSE.

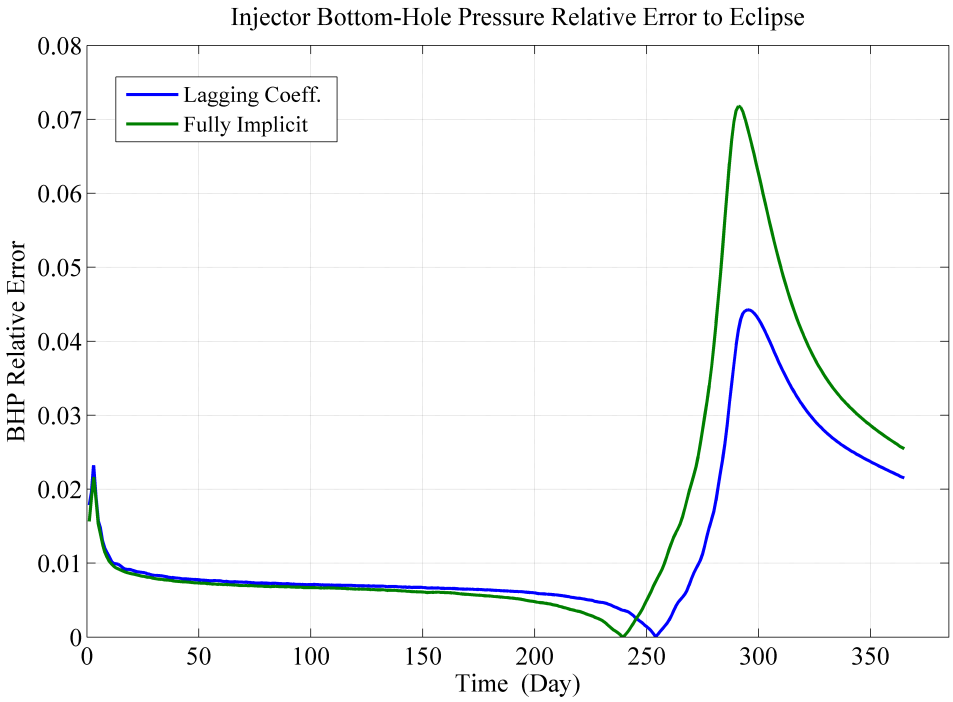

Figure 3.15: Fully implicit and lagging coefficient methods relative error to ECLIPSE curves for BHP in synthetic two-phase reservoir simulation example.

$$\begin{cases} \dot{\mathbf{x}}_r(t) = \mathbf{W}^T \mathbf{F}_r\left(\mathbf{V}\mathbf{x}_r(t), \mathbf{u}(t)\right) \\ \mathbf{y}(t) = \mathbf{H}_r\left(\mathbf{V}\mathbf{x}_r(t), \mathbf{u}(t)\right) \end{cases} \tag{3.63}$$

where $\mathbf{x}_r \in \mathbb{R}^{r\times 1}$. The methodologies in the projection model reduction differ on how one obtains the projection matrices. Some methods can deal with the nonlinear system, whereas some can be used directly with the linearized model [5]. One may also think of projection method, e.g., proper orthogonal decomposition (POD) or principal component analysis (PCA) [132, 7], for a particular large-scale parameter. In this case, one can project for instance the permeability field into a much smaller subspace in a process called parameterization [118]. Model reduction is of highly interest in many science and engineering fields where the order of original system is

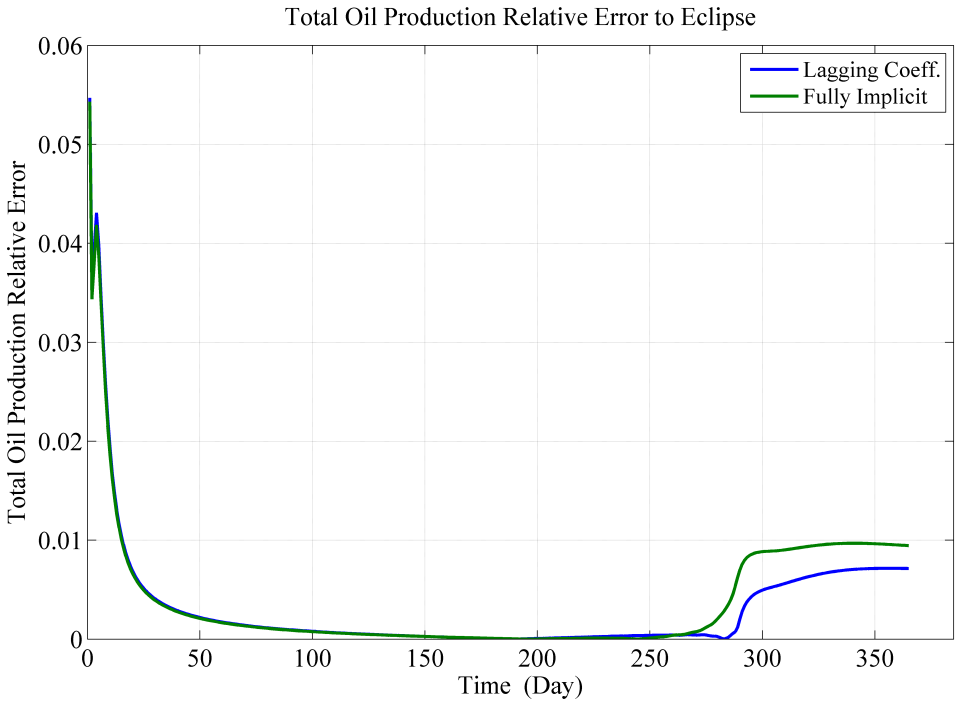

Figure 3.16: Fully implicit and lagging coefficient methods relative error to ECLIPSE curves for total oil production in synthetic two-phase reservoir simulation example.

such high that makes it difficult to work with. In fact, model reduction or parameterization defined as reducing the dimensionality of original model to a lower one to make a costly efficient model. In addition, in all history matching problem, in order to reduce the ill-posedness of the problem, it is necessary to de-correlate the parameters. Proper orthogonal decomposition (POD) as an optimal transformation is widely used in parameterization. To obtain the bases for POD, it is necessary to vectorize the original replicates. Therefore, the higher order statistical information is lost due to slicing the replicates. Another approach that deals with the replicates as they are, is high order singular value decomposition (HOSVD).

3.8 Parameterization

Parameterization techniques have been studied in subsurface modeling since the 1960's in the form of zonation. In a broad sense, parameterization can be divided into two main groups: spatial and transform domain [75]. In the spatial case, one aims at identifying spatial regions (zones) that can be thought as homogeneous pieces of the subsurface, and this can be assigned a single constant property during the inversion process. Although it seems logic to find such zones, problems with geologic discontinuities at the boundary of such regions make the implementation difficult. On the other hand, transform domain methods, can overcome these issues by means of introducing geological spatial correlations into the parameterization process. Several techniques have been developed in recent years [75], including the classical principal component analysis (PCA/SVD), discrete cosine transform (DCT), and the discrete wavelet transform (DWT methods. In all of these cases, the objective is to find an *optimal* basis selection that can explain the main variability in the parameter fields in a pre-defined norm. In this dissertation, we will address some of the shortcomings of the PCA approach.

In the parameterization by PCA/SVD case, one writes the system parameters in terms of smaller number of parameters using the SVD operator. One of the main drawbacks of the SVD framework is the fact that both states and the geological parameters need to be vectorized for the computations of what is known as *the snapshot matrix*. This, in turn, leads to the loss of geological continuity when the parameters are reconstructed for the reservoir model simulation. We will address this issue by extending the projection framework using HOSVD techniques [2, 65], defined in the next subsection.

As we discussed before, in order to optimize reservoir production and to provide

an accurate future production prediction, we need to build a fine detailed reservoir model. Having such a fine reservoir model results in a nonlinear, complex, and large-scale system. Solving such a large-scale inverse problem, e.g., history matching, requires a very expensive computational cost. In addition to computational cost, we note that the efficiency of the solution to the history match problem can be bounded due to numerical instabilities in solution algorithms. A common approach to coup with instability and non-uniqueness concerns corresponding to the solution of reservoir characterization is parameterization. The central idea of parameterization methods is to reduce the number of unknown model parameters, such as permeability or porosity, and to pose the inverse problem in a proper formulation by estimating a less number of unknown model parameters [73, 78, 78, 100, 28, 48, 62, 111, 49]. In other words, field parameters uncertainty can be modeled through two-point geostatistics by fewer parameters utilizing parameterization [118]. The main point with the parameterization method like HOSVD is that its parameters can be tuned continuously so that the desired underlying geostatistical explanation acquired. This also can preserve geological realism to some extent while employing adjoint methods for history matching. Adjoint method is very common approach in solving inverse problems such as history matching and has been first introduced by Chen et al. [33] and Chavent et al. [31] for single-phase problems. A number of research studies have been directed since then, to develop the adjoint models application in inverse problem for multi-phase reservoir problems such as Datta-Gupta [134], Zhang et al. [135] and Reynolds et al. [111].

Efficient parameterization while solving a history matching problem allows us to avoid geostatistical inconsistency in reservoir model parameters specially when we employ gradient-based techniques to solve inverse problems. As a matter of fact, field parameters space such as permeability and porosity are of higher order

dimensionality with highly correlated parameters. Parameterization methods such as HOSVD generate a map from this high dimensional and highly correlated space to a uncorrelated space of lower rank. Therefore, any combination of parameters of the new space produce a permeability field that acquires the underlying two-point geostatistics. Moreover, these new parameters can be adjusted until a perfect production match has been reached [118, 135].

Considering the Bayesian inverse modeling, the solution to the history match problem can be established by integrating prior knowledge obtained from the reservoir measurement data prior probability density function, $f_\Theta(\theta)$, probability density function of reservoir model parameters, $f_P(p)$, and the reservoir forward model, $\Theta = g(p)$, in order to obtain model parameters posterior probability density function, $\Pi_P(p)$, as follows

$$\Pi_P(p) = \gamma f_P(p) f_\Theta(g(p)). \tag{3.64}$$

wherein, γ is a normalization factor. Although, a very common method to solve this nonlinear inverse problem is to perform Monte Carlo random search techniques [], in history matching problem, running forward simulation, e.g., $\Theta = g(p)$, is computationally quite expensive and time consuming. Thus, in this case we usually estimate its probability distribution function through maximum likelihood method and for the case that both prior probability density functions are Gaussian the optimization approach is known as least square method. The reader may note that forward model also is a function of reservoir model states, i.e., oil pressure and water saturation for a two-phase reservoir problem, and some control inputs as well. Thus, the general optimization formulation to solve history matching problem can be stated as follows

$$\underset{p}{minimize}\ J = \left(\hat{p} - p\right)^T C_M^{-1} (\hat{p} - p) + \sum_{i=0}^{N-1} \sum_{j=1}^{N_w} \left(\frac{g_j^i(x^i, u^{i-1}, p) - \theta_{obs_j}^i}{\sigma_j^i} \right)^2. \tag{3.65}$$

where, C_M is the parameter covariance matrix. σ_j^i is the observation standard deviation and N_w is the number of wells. The optimization process has been performed subject to reservoir forward model simulation and initial reservoir conditions that are optimization problem constraints. As stated previously, without a proper parameterization method, the solution of inverse problem can be geologically inconsistent despite of the accuracy of parameter estimation procedure. Therefore, reparameterizing reservoir model parameters like field permeability map, not only results in geologically consistent estimated parameters, but also, significantly decrease the number of unknown reservoir model parameters. The latter advantage of parameterization implies that employing parameterization allows to solve a smaller size problem in an uncorrelated space instead of solving the original ill-posed history matching problem in high dimensional and highly correlated original space.

3.8.1 Efficient Permeability Parameterization Through HOSVD

As mentioned before, the main idea in reservoir model parameter estimation is to approximate the original high dimensional space of correlated unknown and uncertain model permeability with one of the lower rank while preserving geological consistency of the model parameters by capturing the most significant permeability characteristics [118, 99, 1, 2]. A very common parameterization method for performing history matching in petroleum engineering is Karhunen Loeve Transform (KLT) [84, 96]. Although, KLT yields a precise estimation, it is not efficient with respect to implementation cost. Another classical option to obtain parameterization for history matching purposes is singular value decomposition (SVD). It has been shown that SVD and KLT transforms convey similar concept considering the problem of multivariate statistical analysis and given same approximation of column covariance matrix [63]. Moreover, considering multivariate stochastic process, the SVD and the

KLT are computationally equivalent. Implementation of classic SVD requires vectorizing input field permeability map and stacking them up into a matrix in order to perform SVD. This is the other significant drawback with SVD which may result in losing some important features due to vectorizing and consequently yields a weak prediction. In fact, vectorizing may lead to a solution that honors observation data while geologically is inconsistent. This is the main motivation in the present dissertation to perform a parameterization that not only provides a geologically consistent predictions, but also, reduces the cost of implementation. The higher order singular value decomposition (HOSVD) is the techniques that is employed here in order to fulfill the objectives of the work. The discrete cosine transform (DCT) is a new method in performing parameterization for inverse problem in petroleum engineering and discussed in [76].

In the present work, we utilized transform based image compression idea through HOSVD approach to perform efficient low dimensional parameterization for history matching problem in petroleum reservoir simulation field. A linear transformation defines a map between two vector spaces so that conserves the adding and scalar multiplication operators [117]. The central idea is to find a orthonormal transformation between original permeability space and the low dimensionality uncorrelated permeability space. In other words, we would like to represent the original permeability space by a set of orthonormal bases. This set of bases represents the original space and can conserve the signal energy while preserves the most important features of the original space. It also provides a uncorrelated representation of the original space that has strong energy compaction property [76]. Other interesting property of such a transform is that one can reconstruct any member of the space using truncated set of the bases through inverse transform [76, 117]. Therefore, one can characterize the original space utilizing a low dimensional estimated version of it while keep the most

important features of the original space.

The reader notes that there is an important difference between the case of image compression and reservoir parameterization problems. As a matter of fact, in image compression problem, the original space is a known image that we desire to reduce its dimensionality by truncating the its bases set for the sake of transmission and storage. However, it is not the case in general parameterization problem for reservoir history matching. Since, in history matching problem the original field permeability map is unknown that we would like to estimate. Thus, instead of reducing the unknown original space, we apply HOSVD analysis to a set of a known prior permeability maps called training set, in order to find a set of bases that could convey the most important features of the original space. It is believed that this training set may share important characteristics with the unknown permeability field. The idea is to estimate the unknown permeability by utilizing a truncated version of the training set bases [118, 99, 1, 2].

3.9 History Matching Through EnKF

In real reservoir simulation problems the actual permeability or porosity maps are unknown. In order to make the reservoir model more accurate, it is of high interest to provide a reliable estimation of these system parameters. In other words, having a reliable and accurate model requires a well understanding of reservoir rock flow properties. Therefore, in a reservoir simulation problem, in addition to parameterization to reduce the dimensionality of the system, one needs to estimate unknown reservoir parameters such as petrophysical properties including permeability and porosity as well. In this section, we introduce a well-known parameter estimation method in the petroleum industry, known as the ensemble Kalman filter (EnKF)[105, 59, 58].

Predicting reservoir geological properties like permeability and porosity especially

in a heterogeneous rock flow environment is referred to as reservoir characterization. The task in reservoir parameter inference is to estimate millions of unknown geological and petrophysical properties using few and sparse measurements data in hand that resulted in a highly nonlinear and ill-posed inverse problem due to the underdetermined nature of the problem. As a matter of fact, in a reservoir characterization problem the goal is to identify reservoir parameters knowing the reservoir states and outputs such as reservoir production history including oil and water production rates and bottomhole pressure at injectors. Thus, it is an identification or inverse problem, as it is known in reservoir simulation studies, at which the number of unknowns are bigger than the number of measurements by order of magnitudes that makes the problem highly underdetermined and nonlinear[116, 72, 98]. In addition, the ill-posedness nature of reservoir characterization problem leads to many different solutions that all express system properties and behavior accurately while providing dissimilar future reservoir production forecast. This section describes the EnKF method in detail starting with classic Kalman filter definition and proceeding to the fundamentals of EnKF as well as stating history matching, i.e., reservoir characterization, problem and application of EnKF in reservoir parameter inference. [74, 105, 59, 26, 27]

3.9.1 The Classic Kalman Filter

The Kalman filter estimates important parameters of a given system utilizing noisy observations or measurements in a recursive manner in order to treat measurements real time and as they are available [83, 29, 82]. In general, for a Gaussian noise, the Kalman filter minimizes the difference between estimated parameter and its actual value in a least square criterion known as minimum mean square error (MMSE).

For any linear stochastic process, the state-space modeling process is described as follows

$$x(n) = \mathbf{A}(n-1)x(n-1) + \mathbf{B}(n-1)u(n-1) + w(n-1), \tag{3.66}$$

$$y(n-1) = \mathbf{C}(n-1)x(n-1) + v(n-1). \tag{3.67}$$

wherein, x_n represents state vector of the system at current time step, u_n is the current control input vector, y_{n-1} is the modeling process or the observation vector, $\mathbf{A}(n-1)$ is the state transition matrix, and $\mathbf{B}(n-1)$ and $\mathbf{C}(n-1)$ are input and output (observation model) matrices respectively. Also, $w(n-1)$ and $v(n-1)$ are assumed to be uncorrelated Gaussian white noise processes (zero mean) known as process and observation noises respectively which imply the following properties with the linear system assumption

$$E[x_0] = 0, \tag{3.68}$$

$$cov\big(v_n, x_0\big) = cov\big(w_n, x_0\big) = 0, \tag{3.69}$$

$$cov\big(x_0, x_0\big) = \Pi_0. \tag{3.70}$$

Also, the correlation matrix for vector $N_n = \begin{pmatrix} v(n) \\ w(n) \end{pmatrix}$ is defined as follow considering the fact that v_n and w_n processes are uncorrelated

$$cov\big(N_n, N_n\big) = \begin{pmatrix} V\delta_{ij} & 0 \\ 0 & W\delta_{ij} \end{pmatrix} \tag{3.71}$$

Thus, the problem is to estimate system states given initial state and covariance matrix employing the Kalman filter in an optimum manner. The Kalman filter

provides state estimation as well as state error covariance estimation. In other words, the Kalman filter estimates posterior density of states, i.e., $\hat{x}(n|n-1)$, and the error covariance matrix posterior density, i.e., $\Pi(n|n-1)$, given all previous measurements including the current one through a recursive process by minimizing the Bayesian least square loss function [74, 82]. Following are the integrated update steps for the Kalman filter procedure

$$\hat{x}(n+1|n+1) = \hat{x}(n+1|n) + \mathbf{K}(n+1)Y(n+1), \tag{3.72}$$

$$\mathbf{\Pi}(n+1|n+1) = \mathbf{\Pi}(n+1|n) - \mathbf{K}(n+1)\mathbf{M}(n+1)\mathbf{K}^T(n+1). \tag{3.73}$$

wherein $\mathbf{K}(n+1)$ is the Kalman filter gain, $\mathbf{\Pi}(n+1|n+1)$ is the updating step for state covariance matrix, and $Y(n+1)$ is the updated measurement error. Algorithm 3.3 summarizes all steps within the process.

In order to utilize standard Kalman filter, the problem requires to honor three important condition. First, Kalman filter is well defined for linear systems. Second, it is assumed that all states and parameters of system have Gaussian probability distribution, i.e., are Gaussian stochastic process. And the last important assumption in stating a problem in the Kalman filter formulation is that the covariance function of error is known so the Gaussian process can be simply expressed by a mean and covariance matrix. However, as discussed before, this is not the case in reservoir parameterization and history matching problem. First of all, inverse problem is highly nonlinear with high dimensionality which means that it can not be stated by the standard Kalman filter formulation since the relation between states of system and input and output of the system are not linear anymore and nonlinear functions relate states of the system as well as its input and outputs. Furthermore, the large-scale nature of inverse problem leads to estimate a very large covariance

matrix which is computationally too expensive. For the second one, in real reservoir characterization problem, probability field permeability maps are usually not from a Gaussian distribution while the main assumption in the Kalman filter is that states and parameters are Gaussian process. Therefore, we need to restate the standard Kalman filter formulation in a way to consider the stated conditions. This leads us to employ the ensemble Kalman filter (EnKF) [74].

Algorithm 3.3 The Classic Kalman Filter

Input: $\hat{x}(n|n)$, $u(n)$, $\mathbf{\Pi}(n|n-1)$
Output: $\hat{x}(n+1|n+1)$, $\Pi(n+1|n+1)$
procedure State Estimation
    Time update
        $\hat{x}(n+1|n) = \mathbf{A}(n)\hat{x}(n|n) + \mathbf{B}(n)u(n)$ ▷ *state prediction*
        $\hat{y}(n+1|n) = \mathbf{H}(n)\hat{x}(n+1|n)$ ▷ *measurement prediction*
    Measurement update
        $Y(n+1) = y(n+1) - \hat{y}(n+1|n)$ ▷ *measurement residual*
        $\hat{x}(n+1|n+1) = \hat{x}(n+1|n) + \mathbf{K}(n+1)Y(n+1)$ ▷ *updated state*
end procedure
procedure State Covariance Estimation
    $\mathbf{\Pi}(n+1|n) = \mathbf{A}(n)\mathbf{\Pi}(n|n)\mathbf{A}^T(n) + \mathbf{V}(n)$ ▷ state prediction covariance
    $\mathbf{M}(n+1) = \mathbf{C}(n+1)\mathbf{\Pi}(n+1|n)\mathbf{C}^T(n+1) + \mathbf{W}(n+1)$ ▷ measurement prediction covariance
    wherein,
    $\mathbf{K}(n+1) = \mathbf{\Pi}(n+1|n)\mathbf{C}^T(n+1)\mathbf{M}^{-1}(n+1)$ ▷ Kalman gain
    $\mathbf{\Pi}(n+1|n+1) = \mathbf{\Pi}^e(n+1|n) - \mathbf{K}(n+1)\mathbf{M}(n+1)\mathbf{K}^T(n+1)$
end procedure

3.9.2 The Ensemble Kalman Filter (EnKF)

The ensemble Kalman filter (EnKF) is a recursive Monte Carlo method that has been proposed and utilized for solving petroleum reservoir characterization problems which was established by Lorentzen et al study in 2001. Since then, it has been

developed and modified for applications in high dimensional reservoir assisted history matching by Evensen et al and Aanonsen et al. works [55], [56], [57], [102], and [114].

As mentioned before, the ensemble Kalman filter is an adjusted version of the classic Kalman filter and is a suitable tool for large scale, nonlinear geophysical problems at which the covariance matrix is unknown and so approximated by sample covariance matrix instead [124, 92, 53]. Technically speaking, the EnKF employs Bayesian update in order to estimate a covariance matrix, which is replaced by a sample covariance calculated from the ensembles, while integrating new observations given the joint distribution of the reservoir states, geological/prior knowledge of the system, including pressure and saturation, and the data likelihood. There are several classical techniques to tackle the data assimilation problem such as conjugate gradient or quasi-Newton method for the optimization step. There are also several different methods to calculate the gradient of the squared data misfit function, i.e., cost function of inverse problem optimization, including adjoint and sensitivity equations. Moreover, few other options for approximating the Hessian matrix like Broyden-Fletcher-Goldfarb-Shanno (LBFGS)[95, 94]. One should take this point into account that using gradients are not feasible, i.e., too expensive implementation, for high dimensional problems, e.g., predicting reservoir petro-physical properties such as permeability or porosity. Thus, an important advantage of EnKF, comparing to other optimization schemes, is that this method does not involve adjoint gradients of objective function, which actually is the difference between observed and estimated data, in its update step [93], and [97].

As a matter of fact, the EnKF approximates each member of ensemble independently simply by updating mean and covariance of the joint probability density function (pdf) of reservoir states and data likelihood stated beforehand. Finally, the posterior joint pdf will be empirically approximated utilizing new updated ensem-

ble [50, 74, 79]. We have to underscore significant assumptions for implementing EnKF as follows: (1) prior joint pdf must have multivariate Gaussian probability distribution, otherwise EnKF does not yield an accurate estimate of geological properties in hand for the reservoir; (2) EnKF presumes linearity in the system, thus reservoir system equations, including states, parameters and observations, have to be linearly posed in order to get EnKF well performed. Therefore, assuming linearity and having Gaussian distribution are the essential conditions in performing EnKF to obtain results that are geologically consistence with the geological prior knowledge from the reservoir. In other words, these conditions entail an adjustment in standard EnKF formulation if one wants to apply EnKF to non-Gaussian systems as well. Eager reader can refer to [102] to find various approaches proposed for common non-Gaussian reservoir models. One can estimate reservoir parameters such as permeability and porosity by matching the production data through the EnKF optimization involving a two stages procedure referred to as forecast and update.

As discussed previously, the EnKF replaces state pdf covariance matrix by sample covariance matrix or simply by an ensemble of members ,$X^i = \left(x_1^i, x_2^i, \cdots, x_N^i\right)$ that generates samples from a prior distribution. That is to say that the central idea of the EnKF is to propagate an ensemble of initial guesses, of the reservoir model parameters, in time in order to integrate observation data and to employ statistics of the model parameters at each iteration level for updating the model covariance matrix. These ensemble members can be generated by stacking the rock/flow properties in each gridblock and production data up to a state vector called reservoir model state vector and denoted by x_j^i [95, 94, 74, 102]. The EnKF algorithm contains two steps. The first step is to run reservoir forward simulation in order to construct forward forecast. Reservoir states and production data are replaced in the predicted state vector in the first step. The second step in the EnKF methodology is to update the

model through adjusting ensemble members in order to honor measurement data.

One could simply write the following for a nonlinear stochastic process and for all $i = 1, 2, \cdot, N$

$$x^i(n+1|n) = f_n\Big(x^i(n|n), \alpha(n), w^i(n)\Big), \tag{3.74}$$

$$y^i(n+1|n) = g_n\Big(x^i(n+1|n)\Big) + v^i(n+1). \tag{3.75}$$

wherein $\alpha(n)$ is time dependent control variables, $w^i(n)$ and $v^i(n+1)$ are ith state and observation errors at current time step, and nonlinear functions f_n and g_n are state and observation transition functions as well. Again, in a similar fashion to the classic Kalman filter, the EnKF utilizes predicted ensemble to estimate mean and covariance through a least square optimization step for each sample of ensemble. The update equations in the EnKF are established as follows

$$\hat{x}^i(n+1|n+1) = \hat{x}^i(n+1|n) + \mathbf{K}^e(n+1)Y^i(n+1), \tag{3.76}$$

where the Kalman gain is

$$\mathbf{K}^e(n+1) = \mathbf{\Pi}^e(n+1|n)\mathbf{C}^T(n+1)\mathbf{M}^{-1}(n+1) \tag{3.77}$$

$$\mathbf{\Pi}^e(n+1|n+1) = \mathbf{\Pi}^e(n+1|n) - \mathbf{K}^e(n+1)\mathbf{M}(n+1)\mathbf{K}^{e^T}(n+1). \tag{3.78}$$

Employing update equation in 3.76 and given the initial guess for the ensemble of states, one can easily perform the EnKF for a nonlinear large scale problem such as reservoir permeability of porosity estimation. Algorithm 3.4 summarizes all steps within the process. Section 5 explains the process of permeability characterization and provides with a real field reservoir example to show the performance of the EnkF

along with HOSVD parameterization for predicting reservoir permeability. Eager readers can refer to [74, 105, 82] for more details on the EnKF and its implementation process.

Algorithm 3.4 The Ensemble Kalman Filter (EnKF)

Input: ensemble of samples $\hat{X}^i$
Output: $\hat{X}^i$, $\Pi^e(n+1|n+1)$
procedure STATE ESTIMATION
    $\hat{x}^i(n+1|n+1) = \hat{x}^i(n+1|n) + \mathbf{K}^e(n+1)Y^i(n+1)$
    $\mathbf{K}^e(n+1) = \mathbf{\Pi}^e(n+1|n)\mathbf{C}^T(n+1)\mathbf{M}^{-1}(n+1)$
    $\mathbf{\Pi}^e(n+1|n+1) = \mathbf{\Pi}^e(n+1|n) - \mathbf{K}^e(n+1)\mathbf{M}(n+1)\mathbf{K}^{e^T}(n+1)$
    wherein,
    $\mathbf{M}(n+1) = \mathbf{C}(n+1)\mathbf{\Pi}(n+1|n)\mathbf{C}^T(n+1) + \mathbf{W}(n+1)$ ▷ measurement prediction covariance
end procedure

4. EFFICIENT GEOLOGY PRESERVING RESERVOIR PARAMETERIZATION USING HIGHER ORDER SINGULAR VALUE DECOMPOSITION (HOSVD)*

Parameter estimation through reduced-order modeling plays a pivotal role in designing real-time optimization schemes for the Oil and Gas upstream sector through the closed-loop reservoir management framework. Reservoir models are in general complex, nonlinear, and large-scale, i.e., large number of states and unknown parameters. Thus, having a practical approach to reduce the number of reservoir parameters in order to reconstruct the reservoir model with a lower dimensionality is of high interest. Furthermore, de-correlating system parameters in all history matching and reservoir characterization problems keeping the geological description intact is paramount to control the ill-posedness of the system. As mentioned in the previous sections, in this section we will introduce the advantages of a new parameterization method utilizing higher order singular value decomposition (HOSVD) which is not only computationally more efficient than other known dimensionality reduction methods such as, SVD and DCT, but also provides a consistent model in terms of reservoir geology. HOSVD power is due to its ability to supply a reliable low-dimensional reconstructed model while keeping higher order statistical information and geological characteristics of reservoir model. In order to understand the capabilities of HOSVD and to compare it to other common parameterization methods such as SVD, we generated three different sets of experiments. In the first set,

*Part of the material is published with permission from "Permeability parametrization using higher order singular value decomposition (hosvd)," S.Afra, E. Gildin, 2013, International Conference on Machine Learning and Applications (ICMLA'13), Copyright 2013 by IEEE. Also from "Heterogeneous reservoir characterization using efficient parameterization through higher order svd (hosvd).," S.Afra, E. Gildin, 2014, American Control Conference (ACC'14), Copyright 2014 by IEEE.

dimensionality of a known field permeability maps is reduced using HOSVD image compression idea. Then, we show promising power of HOSVD to estimate and construct unknown permeability maps is investigated and results of both parts compared to those of classic SVD. In the second set of experiments, we utilize higher order singular value decomposition (HOSVD) to reparameterize reservoir permeability and perform several forward reservoir simulations by the resulted reduced order map as an input. To acquire statistical consistency we repeat all experiments for a set of 1000 samples using both HOSVD and Proper orthogonal decomposition (POD). The third experiments describes the results of applying this novel parameterization method to the SPE10 benchmark reservoir model to show its promising parameterization performance. Furthermore, to acquire statistical consistency we repeat all experiments for a set of 1000 samples using both HOSVD and classic SVD (PCA) and provide RMSE analysis for a better understanding in process of comparing HOSVD and SVD in the last two sets of experiments.

4.1 Introduction

The development of accurate and fast computational environments for modeling transport and flow in heterogeneous porous media is a problem of national and global interest. This can be readily recognized as important applications involving heterogeneous media arises in energy related environments, e.g, Oil & Gas reservoir simulations and management, CO_2 sequestration and storage, and weather prediction and air quality management [8, 67, 36]. However, the prediction of fluid flow through heterogeneous porous media is a daunting task to be performed with great confidence because, although fluid properties can be determined with reasonable accuracy, the dynamics of the flow is mostly driven by poorly known rock properties, such as porosity, permeability and relative permeability [77, 8]. In this case, con-

fidence in its behavior is only attained, typically, by repeated experience (forward simulations) covering the entire spectrum of the uncertain parameter spaces in a process called uncertainty quantification, or by means of conditioning reservoir model to new information obtained from measured data streamed out of the field in a process called history matching. In fact, the process of adapting geological properties to fit the production data has its roots in the larger umbrella of parameter estimation [104].

The central issue in history matching is, thus, how to construct a reservoir model to predict accurate future reservoir production utilizing observation data. Several parameters describe a reservoir model which each of those parameters may convey a huge amount of data. Some parameters are specified per grid block like permeability and porosity and others for the entire model or a particular layer such as relative permeability and capillary pressure. History matching is a highly underdetermined, nonlinear and ill-posed problem owing to insufficiency and complexity of observed data from reservoir[104]. This means there is a possibility of obtaining reservoir models that fulfill observed measurements but then provide incorrect predictions. This is mainly due to the fact that high fidelity reservoir models come from the discretization of the underlying partial differential equations related to fluid flow in heterogeneous media, which can lead to models of millions of gridblocks, and therefore millions of parameters (permeability, porosity) and states variables (pressure, saturations)[67, 51]. Many workflows in uncertainty quantification and history matching rely on massive computations, and the availability of computing resources is still seen as a limiting factor. Considering that large-scale computer-based simulation provided the only feasible method for producing quantitative predictive information about complex behavior, novel ways to reduce the computational burden related to simulations need to be developed.

In reservoir management, the problems that one faces in controlling petroleum systems are more complex in the sense that one deals with highly non-linear and uncertain models, which are described mathematically, by large-scale dynamical systems - fine scale discretization are very often needed, and massive computational machinery are required for simulation and optimization. Furthermore, porous media properties such as conductivity or permeability contains many small scales and uncertainties. For example, in fractured media, the small scales can be much smaller compared to the field scales. For this reason, it is computationally expensive to solve forward problems directly, and, in particular, it is prohibitively expensive to solve many such forward problems as in the case of uncertainty quantification and controller design. Owing to recent achievements in reservoir engineering, simulating petroleum reservoirs and reservoir management are getting more efficient in terms of running time, accuracy, and using leading edge methods such as high performance computing, than since it began in mid-1950's [107].

A challenging problem in reservoir engineering is to estimate petrophysical properties of a reservoir such as permeability and porosity, by means of its production history in a process called inverse modeling. Having precise predictive reservoir model is of high importance for predicting future production profile of reservoir. The main idea is to optimize reservoir production (e.g., hydrocarbons) by delaying water production and minimizing fluid injection during the reservoir life-cycle. This can be accomplished by setting up a model-based optimization and parameter estimators for proper account of uncertainties. Thus, providing a powerful reservoir characterization method significantly impact the amount of hydrocarbons extracted and, in turn, the volume of global reserves by increasing the recovery factor of conventional reservoirs by only a small fraction.

Although, having a reliable and accurate reservoir model is highly tied to provid-

ing a fine detailed representation of the reservoir, the high resolution model results in a large scale inverse problem both in the parameter space (permeability, porosity) and state-space (pressures, saturations). Therefore, it is of great importance to characterize and reduce the complexity of the model in order to acquire efficiency with respect to computational time and cost. Also, it is beneficial to perform geologically consistent reservoir parameter adjustments as data is being assimilated in the history matching process. This is a daunting task to be performed as one is bounded by the number of data points, i.e., measurements, and very often the inverse problem has more unknowns that can uniquely be estimated from the available data. To this end, having a practical approach to reduce the number of reservoir parameters in order to reconstruct the reservoir model with a lower dimensionality is of high interest.

A number of studies have been conducted to reduce computational efforts in reservoir simulation and history matching [52, 51, 22, 1, 129] as well as reservoir characterization through integrated parameterization [99, 65]. The methodologies basically worked in two fronts: reducing the number of states using model reduction techniques, and reducing the number of unknown parameters in a process known as parameterization [119, 75]. Among all of these methods, a common approach that is applied to history matching is proper orthogonal decomposition (POD) [132, 64, 66], which in different areas, is also known as principal component analysis (PCA) and Karhunen- Loève Decomposition (KL). In the standard PCA (POD), it is necessary to carry out an eigen-decomposition of the random field covariance matrix which is expensive for large models. Furthermore due to the vectorization of the snapshots data in the POD computation, many features may be lost in the reduced space [11, 86, 90].

Here, we introduce the multi-linear algebra based approach, namely the high-order singular valued decomposition (HOSVD) [86, 90, 130, 2], to reduce dimension-

ality representation of reservoir properties, such as permeability, taking into account an ensemble of models. We treat property ensembles as a high-dimensional tensor, and by means of tensor algebra (HOSVD) we show that the reduced models preserve better geometric features keeping them more intact during the reduced basis computations. This is of great importance in the case of reservoirs as the properties in consideration have geological meaning. In other words, HOSVD has the ability to reduce the size of the model and reconstruct it accurately while keeping higher order statistical information and geological characteristics of the reservoir model. As a matter of fact, other parameterization algorithms need to vectorize original replicates in order to obtain basis in process of dimensionality reduction which results in losing geological consistency. In HOSVD, we take the snapshots in a 2D or 3D approach and stack them up in a tensor form, i.e. a multi-way array in multilinear algebra, which leads to performing tensor decomposition as a way to obtain the new reduced basis. Eager reader could refer to authors' other published work on integrating HOSVD based parameterization into history matching process [65].

This section is organized as follows. In subsections 4.2 and 4.3, we briefly restate the reservoir simulation framework and show how permeability is taken into account the the porous media flow. Sections 4.4 and 4.5 describe permeability field parameterization and dimensionality reduction using HOSVD used in the present work as well as the simulation results of forward reservoir simulation based on the obtained geostatistical permeability realization through HOSVD parameterization are presented. We also apply this novel parameterization method to a reservoir engineering benchmark model known as SPE 10. In subsection 4.6, we discuss the running time of all simulation results and then finally subsection 4.7 provides several conclusion remarks.

4.2 The Reservoir Simulation Problem Restatement

Many existing flow and transport models in porous media can be described by a set of partial differential equations representing conservation of mass, momentum and energy as a function of pressure and temperature, and reconciled by the equations of state [8]. For the case of two-phase flow systems (oil-water), the mass balance equation for each phase is

$$\nabla \cdot (\rho_l \mathbf{v}_l) + \frac{\partial (\rho_l \phi S_l)}{\partial t} - \rho_l q_l = 0, \quad l \in \{o, w\}, \tag{4.1}$$

where ρ_l is the fluid phase density, $\mathbf{v}_l$ is the fluid phase superficial velocity, t is time, $\nabla\cdot$ denotes the divergence operator, ϕ is the porosity, S_l is fluid phase saturation, q_l is flow rate per unit volume and finally $l \in \{o, w\}$ represents the oil and water phases, respectively. Applying the empirical Darcy's law, one can write

$$\mathbf{v}_l = -\frac{k_{rl}}{\mu_l}\mathbf{K}\left(\nabla p_l - \rho_l g \nabla h\right), \tag{4.2}$$

where ∇ is the gradient operator, $\mathbf{K}$ is the permeability tensor, μ_l fluid phase viscosity, k_{rl} the relative permeability of each phase (which is a function of water saturation) , p_l is the phase pressure, g is the constant of gravity acceleration and finally h is the depth of the reservoir.

We can consider the mass balance equation for each phase by plugging Eq. 4.2 into Eq. 4.1. This yields two equations in four unknowns: (p_w, p_o, S_w, S_o). Thus, two additional equations are required to complete the system description. These equations are given by a closure equation which states that the sum of all fractional saturations must always be equal to one (since the saturations are the volumetric fractions occupied by each phase), and the oil-water capillary pressure equation,

which gives a relation between phase pressures as function of water saturation. They are respectively:

$$S_w + S_o = 1, \tag{4.3}$$

$$p_o - p_w = p_c(S_w) \tag{4.4}$$

Since the unknowns are not independent, we can formulated the two-phase flow equations in terms of two state variables: p_o, the oil pressure, and S_w the water saturation. yielding

$$\begin{aligned} -\nabla \cdot \left\{ \frac{\rho_w k_{rw}}{\mu_w} \mathbf{K} \left[\left(\nabla p_o - \frac{\partial p_c}{\partial S_w} \nabla S_w \right) - \rho_w g \nabla h \right] \right\} &+ \\ \rho_w \phi \left[S_w \left(c_w + c_r \right) \frac{\partial p_o}{\partial t} + \frac{\partial S_w}{\partial t} \right] - \rho_w q_w &= 0, \\ -\nabla \cdot \left[\frac{\rho_o k_{ro}}{\mu_o} \mathbf{K} \left(\nabla p_o - \rho_o g \nabla h \right) \right] & \\ \rho_o \phi \left[\left(1 - S_w \right) \left(c_o + c_r \right) \frac{\partial p_o}{\partial t} - \frac{\partial S_w}{\partial t} \right] - \rho_o q_o &= 0 \end{aligned} \tag{4.5}$$

As can be seen from Eq. 4.5, multi-phase flow through porous media is given by a set of weakly-nonlinear parabolic PDE's that represents the rate of change of pressure (diffusion) coupled with a set of strongly-nonlinear parabolic - hyperbolic PDE's which describe the rate of change in phase saturations and component concentrations (diffusion-convection). The main idea of reservoir simulation is then to compute the dynamics of the fluids inside the reservoir, given boundary conditions and well constraints, such as hydrocarbon production rates, maximum/minimum well pressures, to name as few.

Applying spatial discretization results in a set of nonlinear ordinary differential equations with high dimensionality. The type of spatial discretization scheme used is

important in developing good models. In the oil industry, it is customary to discretize the pressure and the transport (saturation) equations by means of the finite volumes method using upstream weighting. One of the reasons is that they yield locally conservative schemes [36].

After discretization in space and time, each grid block is related to two states of the reservoir, that is oil pressures and water saturations. Given the fine details of the dynamics, millions of gridblocks are necessary to describe with accuracy the flow in the porous media. This in turn, leads to large-scale systems both in the parameter space (permeability, porosity) and state-space (pressures, saturations). Two of the primary variables related to the fluid dynamics in porous media are the porosity, ϕ, and permeability, $\mathbf{K}$. The porosity accounts for the amount of void spaces in the porous media that can store the hydrocarbon fluids. On the other hand, if the void spaces are not connected, the fluid cannot be moved from one region to the other. In other words, permeability accounts for how easier is to transfer fluid inside the reservoir. So it is of great importance to characterize correctly the permeability of the reservoir. As pointed out before, due to the large number of gridblocks used in the discretization process, permeability can have millions of variables in its representation. Model reduction or parameterization is a necessary step in devising fast and accurate reservoir simulation models.

4.3 Permeability Field Parameterization

As pointed out in the previous sections, the reduction in the number of gridblocks in the description of permeability information is of central importance in reservoir simulation. Indeed, model reduction in this case can be achieved by parameterizing the permeability field or transforming it to a lower dimensional space as if the permeability parameterization is treated as an image compression problem.

A map from space of correlated variables into an uncorrelated space of lower dimension is known as multilinear analysis. Generally speaking, working with uncorrelated space of lower rank is often easier than the original one. For image compression purposes, multilinear techniques are applied to a single known image and the compressed form of image obtained by truncating basis in the lower dimension space. A significant task in image processing procedures is preserving important features of image along with keeping best basis and achieving an efficient compression ratio.

In history matching and reservoir characterization problems, the input permeability image is unknown and has to be estimated through history matching process. Hence, finding a set of basis is impossible. In the present work with the assumption of two-point geostatistics, the unknown permeability field is a random sample from a multivariate Gaussian distribution defined by a variogram or covariance function. A variogram or covariance function define the underlying geological continuity in the formation. Attaining realistic basis function from a large finite number of samples that are drawn from a specific high dimensional Gaussian distribution is very likely. These basis geologically describes unknown permeability field.

Here, we apply HOSVD-ALS first for dimensionality reduction and then for estimating an unknown permeability map to investigate the ability of HOSVD-ALS for supplying a low-dimensional practical and reliable estimated permeability map in a geological sense and how much this estimated model is appropriate for history matching.

4.4 Experiment A: Permeability Parameterization Using HOSVD

For the first example, two different experiments have been conducted in order to show the ability of HOSVD-ALS, first as a method to compress known permeability maps, and second as an approach to estimate unknown maps using basis obtained

from a training set of permeability samples. In the present work, we used an ensemble of 500 permeability realizations as our training set.

A two-point geostatistical simulation algorithm called Sequential Gaussian Simulation (*sgsim*) [47] is utilized to generate 1000 permeability realizations. A specific variogram model properties is also used to represent the geological structure. Each realization contains 45×45 grid blocks. To run simulations, the first 500 samples are considered as training set of known permeability maps and all other samples constructed the unknown test set used for permeability field estimation.

4.4.1 Dimensionality Reduction

We performed HOSVD-ALS for the first 500 permeability replicates as training set to find basis function employed to reduce the dimension of original images for compression purposes. First, HOSVD-ALS is utilized to provide truncated basis matrices and coefficient core tensor. Based on the HOSVD-ALS approach, the reduction procedure requires the selection of basis which express the map with higher accuracy. Here, we perform three different setups. In the first one, we choose $k = 70$ and found the best $(25, 25, 140) - rank$ representation of original tensor. In the second setup we decrease the order of tensor's third mode from 140 to 70. Eventually, for the last simulation we run HOSVD to find the best $(45, 45, 70) - rank$ approximation and again fixed k at 70. Kronecker product is performed in all simulations to compute required coefficients for reconstruction part. Utilizing truncated basis results in a compressed reconstructed version of known permeability maps (3 arbitrary samples drawn from training set). In these experiments, for regular PCA, we first vectorized each sample and then stacked all the vectorized training samples into a matrix.

Figure 4.1 shows that HOSVD not only outperforms PCA in the measure of RMSE, but also overcome it in perceptual sense. Moreover, the capability of reduc-

ing rank in all modes is assisting HOSVD to become more efficient than PCA in the manner of memory and computational costs as well. Although, RMSE increases while the number of basis decreases, it is obvious from Fig. 4.2 that HOSVD still has perceptually better performance and quality in comparison to PCA. Figure 4.3 shows the results for the similar setup in both methods. As expected, in the same simulation setup PCA functions exactly as same as HOSVD which leads to equal RMSE. Therefore, it is evident from the results that HOSVD-ALS has a promising power to compress an image while preserving geological features along with spacial characteristics of permeability maps. Even with small number of significant coefficients large scale features, low and high permeability regions are preserved in reconstructed replicates compared to the true permeability maps. In addition to preserving the most important features, the low computational cost is the other significant capability of HOSVD. In fact, in the real reservoir parameterization problems which the system is of order of million, low computational cost and the ability to reduce to a lower rank become important.

4.4.2 Unknown Permeability Field Estimation

Thus far, we investigated the compression power of HOSVD-ALS and showed comparisons between its results and regular POD. Having reliable compression power is a required necessity for a useful compression method in history matching. However, it is not sufficient since, as it was mentioned previously, the permeability image in reservoir history matching problem is unknown.

The other important characteristic of a useful compression method for reservoir history matching is capability of the basis to reconstruct an unknown image with optimum coefficients. Moreover, in the present experiments, basis are obtained using prior knowledge of reservoir permeability. In other words, we use a set of training

samples to compute required set of basis that is necessary for reconstruction and estimation part. In the second set of experiments, we employ HOSVD-ALS and regular POD to estimate unknown permeability samples using basis obtained from prior knowledge (training set).

The coefficients required for reconstructing unknown permeability maps are estimated utilizing the truncated basis computed by applying the HOSVD-ALS or regular PCA methods to the training ensemble of permeability replicates. Therefore, using the basis from the reduced dimension space we could do both estimation and dimensionality reduction of the unknown permeability maps at the same time. In this work, we set k to 300 in PCA and found the best $(15, 15, 500) - rank$. Results of HOSVD-ALS are compared to those of regular PCA (see Fig. 4.4). Again, here the advantage of lower compression rate along with a better performance is evident. As mentioned before, we repeated experiment for all samples to validate our results and corresponding RMSE PDFs are discussed in authors' other submitted work. Here, we only presented randomly selected samples to compare the results.

4.5 Experiment B: Heterogeneous Reservoir Forward Simulation using Efficient Parameterization through HOSVD

Having a reliable compression method is paramount in history matching. However, it is not sufficient since, as it was mentioned previously, the permeability image in reservoir history matching problem is unknown. The other important characteristic of a useful compression method for reservoir history matching is the capability of the basis to reconstruct an unknown image with optimum coefficients. In the present experiments, the basis are obtained using prior knowledge of the reservoir permeability. In other words, we use a set of training samples to compute the required set of basis that is necessary for reconstruction and estimation. Using the basis from

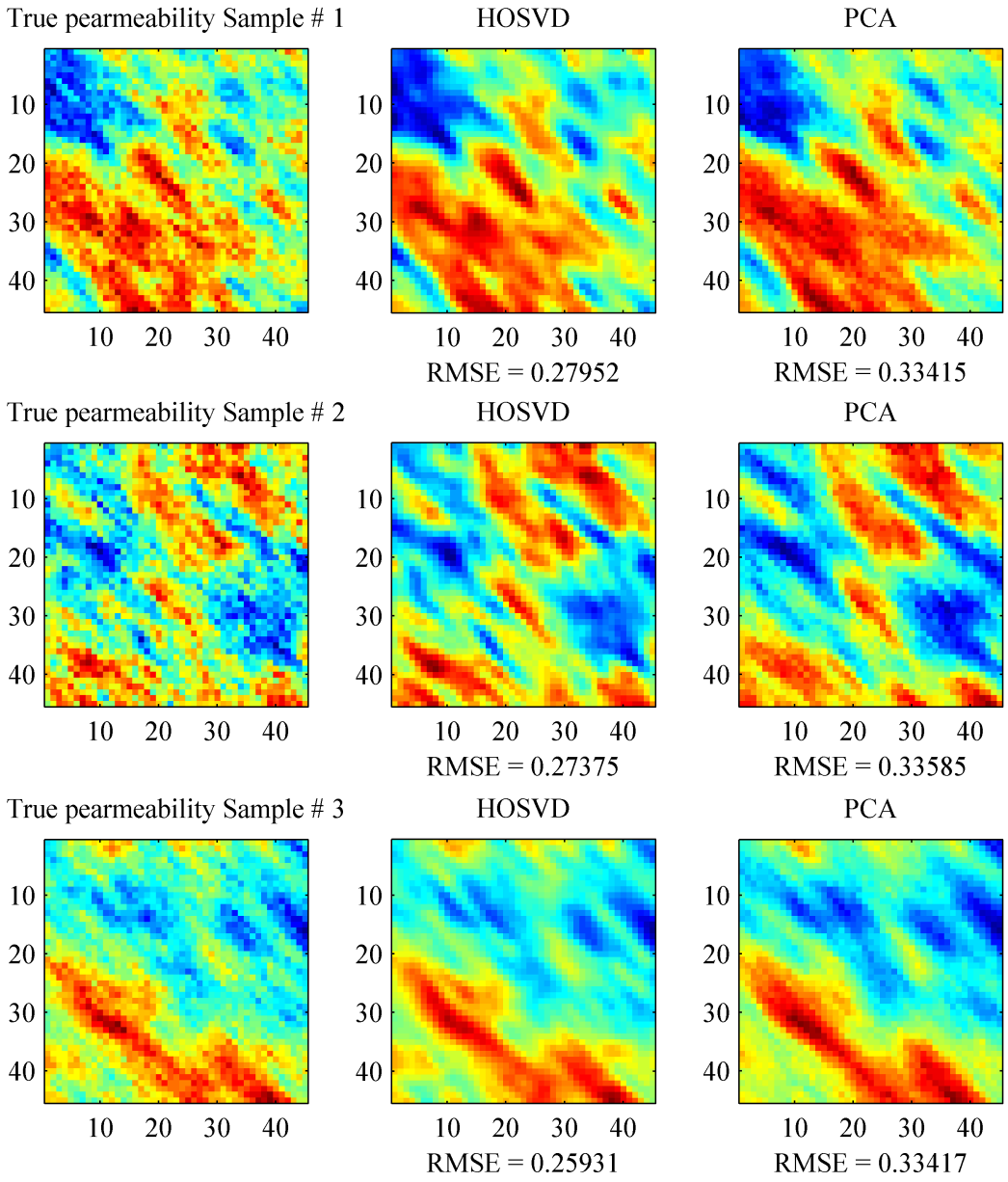

Figure 4.1: Compressed permeability of 3 samples using HOSVD and PCA and corresponding RMSEs for $k = 70$ for PCA. The rank of reduced space using HOSVD is $25 \times 25 \times 140$.

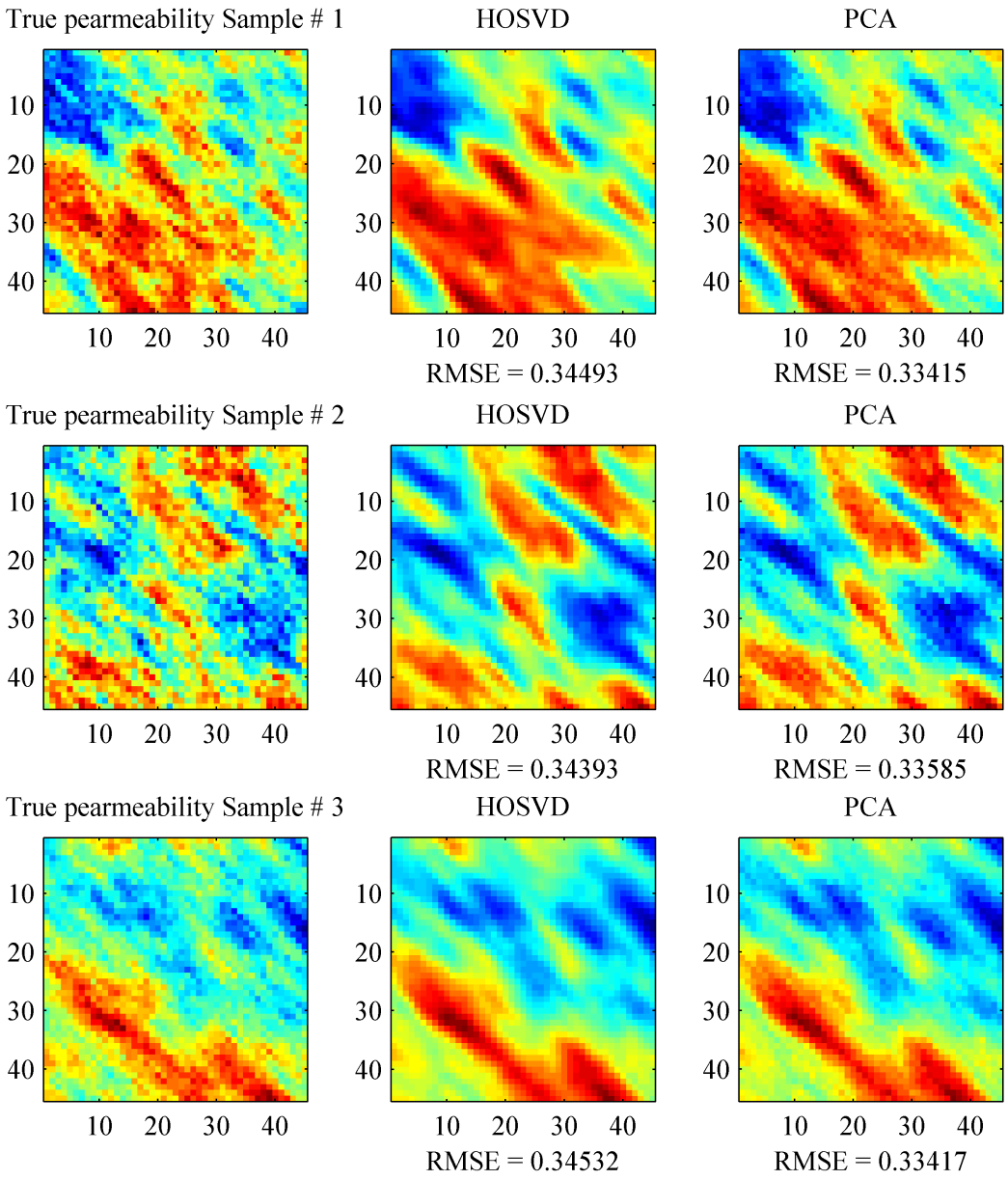

Figure 4.2: Compressed permeability of 3 samples using HOSVD and PCA and corresponding RMSEs for $k = 70$. The rank of reduced space using HOSVD is $25 \times 25 \times 70$.

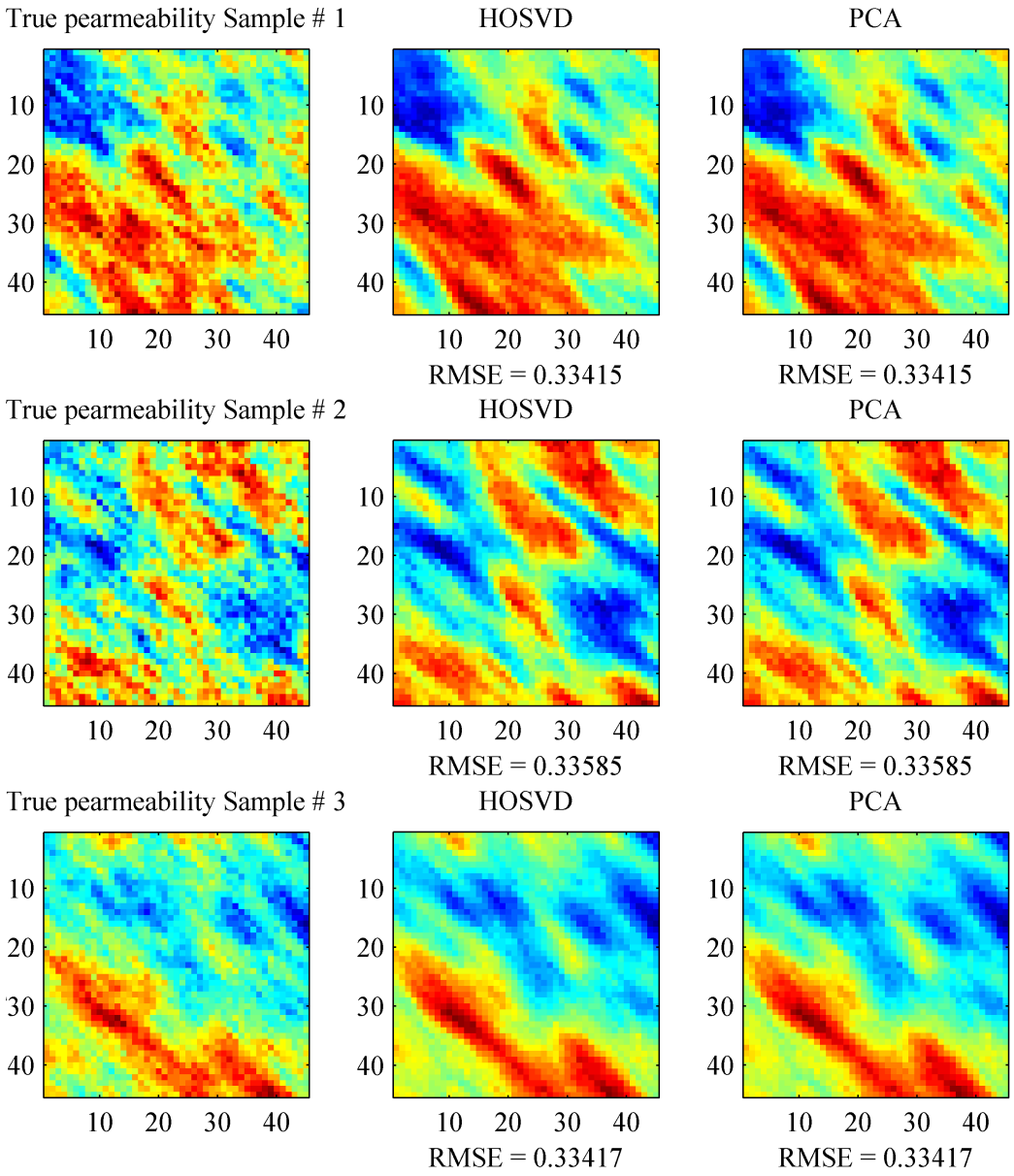

Figure 4.3: Compressed permeability of 3 samples and corresponding RMSEs for $k = 70$.

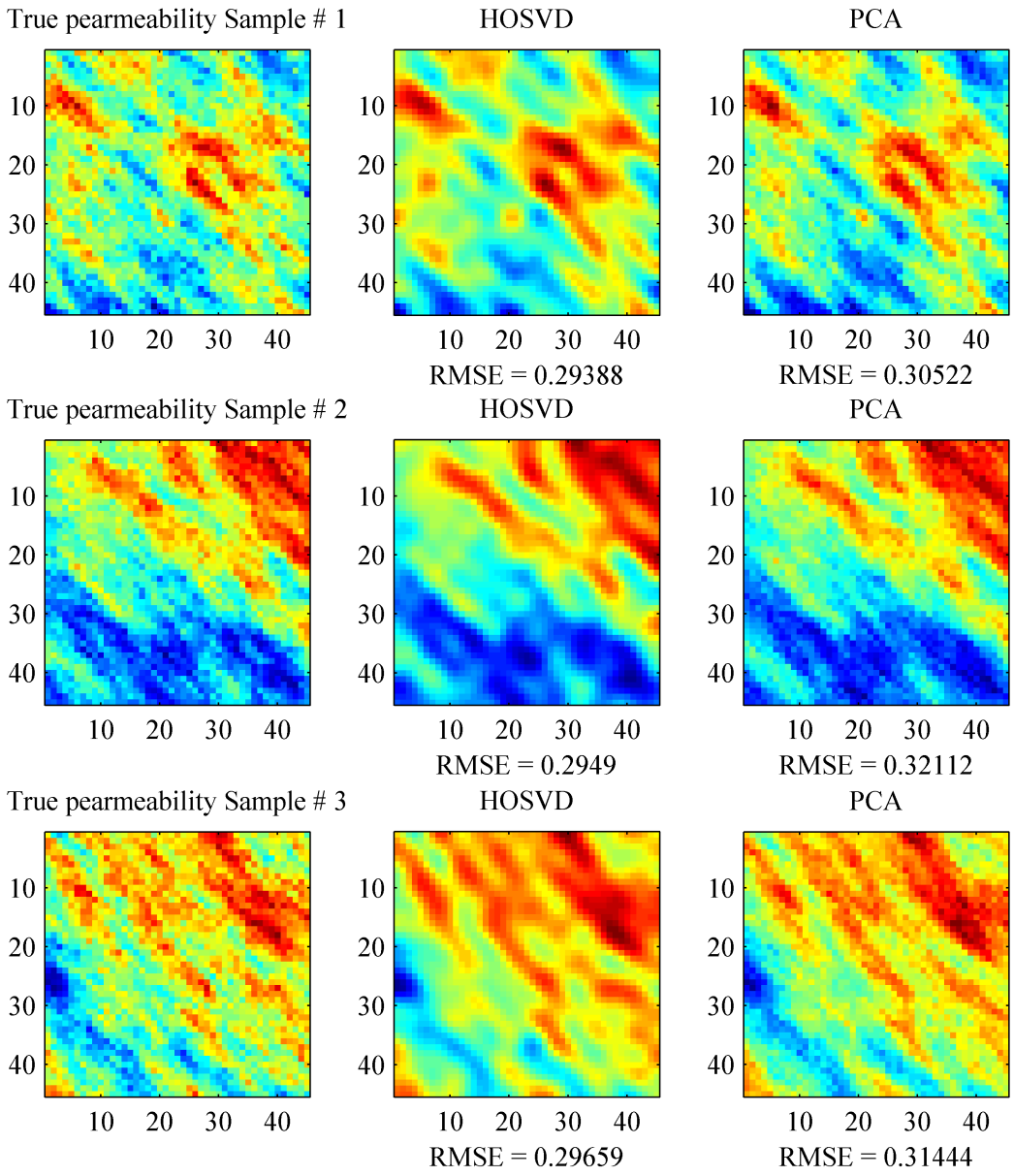

Figure 4.4: Estimated unknown 3 different permeability samples using HOSVD and PCA and corresponding RMSEs for $k = 300$. The rank of reduced space is $15 \times 15 \times 500$.

the reduced dimension space allow us to do both estimation and dimensionality reduction of the unknown permeability maps at the same time. Here, we repeated the experiments for all samples to validate our results and the corresponding RMSE PDFs are discussed next. Furthermore, an appropriate permeability parameterization and compression method not only has to yield consistent permeability maps but also should result in the similar response of the highly nonlinear and complex reservoir system.

4.5.1 Statistical Analysis

Two different sets of experiments have been conducted in order to demonstrate the ability of HOSVD-ALS as a parameterization method to reduce the dimensionality of the original permeability map and to show the capability of the obtained reduced map to reproduce similar system response to that of original permeability.

In both experiments, we used an ensemble of 1000 permeability realizations as our sample set. It should be pointed out that here we work with only permeability, but HOSVD can be used for any grid-based property, such as porosity. In our experiments, we assume porosity is a known property, although large dimensional, we do not perform its parameterization.

To analyze the reconstruction performance of the SVD and HOSVD we calculate the observation root mean square error (RMSE) of the samples. In this work, RMSE of j^{th} observation (each well's BHP, oil or water rate) is defined as:

$$RMSE_j = \sqrt{\frac{1}{N}\sum_{i=1}^{N}\left(\hat{d}_j^i - d_j^i\right)^2}. \tag{4.6}$$

where i is the time step index. Also, the original and estimated observation are represented by d and $\hat{d}$, respectively. In our computations, we do not subtract the

mean of the snapshots. It has been shown that this may not make a difference in the case of history matching [119]. Also, we work with the $\ln(K)$ and thus no negative values of permeability is possible in our decomposition.

It is of great interest to have a single representative observation RMSE for each permeability sample. As a matter of fact, having this parameter simplifies comparison of the permeability reconstruction performance of SVD and HOSVD. Since observation RMSEs have different units, we need to make dimensionless RMSEs. To achieve this purpose we utilized the original observation's L^2 *norm*. Finally, we define the total dimensionless observation RMSE as follows:

$$RMSE_{total} = \sum_{j} \frac{RMSE_j}{\|d_j\|_2}. \tag{4.7}$$

To explore HOSVD-based parameterization properties and compare its capability and power in permeability parameterization with classic SVD, we perform two sets of experiments. In the first experiment a synthetic 2D model is utilized and for the second experiments a 3D model is generated using the first top 5 layers of SPE 10 benchmark [37].

4.5.2 Experiment B-1: Synthetic Model

The synthetic model is generated utilizing the two-point geostatistical simulation algorithm, namely the Sequential Gaussian Simulation (*sgsim*) [47]. In fact, 1000 permeability realizations are generated employing a specific covariance function to represent the geological structure. An exponential variogram model is employed with same correlation length properties of 60 in the x and y directions. Each permeability realization is a 45×45 map of $30 \times 30 \times 30$ feet grid block size and the reservoir assumed to act as a 2D two-phase flow of slightly compressible oil reservoir. For-

ward simulations are performed using ECLIPSE [120]. Overall, we conducted three distinct sets of forward simulation experiments. In the first setup the ensemble of original permeability samples are used as an input to the simulator and the other two setups are implemented for ensembles of reduced order permeability samples using SVD and HOSVD respectively. Therefore, we performed three sets of 1000 forward reservoir simulations. Two randomly drawn permeability realizations along with corresponding reduced ordered representatives using classic SVD and HOSVD are shown in Fig. 4.5. Four producers are operating with a constant bottom-hole pressure (BHP) of 2900 psi and one water injector with a constant injection rate of 300 bbl/day, all operating in an inverted five-spot waterflooding scenario. As stated previously, porosity is not parameterized in this work and therefore is fixed at 0.22. Furthermore, 1 pore volume of water is injected through the simulation time of 1 year. Table 1 summarizes all information regarding simulation description and reservoir specifications.

In simulating a reservoir system, permeability realization is the input and production data is the output of this system. The production data includes bottom hole pressure (BHP) of injection wells, oil and water rate of production wells. In this synthetic model experiment, there are 4 production wells and one injection well resulting in 9 different observations where each observation is available in 12 time steps (of 30 $days$). Consequently, one could come up with a total 9×12 distinct observation values in each experiment.

We performed HOSVD-ALS employing permeability replicates as a training set to find the basis function employed to reduce the dimension of the original images for compression purposes. First, HOSVD-ALS is utilized to provide truncated basis matrices and a coefficient core tensor. Based on the HOSVD-ALS approach, the reduction procedure requires the selection of basis which express the map with higher

accuracy. Here, the following scenario is performed to obtain re-parameterized permeability representatives. In parameterization with the classic SVD, all samples are vectorized and stacked into a matrix namely the training set, and SVD is performed to find the space basis required for the reconstruction. Then, the singular vectors associated with the largest 55 singular values of the covariance matrix, which conserve the most of the energy, are selected as reduced order space's basis. In the SVD case we used those selected basis to compute reduced order version of the original permeability maps to reduce the dimensionality of original space. This is not the case in the HOSVD, as we keep the snapshots *as it is*. For the HOSVD parameterization, the best $(15, 15)-rank$ representation of the original tensor is approximated and then Kronecker product is performed in all simulations to compute required coefficients for the reconstruction step. Utilizing truncated basis results in a compressed reconstructed version of known permeability maps.

Figures 4.5a and 4.8a show that HOSVD not only outperforms classic SVD in the measure of RMSE, but also overcomes it in perceptual sense. One can see that HOSVD-based parameterization is able to better capture the high and low permeability edges comparing to the SVD-based method. It is evident from the results that HOSVD-ALS has a promising power to compress an image while preserving geological features along with spacial characteristics of permeability maps. In addition to preserving the most important features, the low computational cost is the other significant capability of HOSVD. In fact, in practical reservoir parameterization problems with system of order of millions, low computational cost and the ability to reduce to a lower rank become important. Eager reader can refer to [1, 2] for more detailed analysis and discussion about the capabilities of HOSVD parameterization.

Figures 4.5b and 4.8b demonstrate bottom hole pressure curves for the injector. One could undoubtedly see that for the first sample classic SVD curve can not follow

the trend of original response of the system and for the second sample the HOSVD method response lay exactly on the original response. Actually, performing HOSVD-based parameterization yields better reduced order versions perceptually and in terms of RMSE and generates similar responses to that of original maps as well.

Comparing oil production rate curves in Figs. 4.6 and 4.9 illustrate the advantage of using HOSVD over the classic SVD even more particularly for the second sample that the SVD response could not follow the trend of original response correctly. For instance,in the producers 2 and 4 in Fig. 4.9 and producer 2 in Fig. 4.6, the SVD-based results are way off in values and trend comparing to those of original and HOSVD-based. Figures 4.7 and 4.10 present water production rates as well. Interestingly, in producer 2, the SVD based parameterization method causes a breakthrough while in the original response no breakthrough happens during the simulation time in that specific producer and one can see that the HOSVD curve exactly fit to the true system response as expected.

An important characteristic of a powerful compression method for reservoir history matching is the capability of the basis to reconstruct an unknown image with optimum coefficients. Moreover, in the present experiments, basis are obtained using prior knowledge of reservoir permeability. In other words, we use a set of training samples to compute required set of basis that is necessary for reconstruction and estimation part. As mentioned before, we repeated experiment for all samples to validate our results and corresponding RMSE PDFs are discussed in the next subsection. Here, we presented two randomly selected samples to compare the results.

In order to statistically demonstrate the advantage of HOSVD over SVD we applied both methods to 1000 permeability samples. Also, we repeated the forward reservoir simulation for all 1000 permeability samples to perform statistical analysis for comparing the performance of HOSVD-based and classic SVD-based parameter-

ization. Figure 4.11 which includes permeability RMSE PDFs clearly shows that HOSVD results in considerably less reconstruction error than SVD in the parameterization process. This convey the fact that HOSVD-ALS has a promising power to compress an image while preserving geological features along with spatial characteristics of the permeability map. Figure 4.12 express the probability density function of total dimensionless observation RMSE using the results of all 1000 forward simulations. Statistics of these PDFs are concluded in table 4.2. It should be noted that 90% of total dimensionless observation RMSE values lay within the shown interval in Fig. 4.12.

4.5.3 Experiment B-2: SPE10 Model

To probe the advantages of the proposed HOSVD parameterization method, we employ the top 5 layers of SPE 10 benchmark [37]. Analogous to the synthetic model, two-point geostatistical simulation algorithm is utilized to generate 1000 permeability realizations. Here, to represent the geological structure, we incorporated patterns from top 5 layers of SPE 10 to an exponential variogram model with correlation length properties equal to 100 and 80 in the x and y directions, respectively. Moreover, a proper permeability covariance matrix is assumed in order to assure each map includes the desired permeability range in the top 5 layers of SPE 10 model. Each permeability realization is a $60 \times 220 \times 5$ map of $33 \times 33 \times 33$ feet grid block size. We run ECLIPSE reservoir simulator for a **3D two-phase** (oil and water) black oil during 360 days or 6 time intervals of 60 days. All the simulation setup and parameterization procedure are done in a similar fashion to the synthetic example. Again, we conducted three distinct sets of forward simulation experiments for original, classic SVD, and HOSVD parameterized maps. Two randomly drawn true permeability

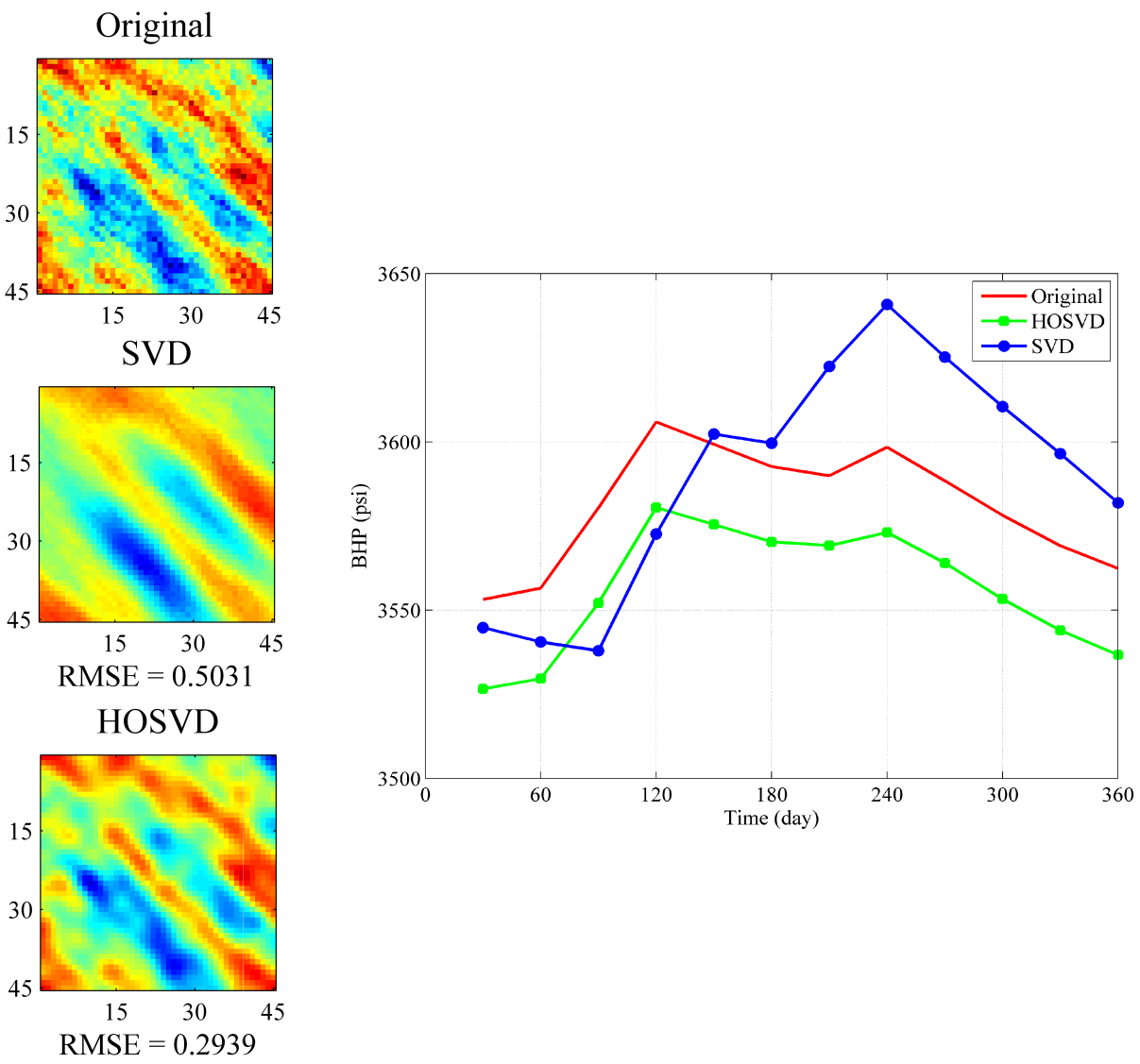

Figure 4.5: First permeability sample along with its reconstructed versions by SVD and HOSVD.

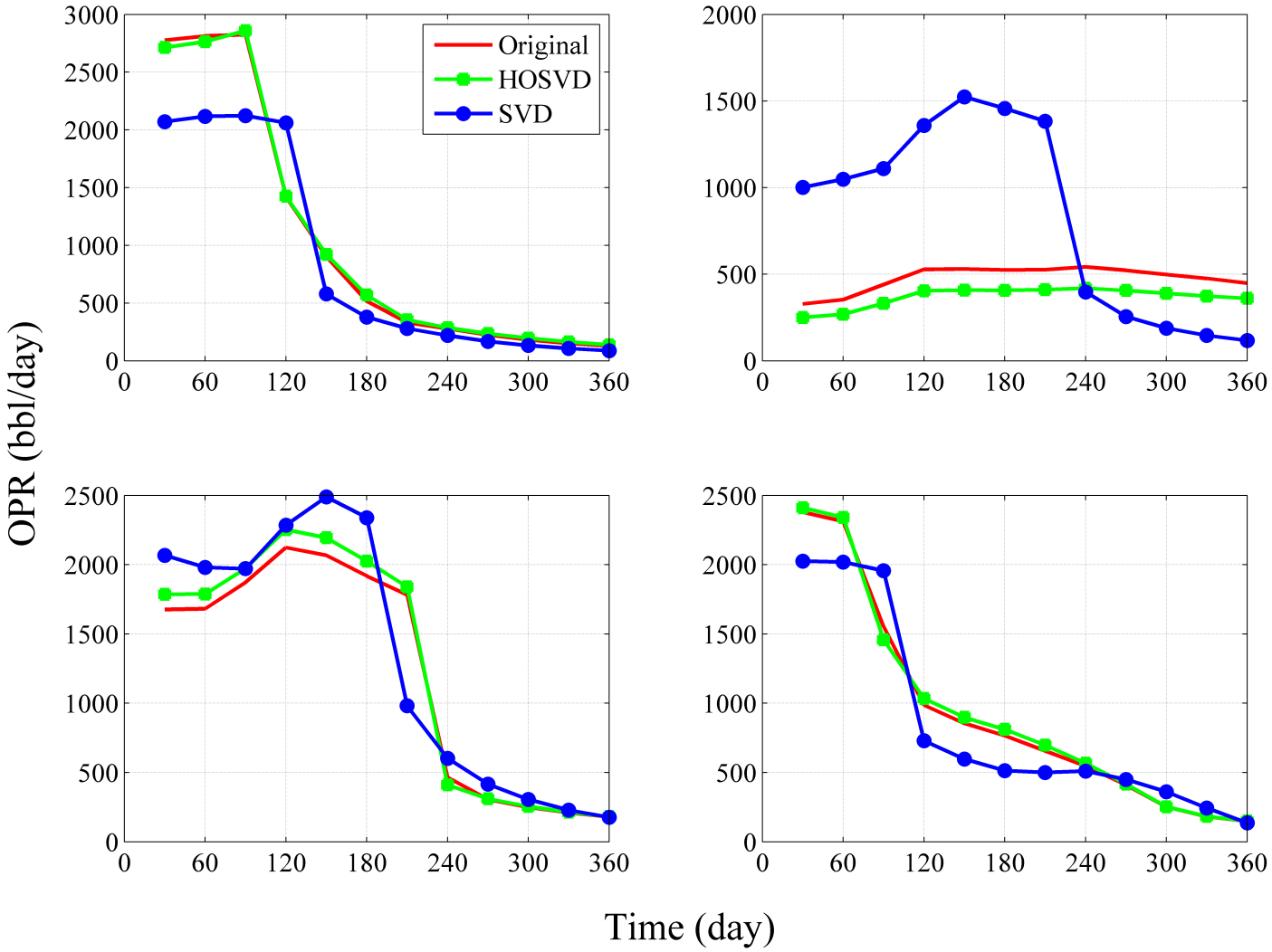

Figure 4.6: Oil production rate curves of all producing wells for the first sample. System responses are plotted for original map, classic SVD and HOSVD based parameterized maps.

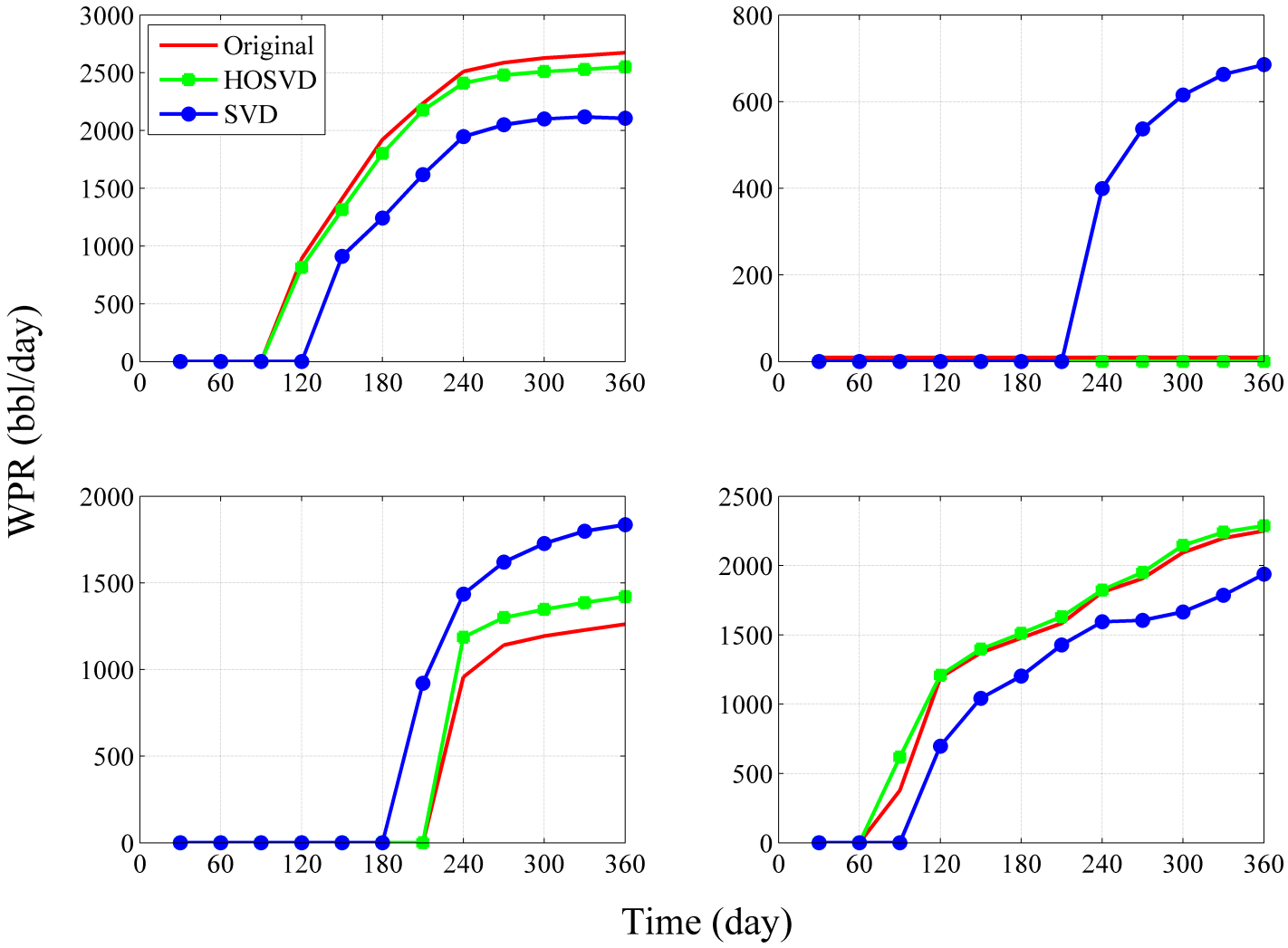

Figure 4.7: Water production rate curves of all producing wells for the first sample. System responses are plotted for original map, classic SVD and HOSVD based parameterized maps.

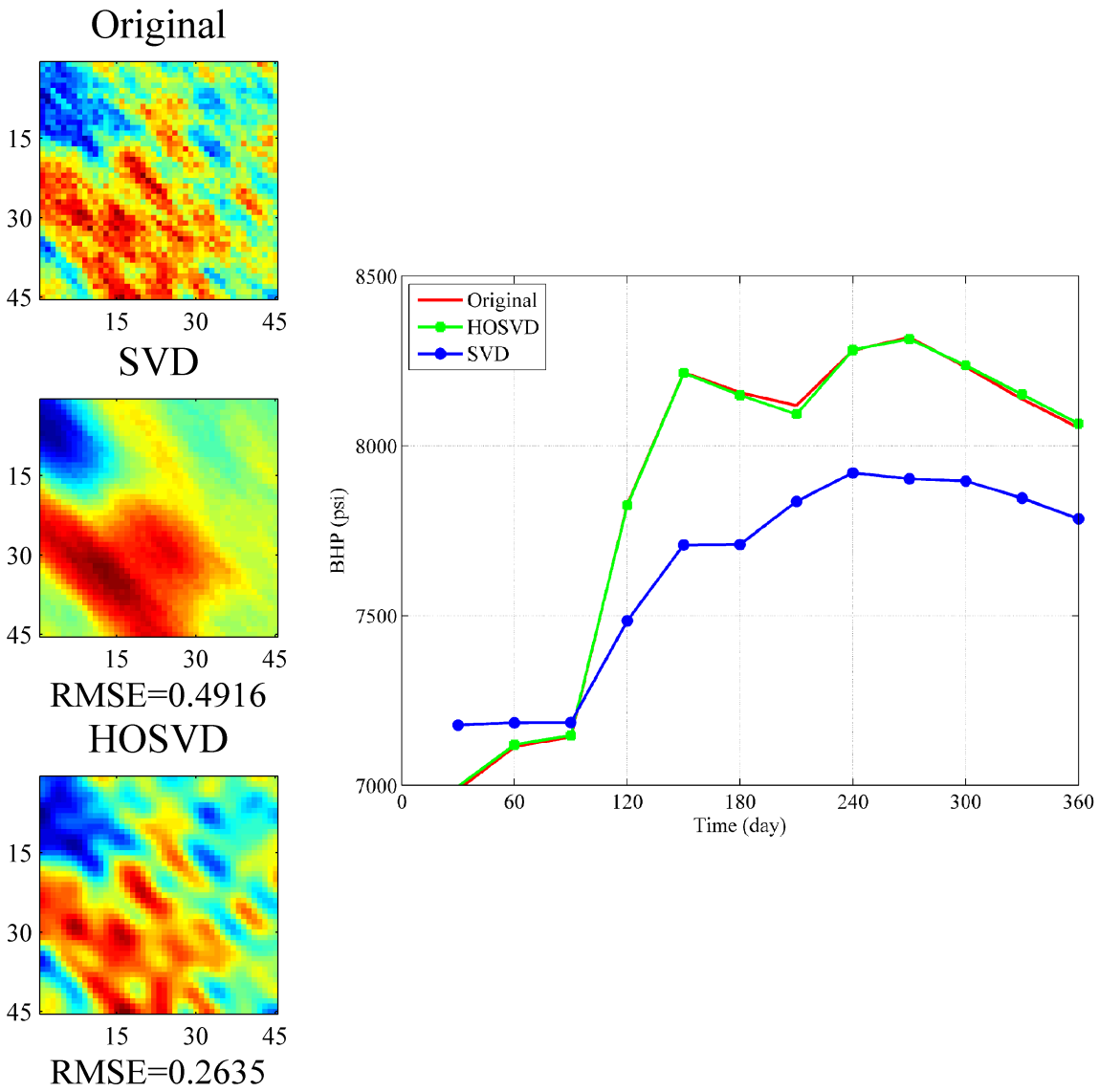

Figure 4.8: Second permeability sample along with its reconstructed versions by SVD and HOSVD.

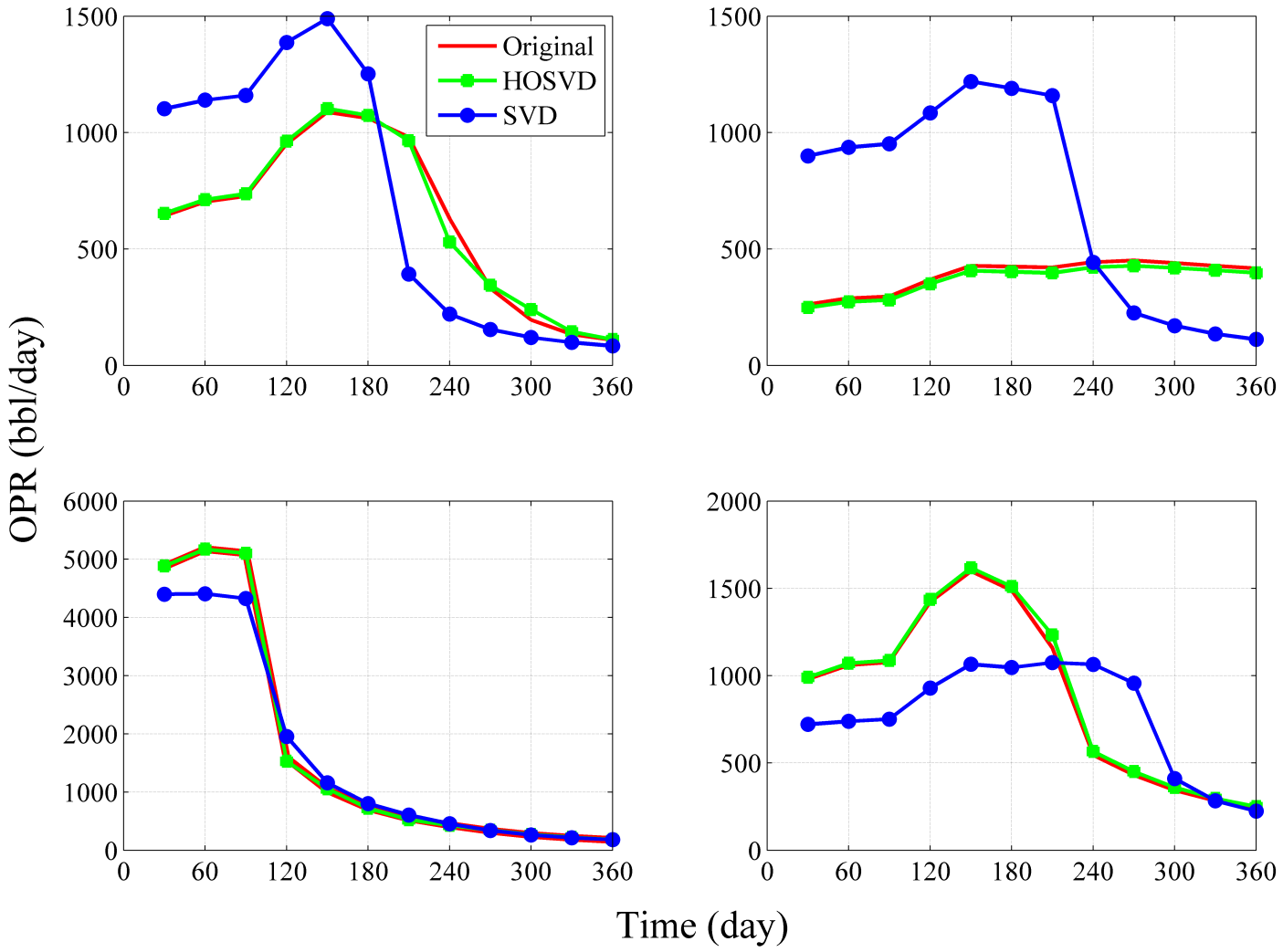

Figure 4.9: Oil production rate curves of all producing wells for the second sample. System responses are plotted for original map, classic SVD and HOSVD based parameterized maps.

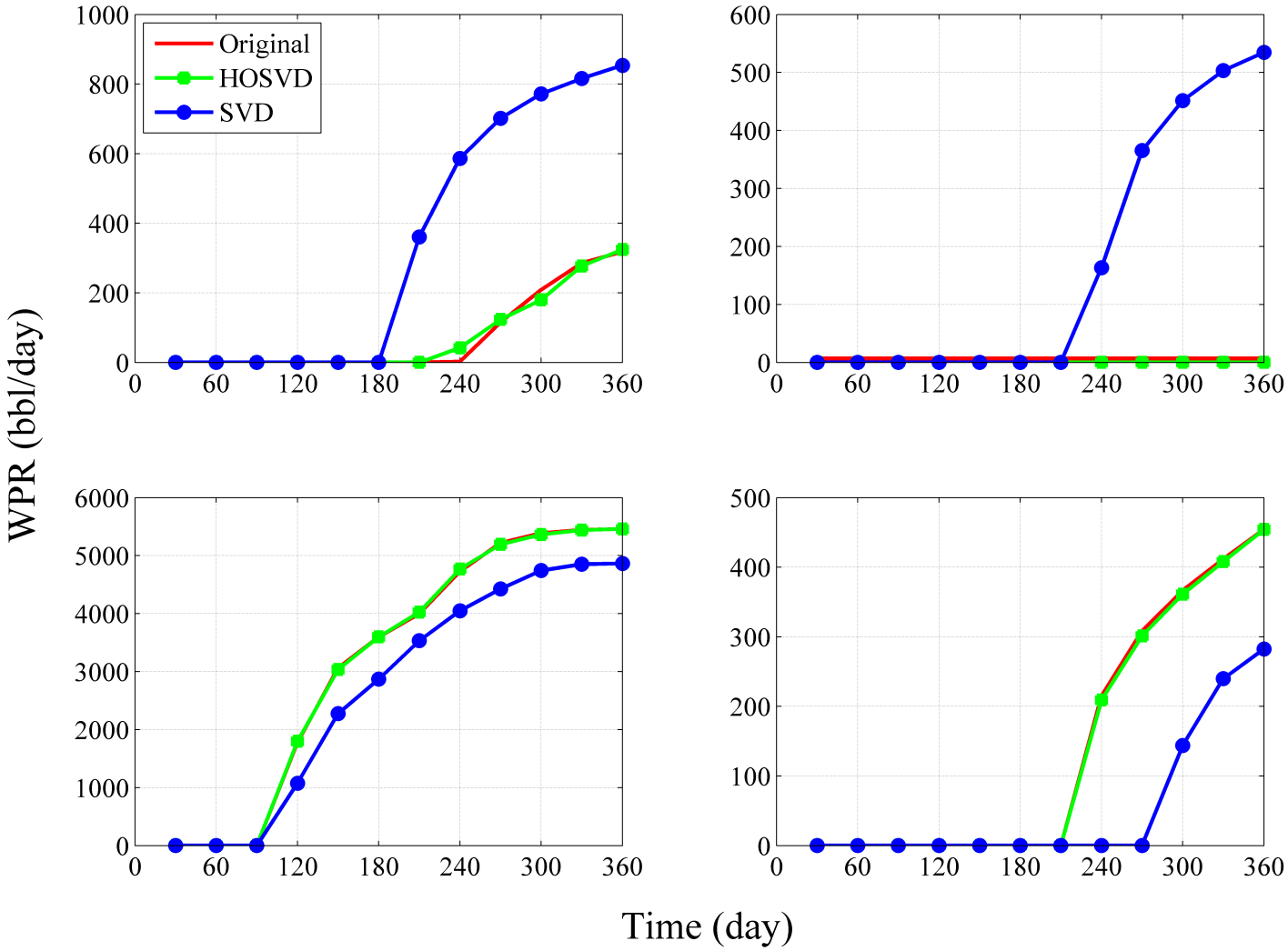

Figure 4.10: Water production rate curves of all producing wells for the second sample. System responses are plotted for original map, classic SVD and HOSVD based parameterized maps.

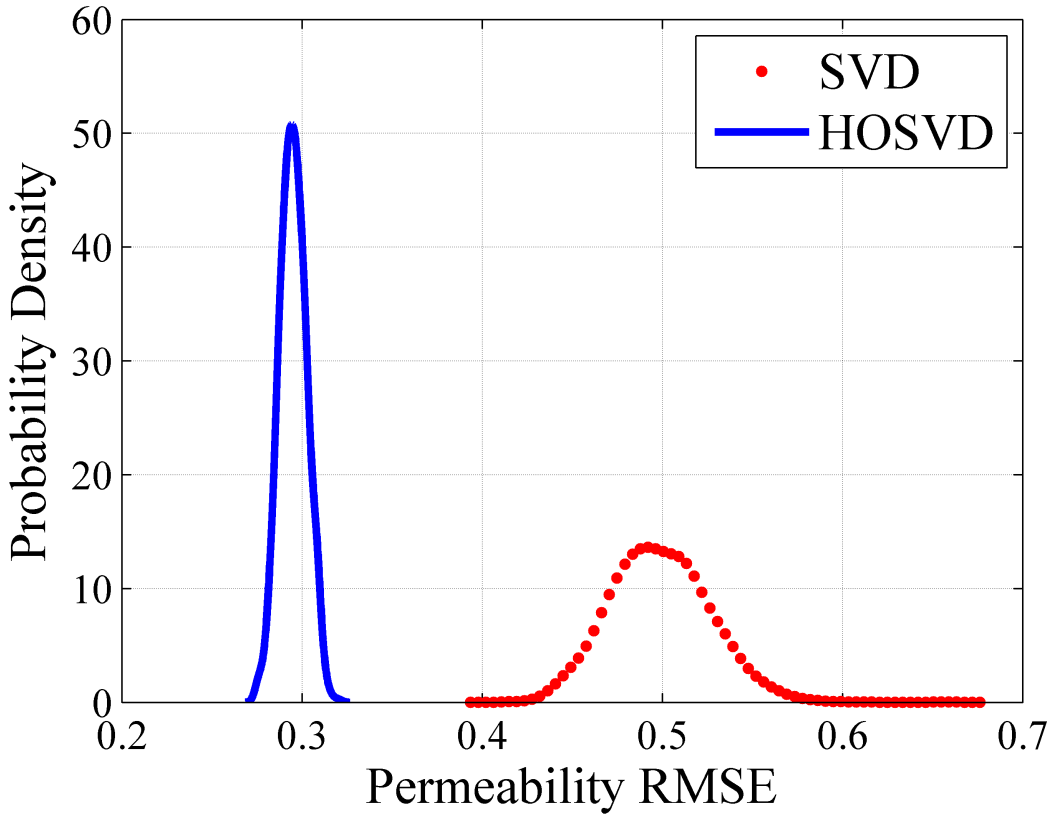

Figure 4.11: PDFs of permeability RMSE for SVD and HOSVD; The synthetic 45×45 example.

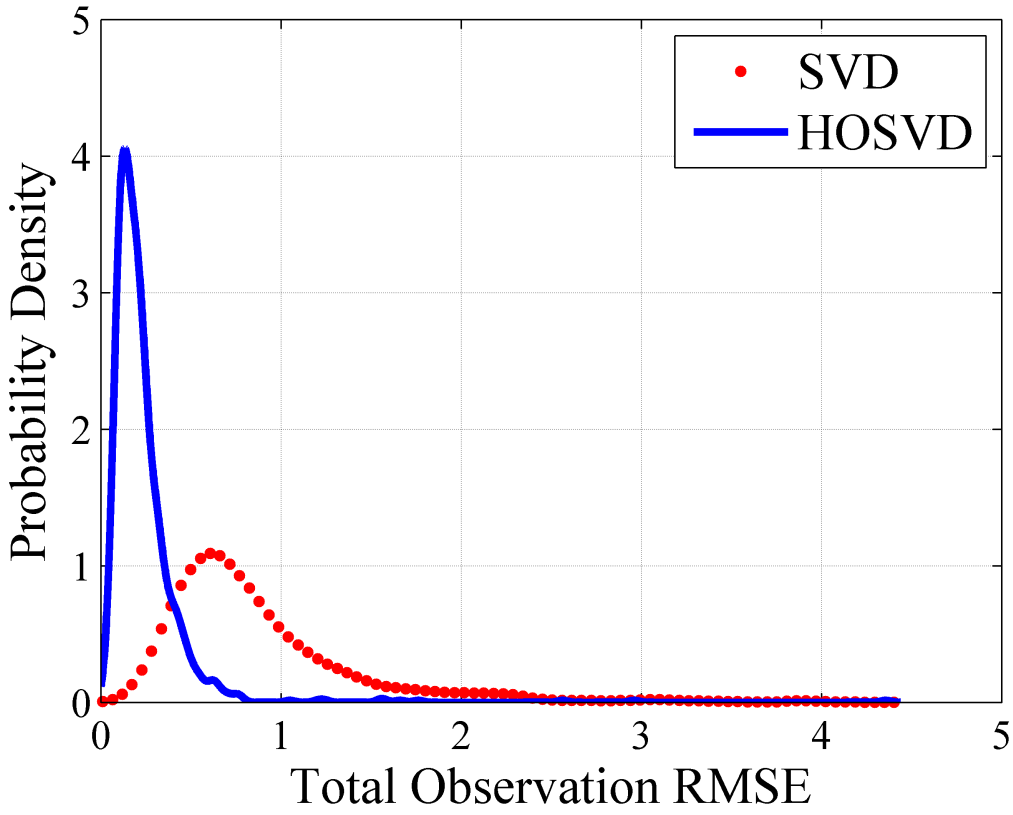

Figure 4.12: PDFs of total dimensionless observation RMSE for SVD and HOSVD. The synthetic 45×45 example.

realizations along with corresponding reduced ordered representatives using classic SVD and HOSVD are shown in Figs. 4.13 and 4.17. Eight producers are operating along with 15 injectors constructing a network of eight inverted 5 spot configuration all in a waterflooding scenario. As stated previously, porosity is not reparameterized in this work and therefore is fixed at 0.22. Furthermore, 1 pore volume of water is injected through the simulation time of 6 year. Table 4.1 summarizes all information regarding simulation description and reservoir specifications for both experiments.

Even with small number of significant coefficients, large scale features and high/low permeability regions are preserved in reconstructed replicates compared to the true permeability maps. Although HOSVD has a higher overhead in terms of basis computations, it yields models with higher compression ratios, and thus, lower computational cost for using the reduced models.

Table 4.1: Reservoir description and fluid properties for experiments 1 and 2.

Property	**45x45**	**SPE 10**
Simulation	Two-phase	Two-phase
Simulation Time	1×360 day	6×360 day
Number of grid blocks	45×45	$60 \times 220 \times 5$
Grid block size	$30 \times 30 \times 30\ ft$	$33 \times 33 \times 33\ ft$
Porosity	$0.22\ uniform$	$0.22\ uniform$
Rock compressibility	$3.0E-6\ psi^{-1}$	$3.0E-6\ psi^{-1}$
Reservoir geometry	2D	3D
Reservoir depth	$2000\ ft$	$4000\ ft$
Number of injectors	1	15
Number of producers	4	8
Oil Viscosity	$1\ cp$	$1\ cp$
Oil density	$62.4\ \frac{lb}{ft^3}$	$62.4\ \frac{lb}{ft^3}$
Water Viscosity	$1\ cp$	$1\ cp$
Initial reservoir pressure	$3100\ psi$	$6000\ psi$
Producers constant BHP	$2900\ psi$	$5900\ psi$
Water saturation	0.3	0.3

Figures 4.13-4.22 summarize all results for two randomly picked replicates of SPE 10 ensembles. We plotted bottom hole pressure for 9 selected injectors and oil and water production rates for 6 producers for the sake of simplicity to compare results and values for these two representative samples. The two permeability maps have both low and high permeability regions. With respect to trend, the first sample has

a significant high perm region in the middle of the map; However, the second one has two distinct high perm regions at the sides and near the boundaries along with a recognizable low perm area at the middle. Overall, the first permeability sample has a more complex trend comparing to the second one.

Similar to the synthetic example, Figs. 4.13 and 4.17 illustrate that HOSVD not only outperforms SVD in terms of permeability RMSE, but also overcomes it in perceptual sense. Moreover, the capability of reducing rank in all modes is assisting HOSVD to become more efficient than SVD in the manner of memory and computational costs as well even more than the previous example due to the higher dimension nature of the second example. Figures 4.14 and 4.18 show the bottom hole pressure curves for the original samples and corresponding HOSVD-based and SVD-based reparameterize versions. In all injectors the corresponding results of HOSVD-based parameterization tends to follow the trend of original response both in shape and values. Furthermore, for the first sample, in injector number $3, 12$ and 13 the HOSVD response perfectly fits to the true response. For the second sample, one easily could see the same trend and perfect fit in more injectors due to lower complexity of permeability map. In fact, it is obvious from the results that utilizing HOSVD-based parameterization not only result in better reduced order versions perceptually and in terms of RMSE, but also produces similar responses to that of original maps which is more important for our purpose.

Oil production rates are depicted in figures 4.15 and 4.19. One can simply compare the HOSVD method results with that of SVD method. Again, it is apparent form the results that even for the simpler permeability map with a non-complex trend, HOSVD-based parameterization curves outperforms those of classic SVD parameterization. For instance,in the producers 1, 2 and 7 for the first case and 2, 5, 6, and 7 for the second case, the SVD-based results are way off in values and trend

comparing to those of original and HOSVD-based. Figures 4.16 and 4.20 display water production rate curves as well. In contrast to the first example, we do not observe breakthrough in any of the producers during the simulation period. Although, no breakthrough happened in the experiments, the difference between HOSVD and classic SVD is noticeable specifically for more complex trends in permeability maps.

As mentioned previously, in order to statistically demonstrate the advantage of HOSVD over SVD we applied both methods to 1000 permeability samples. Also, we repeated the forward reservoir simulation for all 1000 permeability samples to perform statistical analysis for comparing the performance of HOSVD-based and classic SVD-based parameterization. Figure 4.21 which includes permeability RMSE PDFs clearly shows that HOSVD results in considerably less reconstruction error than SVD in parameterization process. Which clearly convey the fact that HOSVD-ALS has a promising power to compress an image while preserving geological features along with spacial characteristics of permeability map. Figure 4.22 express the probability density function of total dimensionless observation RMSE using the results of all 1000 forward simulations. Statistics of these PDFs are concluded in Table 3. It should be noted that 90% of total dimensionless observation RMSE values lay within the shown interval in Fig. 4.22. As matter of fact, the advantage of HOSVD over SVD in terms of system response and reconstruction capability are also illustrated by Figs. 4.21 and 4.22 and table 4.2.

Table 4.2: Error distribution statistical parameters summary for the experiments.

Method		Mean	Median	Mode
45x45	HOSVD	14.3467	0.1919	0.132
	Classic SVD	77.5178	0.7971	0.6154
SPE 10	HOSVD	0.3437	0.3274	0.3232
	Classic SVD	0.7382	0.7204	0.6873

4.6 Running Time Comparison

Comparison between classic SVD and HOSVD with respect to running time is of high importance in order to evaluate their performance as well as their efficiency. As mentioned previously, we generate two ensemble of 1000 permeability realizations employing two-point geostatistical simulation algorithm (SGSIM) and an exponential variogram with specific assumed covariance and correlation parameters. It should be noted that variogram properties are set independently for 45×45 and SPE 10 cases. In order to perform the present simulations, all 1000 samples in each ensembles are considered as training sets of known permeability maps. Then, we apply classic SVD and HOSVD based parameterization method to the ensembles and observe running time of each scheme first for computing basis and coefficients of the parameter space and second for compression process (reducing the order of each map). The results are summarized in the table 4.3. One must note that for SPE 10 example we repeated the noted process for each layers of each realization separately and independently and then the mean of all running times is reported to acquire statistical consistency. Results show that HOSVD method outperforms classic SVD with respect to run time

in computing the basis and coefficients as well as reconstructing step. Considering the fact that running time for classic SVD is roughly 10 times that of HOSVD in an experiment of lower dimensionality comparing to a real reservoir problem, the HOSVD has a promising performance concerning running time efficiency.

Table 4.3: Running time comparison between HOSVD and classic SVD (in seconds).

Method	**Computing Time**	**Reconstructing Time**
HOSVD	2.0639	37.1983
Classic SVD	39.5381	456.4611

4.7 Summary

The results of this experiments illustrate the promising power of HOSVD-ALS to compress known permeability realizations. Furthermore, the results are compared to classic SVD approach. In addition to the compressing capability, this section indicates that HOSVD-ALS can successfully estimate unknown permeability maps utilizing truncated basis obtained from prior knowledge. Although, classic SVD has lower root mean square error in comparison to HOSVD-ALS, it has a poor perceptual quality. Furthermore, the approach employed in the present section can strongly capture all important spatial features and all spatial geological characteristics in an efficient manner. As a matter of fact, classic SVD cannot preserve spatial features due to the snapshots vectorization. In conclusion, the present work shows that HOSVD-ALS provides a mean for permeability parameterization in reservoir characterization required for history matching processes.

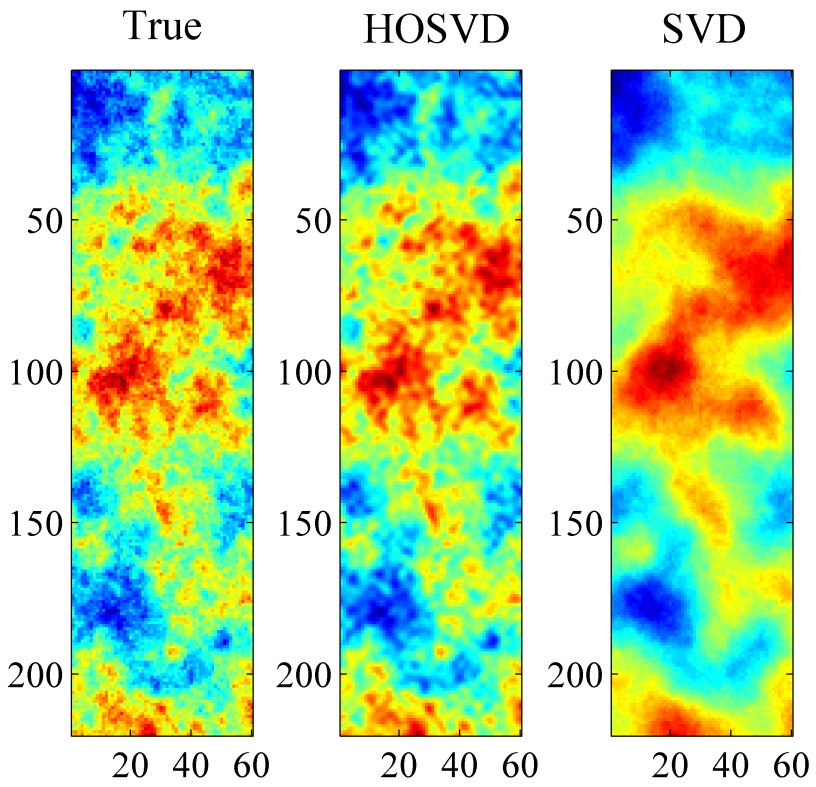

Figure 4.13: First permeability sample along with its reconstructed versions by SVD and HOSVD. SPE 10 example.

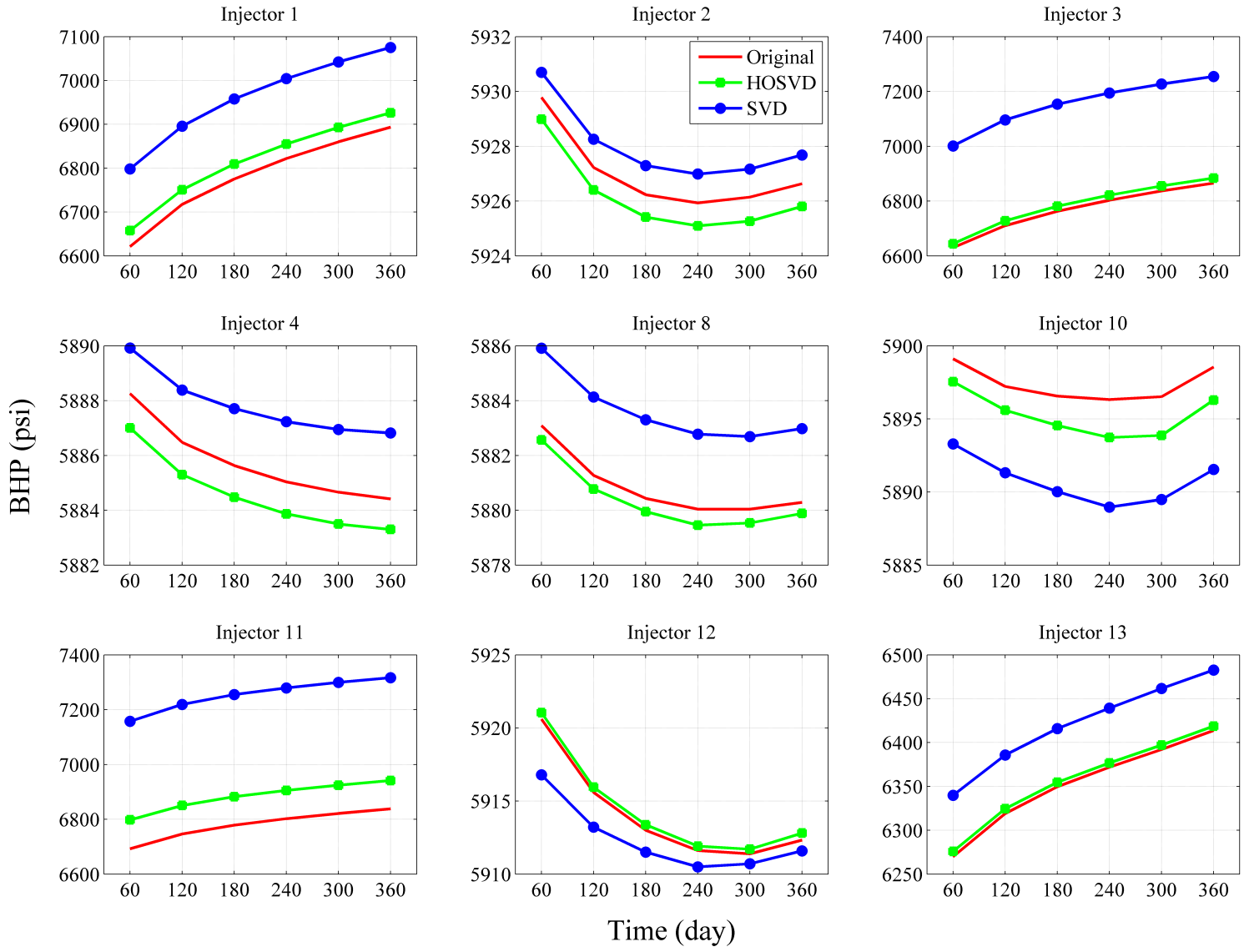

Figure 4.14: Bottom hole pressure curves of all injectors for the first sample. System responses are plotted for original map, classic SVD and HOSVD based parameterized maps.

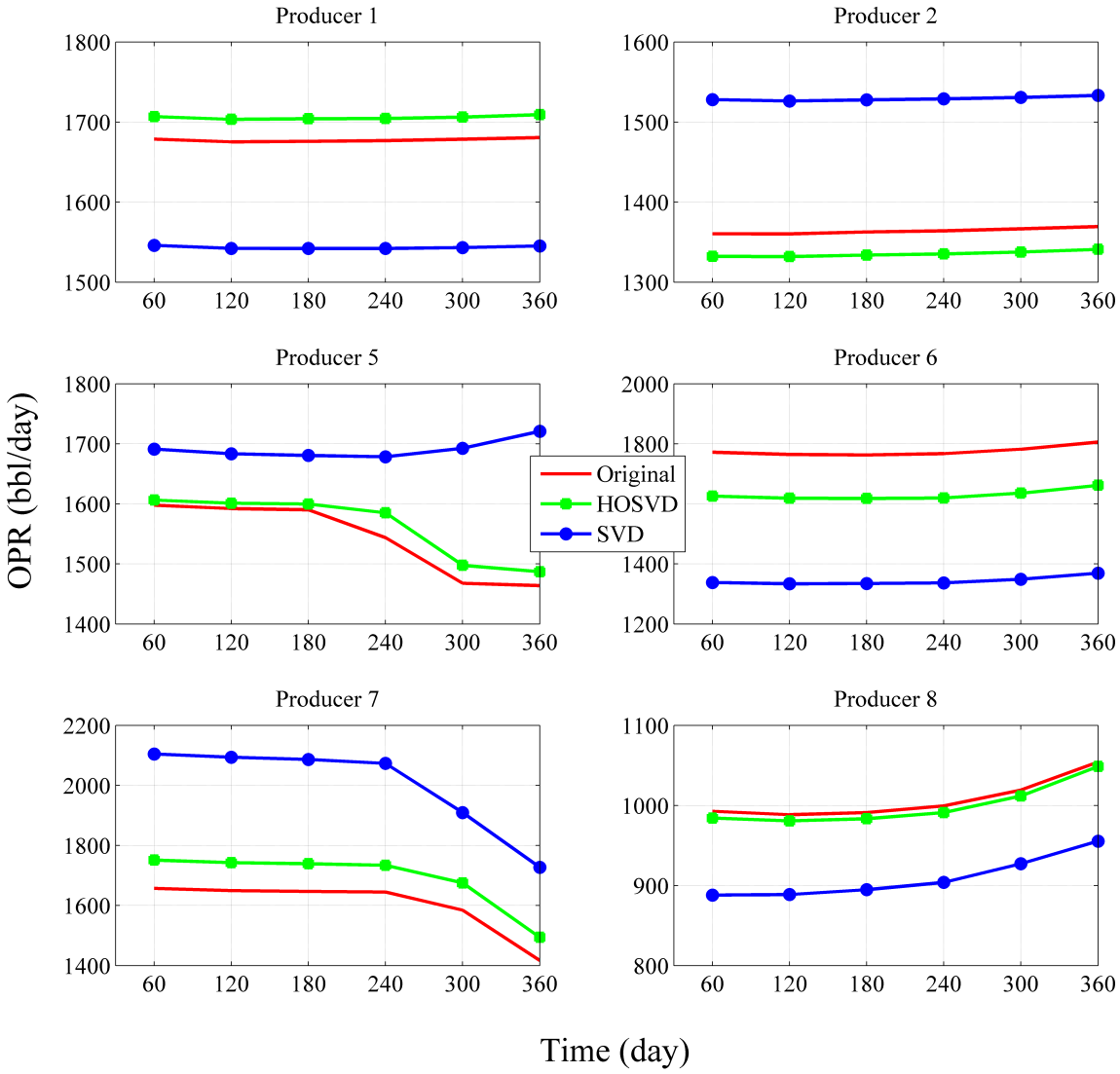

Figure 4.15: Oil production rate curves of all producers for the first sample. System responses are plotted for original map, classic SVD and HOSVD based parameterized maps. SPE10 example.

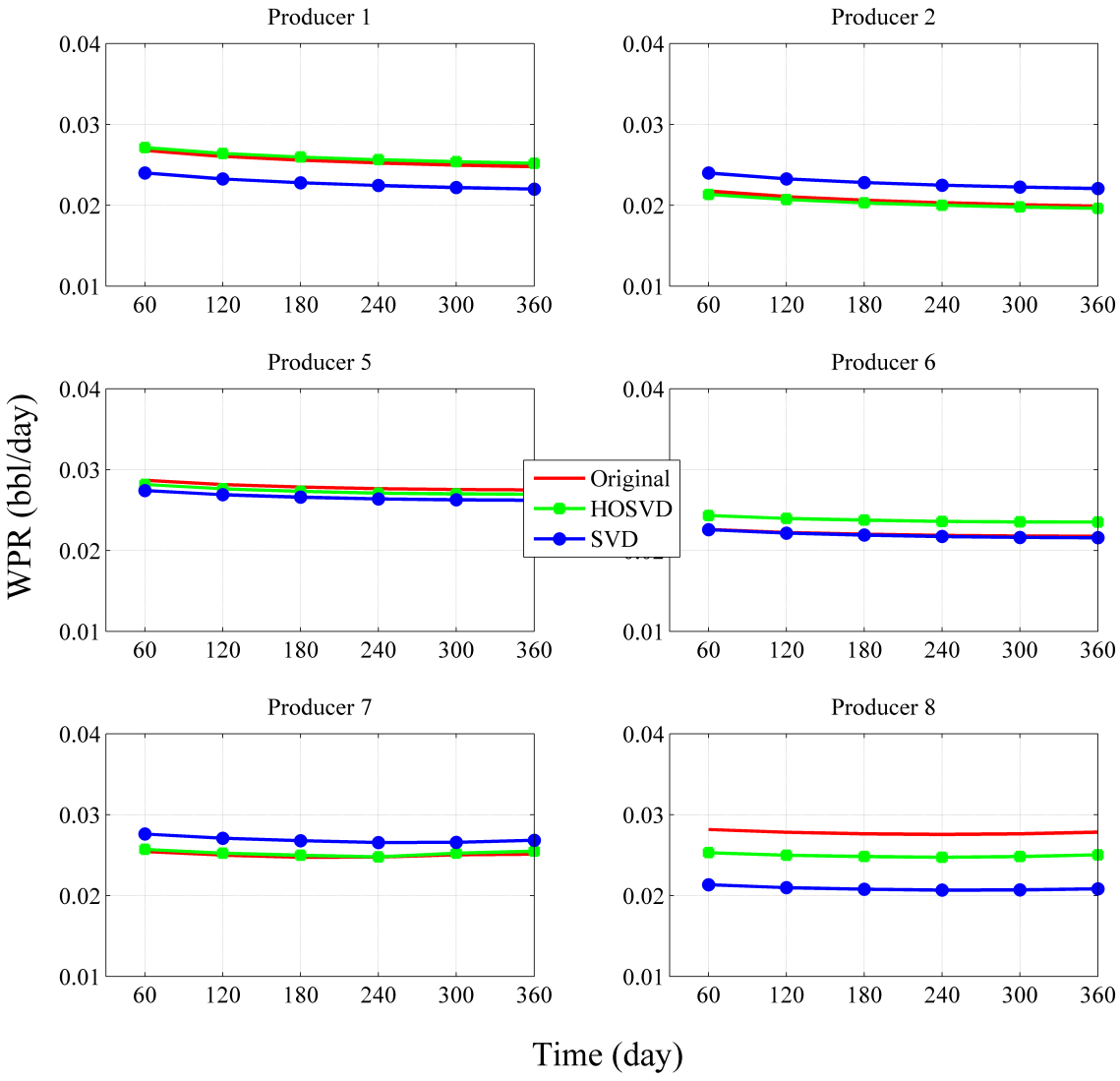

Figure 4.16: Water production rate curves of all producers for the first sample. System responses are plotted for original map, classic SVD and HOSVD based parameterized maps. SPE10 example.

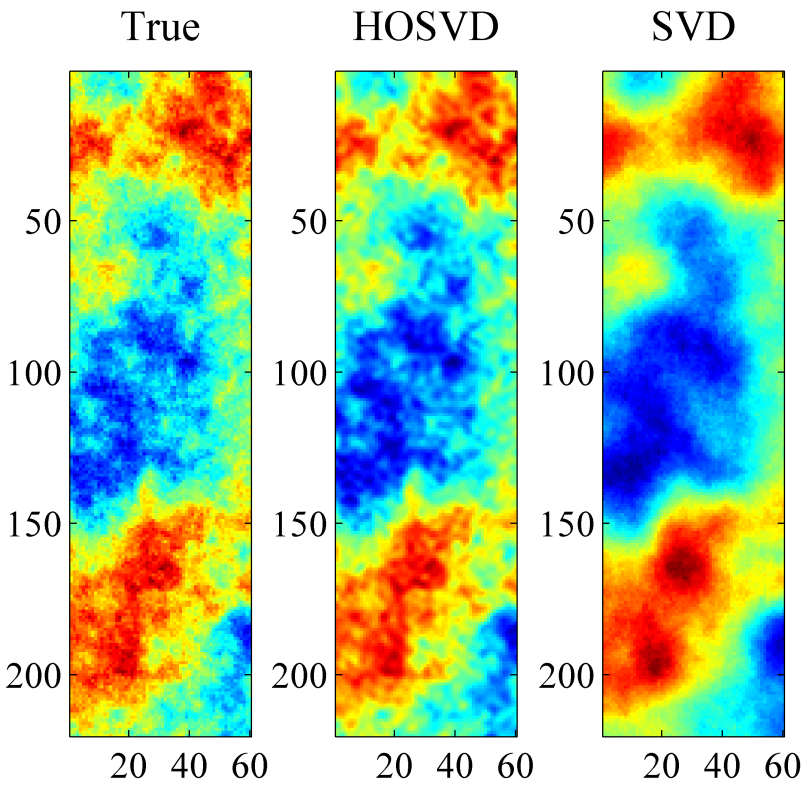

Figure 4.17: Second permeability sample along with its reconstructed versions by SVD and HOSVD. SPE 10 example.

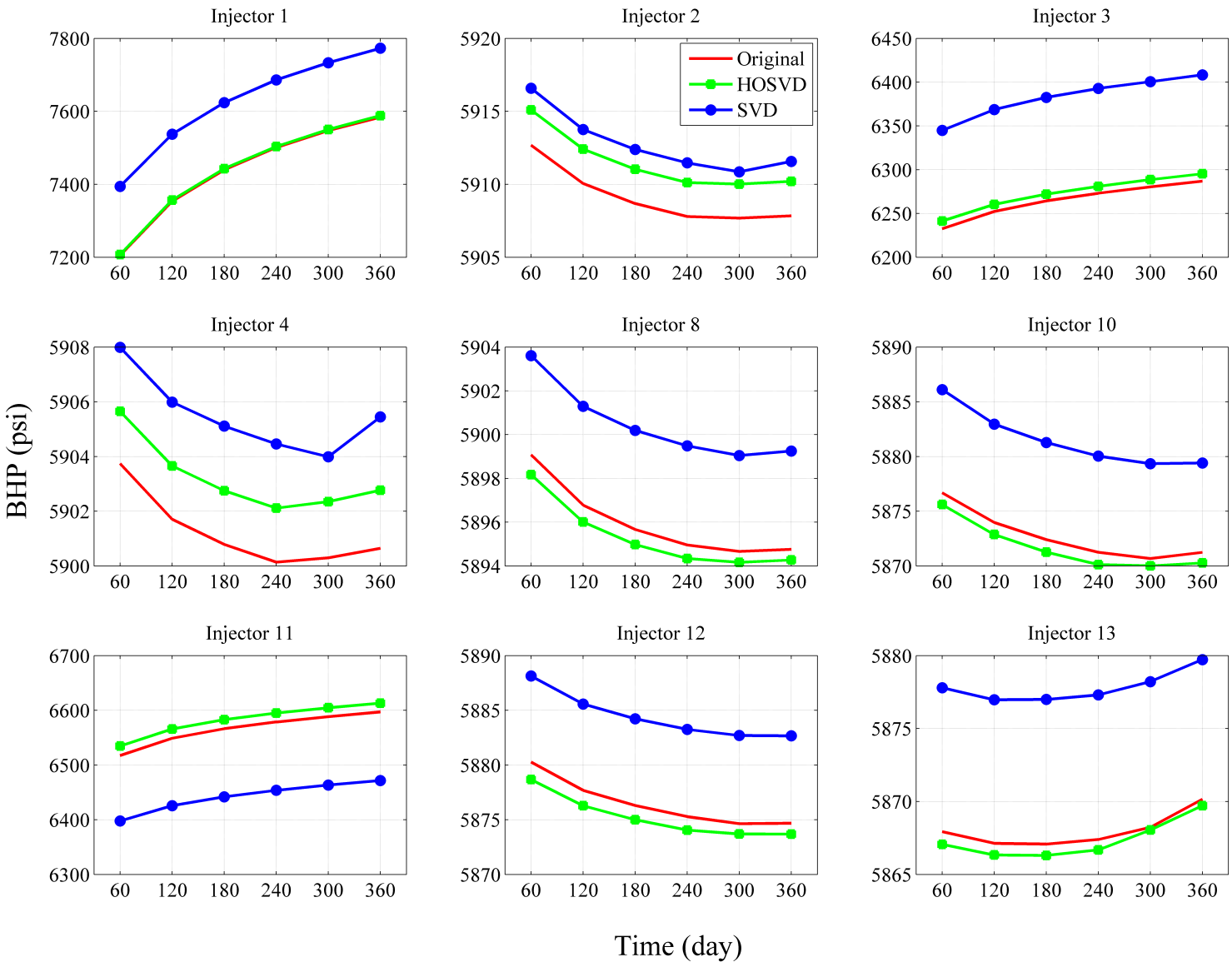

Figure 4.18: Bottom hole pressure curves of all injectors for the second sample. System responses are plotted for original map, classic SVD and HOSVD based parameterized maps. SPE10 example.

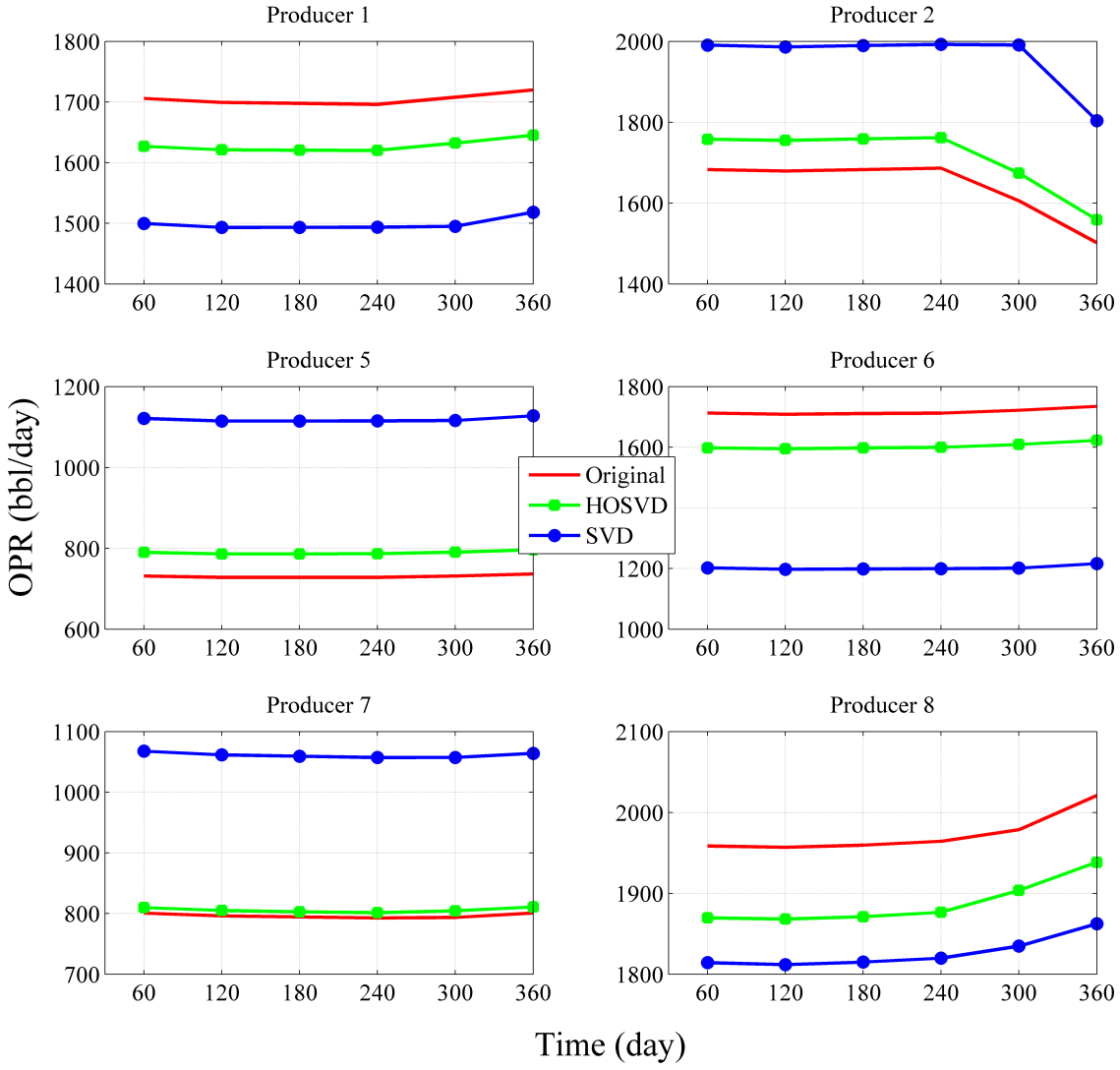

Figure 4.19: Oil production rate curves of all producers for the second sample. System responses are plotted for original map, classic SVD and HOSVD based parameterized maps. SPE10 example.

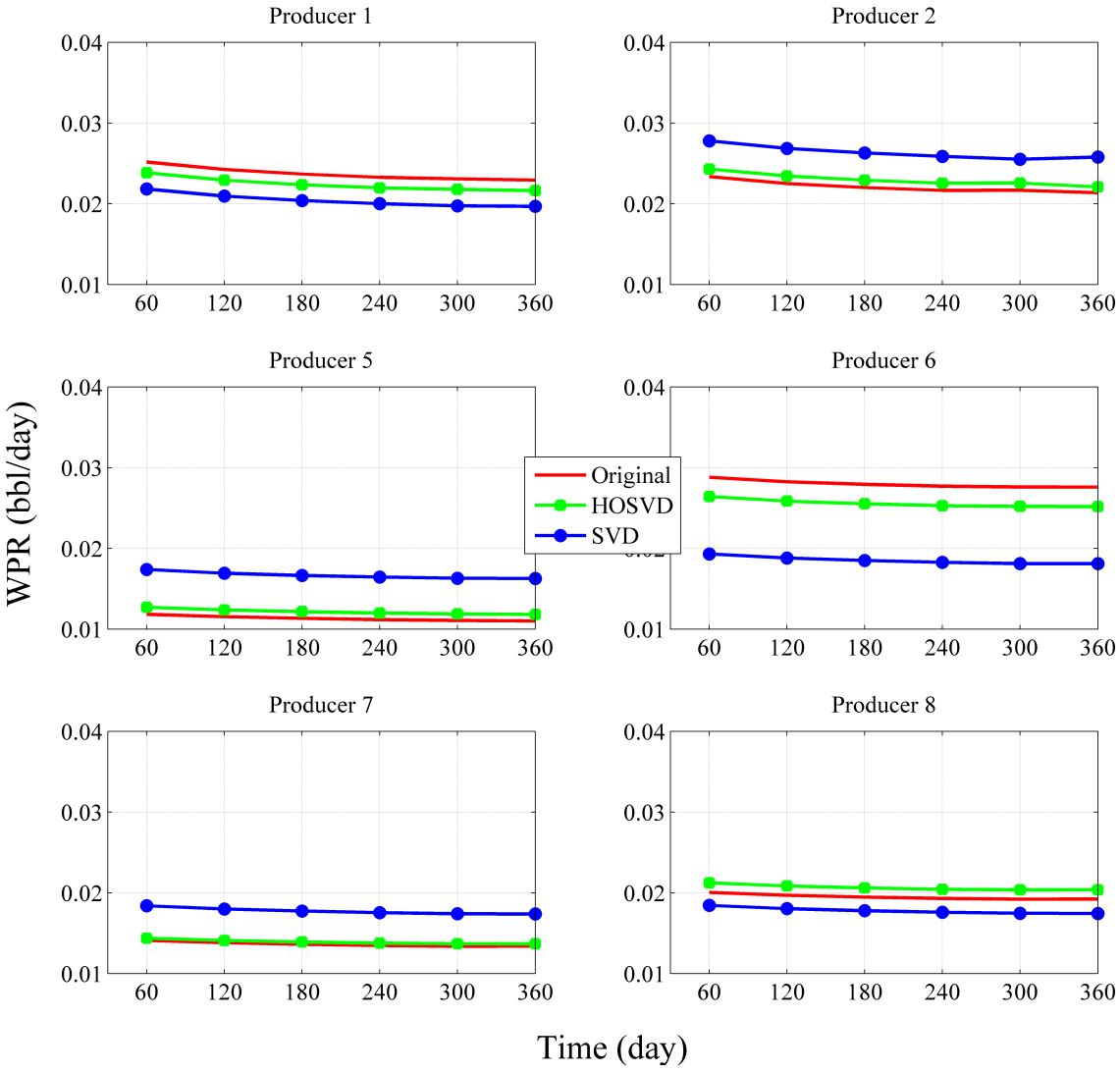

Figure 4.20: Water production rate curves of all producers for the second sample. System responses are plotted for original map, classic SVD and HOSVD based parameterized maps. SPE10 example.

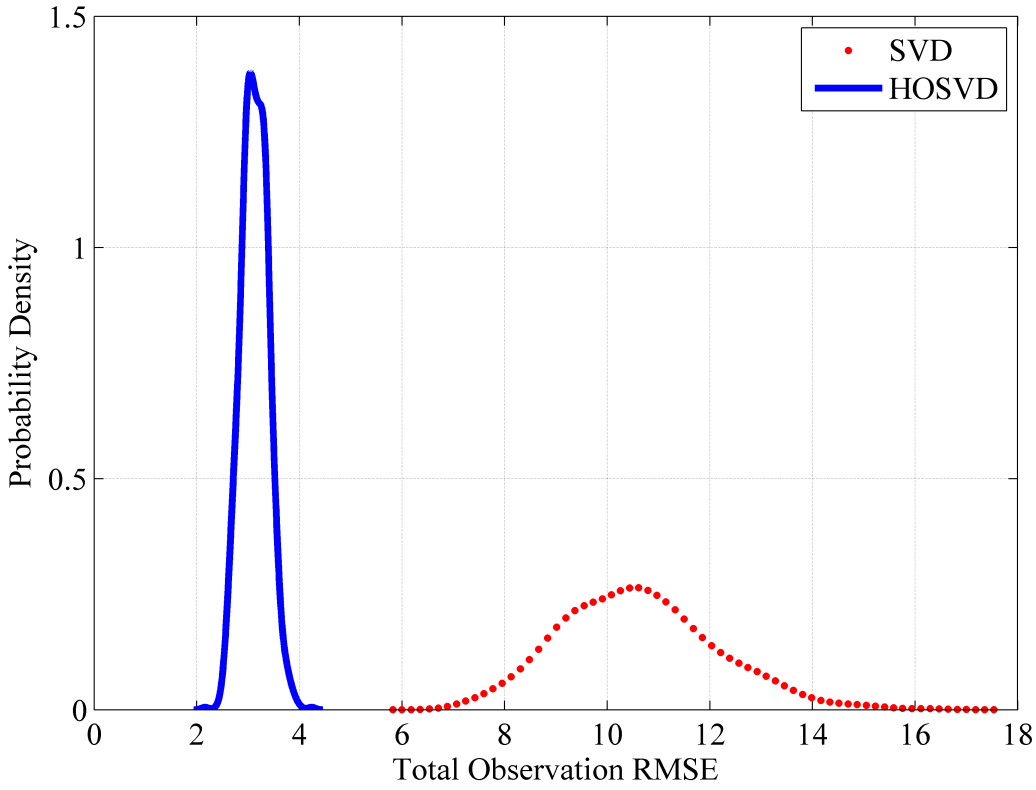

Figure 4.21: PDFs of permeability RMSE for SVD and HOSVD. SPE 10 example.

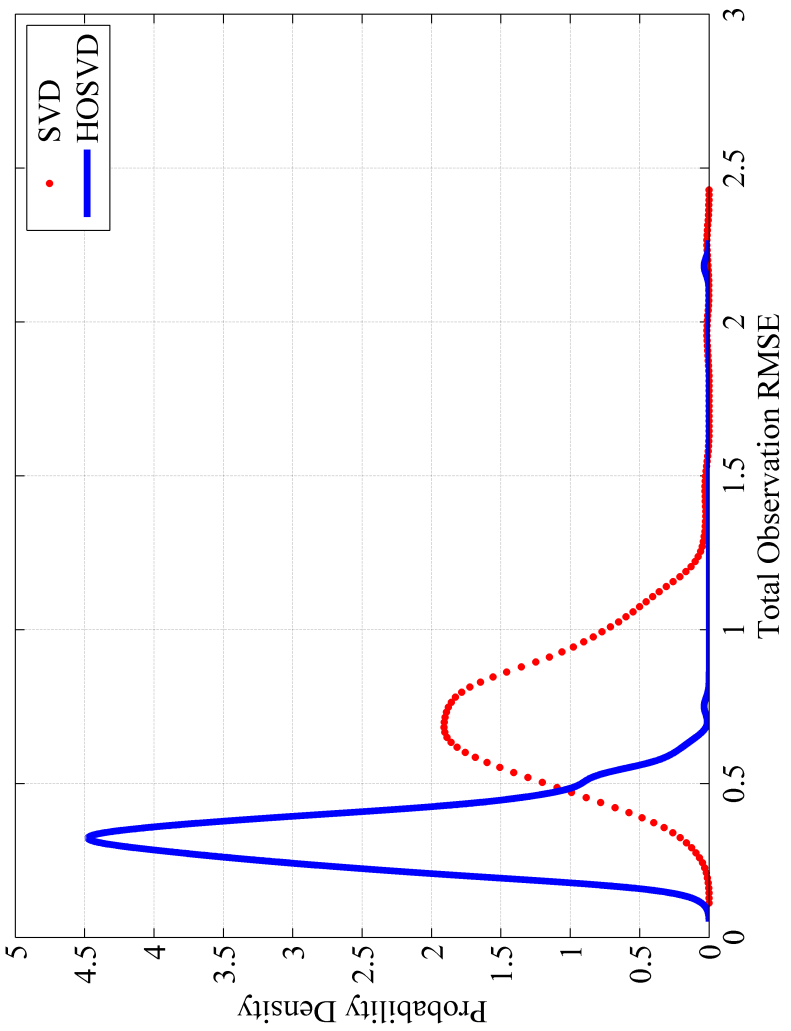

Figure 4.22: PDFs of total dimensionless observation RMSE for SVD and HOSVD. SPE 10 example.

5. EFFICIENT INFERENCE OF RESERVOIR PARAMETER DISTRIBUTION UTILIZING HIGHER ORDER SINGULAR VALUE DECOMPOSITION REPARAMETERIZATION*

Reservoir parameter inference is a challenging problem to many of the reservoir simulation workflows, especially when it comes to real reservoirs with high degree of complexity and non-linearity, and high dimensionality. In a history matching problem that adapts the reservoir properties grid blocks, the inverse problem leads to an ill-posed and very costly optimization schemes. In this case, it is very important to perform geologically consistent reservoir parameter adjustments as data is being assimilated in the history matching process. Therefore, ways to reduce the number of reservoir parameters need to be sought after. In this section, we introduce the advantages of a new parameterization method utilizing higher order singular value decomposition (HOSVD) which is not only computationally more efficient than other known dimensionality reduction methods such as, SVD and DCT, but also provides a consistent model in terms of reservoir geology. HOSVD power is due to its ability to supply a reliable low-dimensional reconstructed model while keeping higher order statistical information and geological characteristics of reservoir model. In HOSVD, we take the snapshots in a 2D or 3D approach, i.e., do not vectorize original replicates, and stack them up into a tensor form, i.e. a multi-way array in multilinear algebra which leads to implementing tensor decomposition. Technically, we performed HOSVD to find the best lower rank approximation of this tensor that is an optimization problem utilizing alternating least square method. This results in a

*Part of the material is published with permission from "Efficient Inference of Reservoir Parameter Distribution Utilizing Higher Order Singular Value Decomposition Reparameterization," S. Afra, E. Gildin, 2014. ECMOR XIV-14th European conference on the mathematics of oil recovery, Sicily, Italy, Copyright 2014 by EAGE.

more consistent reduced basis. We applied this novel parameterization method to the SPE10 benchmark reservoir model to show its promising parameterization performance. We illustrate its advantages by comparing its performance to the regular SVD (PCA) in a history matching framework using EnKF, as well as characterization performance of the ensemble-based history matching approaches along with HOSVD. Overall, HOSVD outperforms SVD in terms of reconstruction and estimation performance.

5.1 Introduction

In recent years, reservoir management has evolve to a more structured workflow, in which one can optimize the reservoir production strategies and assimilate new production information, simultaneously basically in a real-time fashion. One of very interesting and challenging problems in reservoir engineering is to estimate petrophysical properties, such as permeability and porosity, by incorporating production history in an inverse process. Having an accurate geological descriptions of the reservoir model is of high importance for predicting future production profiles and decision strategies. Proposing accurate predictions for reservoir history matching problems is highly tied to the capability of data assimilation techniques that have been used as well as data collecting methods. Although, lots of different methods of collecting data and sensing observations can be conducted in field, their costs are still seen as the limiting factor in deploying them into the field and thus, lack of prior knowledge of the reservoir become a daunting challenge to be explored[12, 14, 60].

Several parameters describe a reservoir model which each of those parameters may convey a huge amount of data. Some parameters are specified per grid block like permeability and porosity and others for the entire model or a particular layer such as relative permeability and capillary pressure. History matching is a highly

underdetermined, nonlinear and ill-posed problem owing to insufficiency and complexity of observed data from reservoir [104, 60]. This means there is a possibility of obtaining reservoir models that match observed measurements but then provide incorrect predictions. Thus, another significant task in the reservoir characterization is reducing the number of unknown model parameters and/or states to improve the estimation results as well as decreasing the costs of operating history matching and data collecting methods.

A number of studies have been conducted to reduce computational efforts in reservoir simulation and history matching [67, 51, 22] and [1, 2, 64, 65]. Of especial interest in this section is to reduce the number of unknown parameters in a process known as parameterization [119, 99]. There is a great number of papers devoted to reducing the number of unknown parameters. They are broadly classified into spatial (e.g., zonation) and transform-domain (e.g., PCA, KPCA, DCT, HOSVD) methods [99]. Since, the central issue in this section is not to bring up a comprehensive assessment of all of these methodologies, we will pay attention here to only SVD-based (PCA) methods.

It is known that PCA does not provide an effective parameterization for complex geological structures, due mainly to its intrinsic two-point statistics nature [99]. In order to overcome this issue, Kernel PCA and other form of nonlinear versions of PCA have been developed [119]. Here, we will take a slightly different approach, which relies on "higher-order" statistics with the introduction of the High-Order Singular Value Decomposition (HOSVD) method [1, 2]. HOSVD is a multi-linear algebra-based approach and it has been developed in the context of images reduction [86, 90, 130]. In the standard PCA, it is necessary to carry out an eigen-decomposition of the random field covariance matrix which is expensive for large models. Furthermore, due to the vectorization of the snapshots data in the PCA computation, many features

may be lost in the reduced space [11, 86, 90]. This new method allows us to treat property ensembles as a high-dimensional tensor, and by means of tensor algebra (HOSVD) we can show that the reduced models preserve better geometric features keeping them more intact during the reduced basis computations. This is of great importance in the case of reservoirs as the properties in consideration have geological meaning.

We consider the problem of data assimilation using the Ensemble Kalman Filter [104], in such a way that the permeability of the reservoir is parameterized by the HOSVD. We compare with the standard SVD approach in terms of accuracy and computational efforts. As pointed out before, the we do not compare with other forms of discretization, and thus, the conclusions taken here should be considered within this context. A forthcoming paper is being developed in this area.

This section is organized as follows. In subsection 5.2 petroleum reservoir characterization, i.e., history matching problem, through ensemble Kalman filter (EnKF). Section 5.3 presents experiments description and provides more details on the underlying history matching process with and without incorporated reservoir parameterization. In subsection 5.4, experiments results are explained properly for 3 different history matching scenarios and then all results are compared with respect to the corresponding RMSEs. More details on EnKF can be found in subsection 3.9.

5.2 Reservoir Characterization Through Ensemble Kalman Filter

In the present work, we are interested in characterizing reservoir permeability map and assuming that porosity is a known parameter in the model. Thus, in order to perform the prediction step in EnKF scheme we simply run forward reservoir simulation using an ensemble of reservoir unknown permeability maps as simulator input. This ensemble of reservoir parameters can be initiated by picking random

samples from model states such as oil pressure, water saturation. One may note that in case of SVD or HOSVD parameterization, initial ensemble has to be generated using the corresponding coefficients of SVD or HOSVD basis vectors or matrices (in HOSVD parameterization scheme). Afterwards, utilizing Kalman gain in EnKF update step we can adjust ensembles by measuring the difference between the observed and simulated data. The EnKF formulation can be stated as follows:

$$z_i^t = \begin{pmatrix} m_i^t & g_i^t(m_i^t) & y_i^t \end{pmatrix} \tag{5.1}$$

$$Z^t = \begin{pmatrix} z_1^t & z_2^t & \cdots & z_M^t \end{pmatrix} \tag{5.2}$$

Wherein, z_i^t is the i^{th} member of ensemble at time t, m_i^t is the static vector which is supposed to be fixed during prediction step, g_i^t denotes directing reservoir simulator, here ECLIPSE 100 is utilized, in order to obtain new updated ensemble, y_i^t is the observed data at time t and Z^t represents the whole ensemble at time step t. Once, forecast step of the EnKF method is completed the analysis part is conducted to generate updated reservoir parameter realizations. The EnKF analysis equation presented as follows:

$$\hat{z_i^t} = z_i^t + K_e\Big(y_i^t - H_e z_i^t\Big) \tag{5.3}$$

Where, $\hat{z_i^t}$ represents updated realization, K_e denotes Kalman gain matrix calculated by

$$K_e = C_z H_e^t\Big(H_e C_z H_e^T + C_y\Big)^{-1} \tag{5.4}$$

C_z indicate unbiased sample covariance matrix and can be computed as follows:

$$C_z = \frac{1}{M-1}\big(Z^t - \hat{Z}^t\big)\big(Z^t - \hat{Z}^t\big)^T \tag{5.5}$$

Where, $\hat{Z}^t$ is the mean of reservoir parameter ensemble. C_y is actually observation data noise covariance matrix. We perturb observation data by adding randomly drawn sample from a zero mean normal distribution with a known covariance matrix, Gaussian white noise, to the observation data. H_e is a zero or one matrix that expresses the relation between model states and observation. One can find more details in [93].

5.3 Experiment Description

Reducing the number of gridblocks in order to express permeability or porosity information much more cost efficient is of high interest in reservoir simulation and history matching problems. As a matter of fact, one can define a projection, a map, from reservoir parameters space into a subspace of lower dimension by means of reservoir parameterization. This can be thought of considering the permeability and/or porosity parameterization problem as an image compression problem.

In reservoir characterization problems, the input permeability image is unknown and has to be estimated through a history matching process. Hence, finding a set of basis is impossible. In the present work with the assumption of two-point geostatistics, the unknown permeability field is a random sample from a multivariate Gaussian distribution defined by a variogram or covariance function. A variogram or covariance function defines the underlying geological continuity in the formation using SPE 10 benchmark [37]. Attaining realistic basis function from a large finite number of samples that are drawn from a specific high dimensional Gaussian distribution is very likely. These bases geologically describe unknown permeability fields.

Here, we apply HOSVD-ALS in order to generate reduced order ensemble of initial guesses and then performing history matching utilizing EnKF scheme to update the

corresponding coefficients of HOSVD basis. All the steps are repeated using classical SVD as the parameterization part.

Sequential Gaussian Simulation (*sgsim*) [47], a two-point geostatistical simulation algorithm, is utilized to generate 200 initial permeability realizations. A specific variogram model property is also used to represent the geological structure; here we incorporated patterns from SPE 10 first layer. Each realization contains 60×220 grid blocks. Furthermore, we conducted forward simulations using ECLIPSE reservoir simulator [120] for a 2D three-phase flow (oil, gas and water) black oil during 2160 days or 6 time intervals of 360 days.

In the present experiment, reservoir model has 15 injectors as well as 8 producers. We have to point out that here we work only with permeability, but HOSVD can be used for any grid-based property, such as porosity. In our experiments, we assume porosity is a known property, although large dimensional, we do not perform its parameterization. Overall, we conducted three distinct sets of forward simulations involving in history matching experiments. In the first setup the ensemble of original permeability initial guesses are used as an input to the algorithm and the other two setups are implemented for ensembles of initial permeability guesses randomly drawn from a set of reduced order permeability samples generated by applying classic SVD and HOSVD respectively. Therefore, we performed a 6-steps EnKF optimization for three ensembles of 200 permeability realizations independently.

A true permeability realization for our 2D model is shown in Figure 1 along with its corresponding reduced order realizations using classic SVD and HOSVD-ALS. Table 5.1 summarizes all information regarding simulation description and reservoir specifications.

Table 5.1: Reservoir and fluid properties.

Property		Quantity	Unit
Model Properties	Simulation	Three-phase	N/A
	Simulation Time	6×360	day
	Grid blocks	60×220	ft
	Grid block size 33×33	ft	
	Reservoir depth	4000	ft
	Porosity	0.22	md
	Rock compressibility	$3.0E-6$	psi^{-1}
	Reservoir geometry	2D	N/A
	Number of injectors	15	N/A
	Number of producers	8	N/A
Oil Properties	Viscosity	1	cp
	Compressibility	$3.0E-6$	psi^{-1}
	Oil density	62.4	$\frac{lb}{ft^3}$
Water Properties	Viscosity	1	cp
	Compressibility	$3.0E-6$	psi^{-1}
	Water density	62.4	$\frac{lb}{ft^3}$
Initial Conditions	Pressure	6000	psi
	Water saturation	0.3	N/A

5.4 Results and Discussion

In this subsection, we compare the performance of history matching using EnKF through classic SVD and HOSVD parameterization for the specified reservoir description in the previous part. In fact, we investigate the capability of HOSVD parameterization in terms of providing the best lower rank approximation of each member of ensemble in the second step of EnKF scheme (update). In the other

words, in each update step, we replace the exact value of predicted reservoir parameter, which we would like to estimate (update), with its corresponding coefficients from the best lower rank approximation of that realization.

To obtain the corresponding coefficients of each realization, we apply HOSVD-ALS to the ensemble of reservoir permeability realizations in order to compute the best lower rank estimation of the tensor of permeability realizations. Thus, in each analysis step, we simply update the corresponding coefficients, obtained from truncated HOSVD parameterization, rather than the unknown parameter, in our case permeability field map, itself.

Integrating parameterization step interestingly decreases the number of the unknown geological parameters of the reservoir model which effectively can treat ill-posedness of the history matching problem with respect to its under determined nature. Technically speaking, by truncating HOSVD basis one could easily underline the most important features of the geological property that we are interested in estimating. Indeed, the most important features are those that conserve more energy and express the original map more accurately. We have to point out that in the present work we do not perform state estimation which means we just update the desired parameters (permeability) and not the states of the reservoir model, such as pressure and saturation.

After updating the coefficients of the HOSVD parameterization through EnKF analysis step, we reconstruct the permeability ensemble using these updated coefficients in order to build new ensemble for the next forecast process. The same scenario is directed for operating reservoir characterization utilizing EnKF through classic SVD parameterization. Moreover, the same ensemble of initial guesses is employed for all 3 history matching experiments.

For SVD we chose the coefficients associated with the largest 40 singular val-

ues of the covariance matrix as the reduced order basis. We also found the best $(30, 90)-rank$ representation of each member of permeability ensemble. Kronecker product is performed in HOSVD procedure to compute the required coefficients for the reconstruction step. Here, we utilize the truncated basis which results in a compressed reconstructed version of the original permeability maps. We can highlight that for the regular SVD, we first vectorize each permeability map and then stack all the vectorized samples into a matrix to be used in the SVD decomposition. This is not the case in the HOSVD, as we keep the snapshots *as it is*.

Figure 5.1 depicts top five layers of the SPE 10 model in 3D. Figure 5.2 shows the true permeability map and its corresponding reduced order reconstruction using classic SVD and HOSVD to compare their performance with respect to their ability to represent more accurate estimation of the original map. As it was stated previously, we integrated these projection methods as the parameterization step in the EnKF scheme, so as to reduce the number of unknown geological properties during the update step. Figure 5.3 depicts the results of regular EnKF history matching without parameterization. Figures 5.4 and 5.5 demonstrate the permeability estimation results for EnKF history matching through classic SVD and HOSVD parameterization scenarios respectively. For the sake of space and ease of comparison, we presented the mean of updated permeability ensemble instead of plotting all realizations log permeability. Figure 5.6 shows the root mean square error, RMSE, analysis of the history matching process with EnKF through parameterization and without it. One can observe that the results of reservoir characterization with HOSVD parameterization outperform those of classic SVD parameterization in relation to geological continuity. This demonstrates the capability of HOSVD parameterization to keep important spatial geological features while reducing the dimensionality of parameter space order of magnitude.

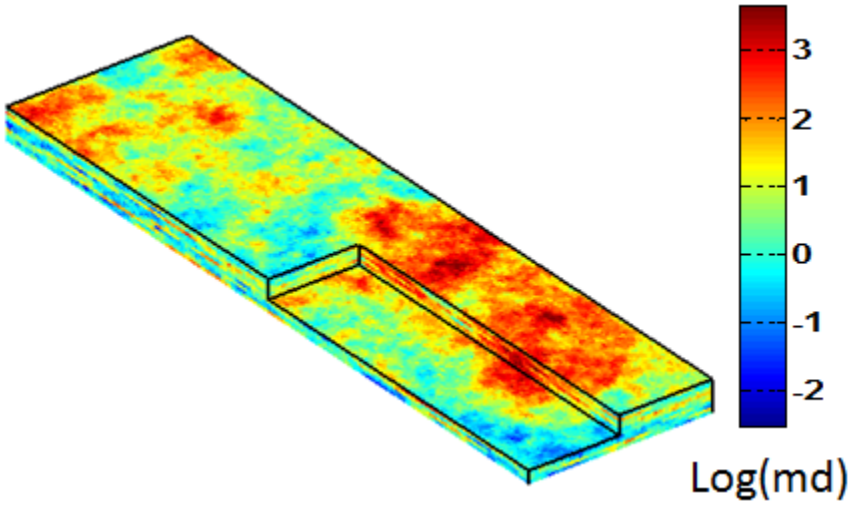

Figure 5.1: SPE 10 benchmark configuration.

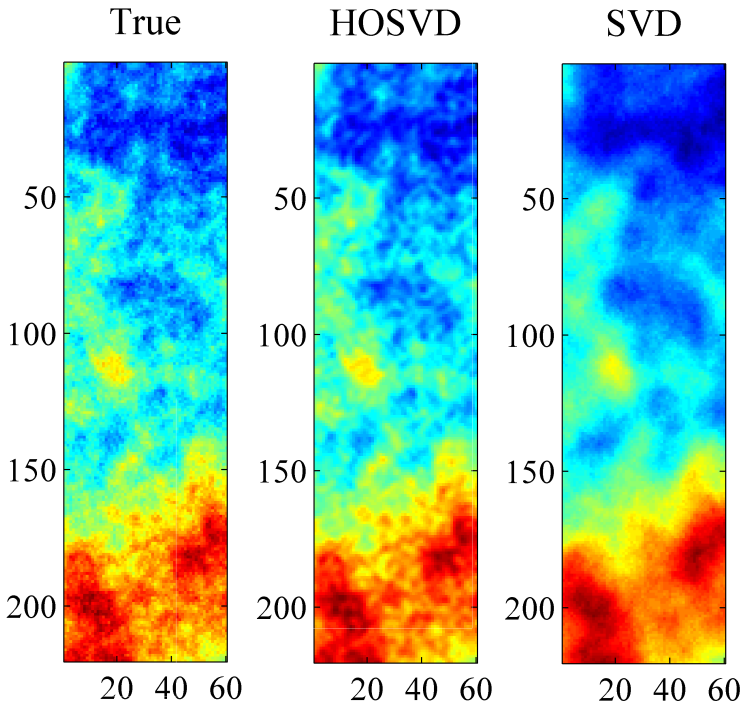

Figure 5.2: True permeability realization along with its reconstructed versions by SVD and HOSVD. We employed SPE 10 patterns to generate permeability realizations.

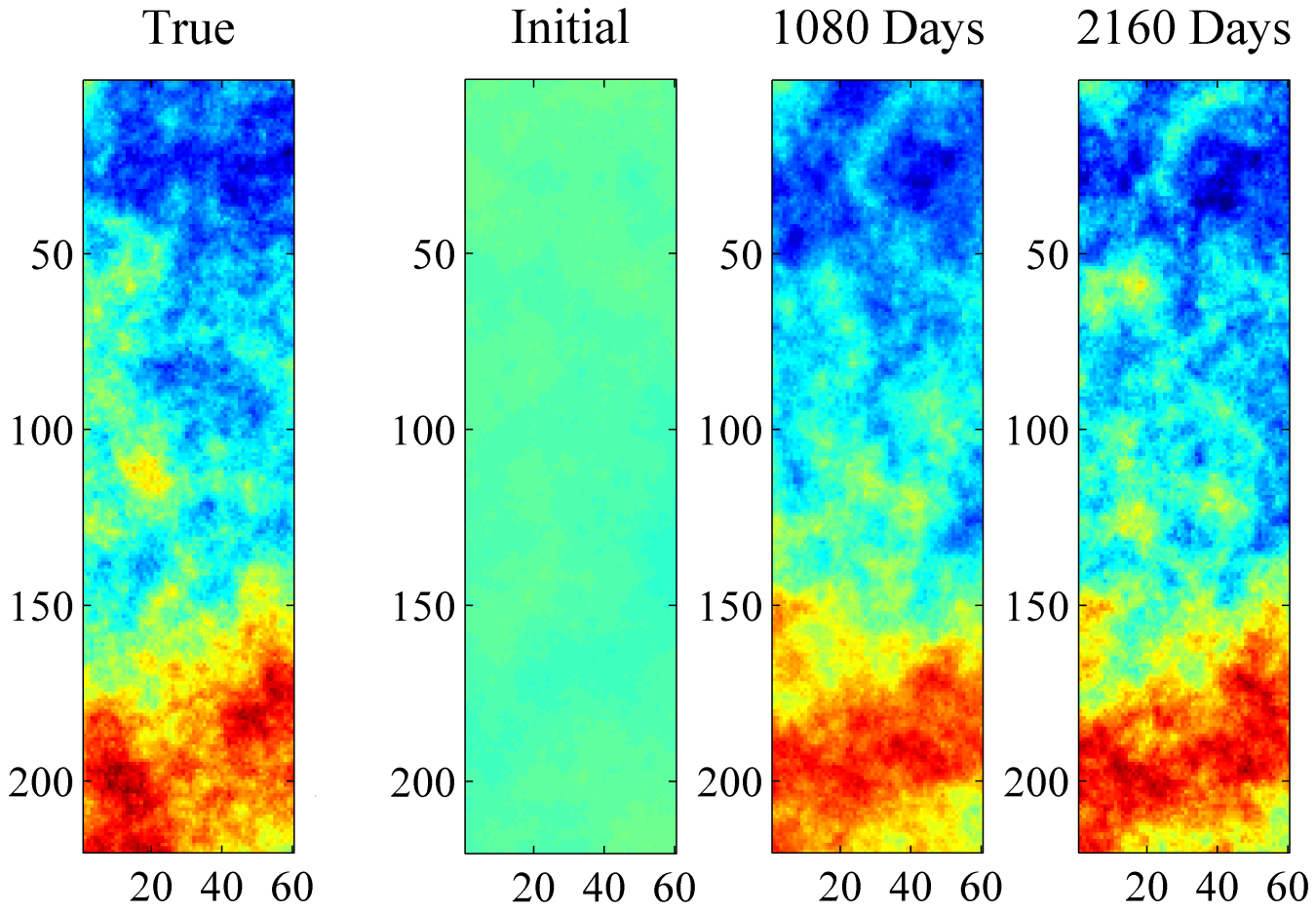

Figure 5.3: True permeability realization along with its corresponding ensemble mean of the initial and estimated realizations after 1080 and 2160 days for standard EnKF.

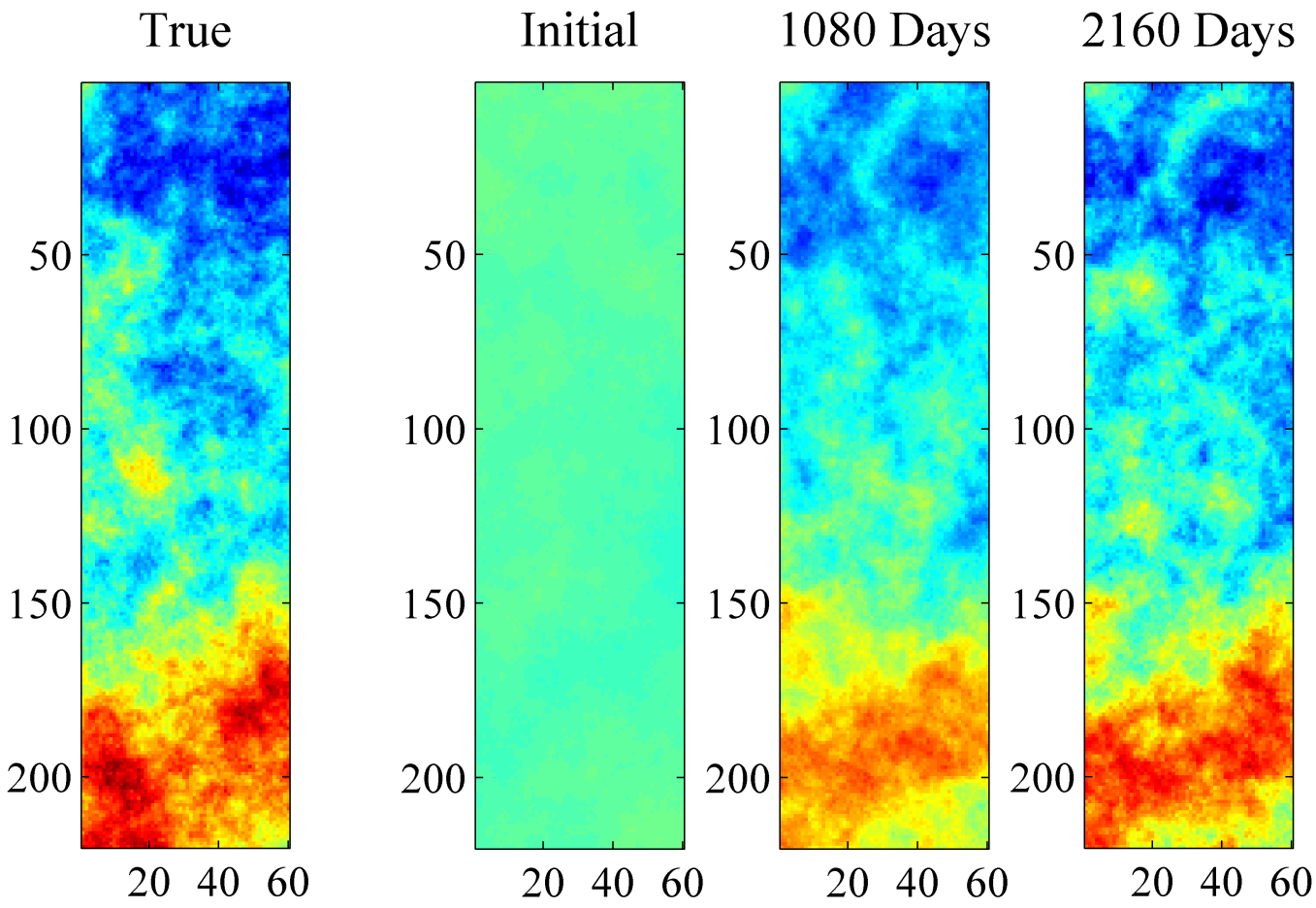

Figure 5.4: True permeability realization along with its corresponding ensemble mean of the initial and estimated realizations after 1080 and 2160 days for EnKF through SVD parameterization

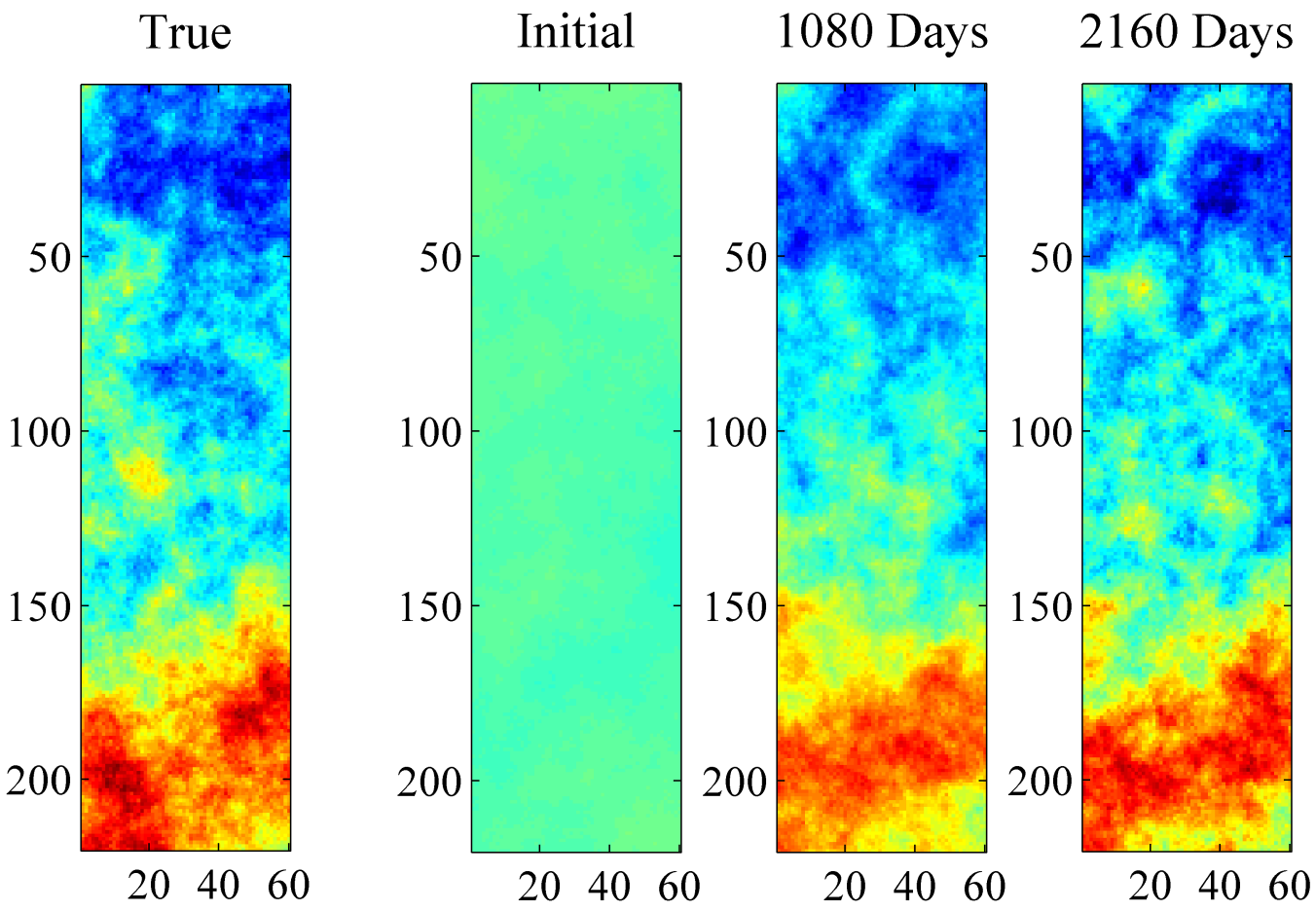

Figure 5.5: True permeability realization along with its corresponding ensemble mean of the initial and estimated realizations after 1080 and 2160 days for EnKF through HOSVD parameterization.

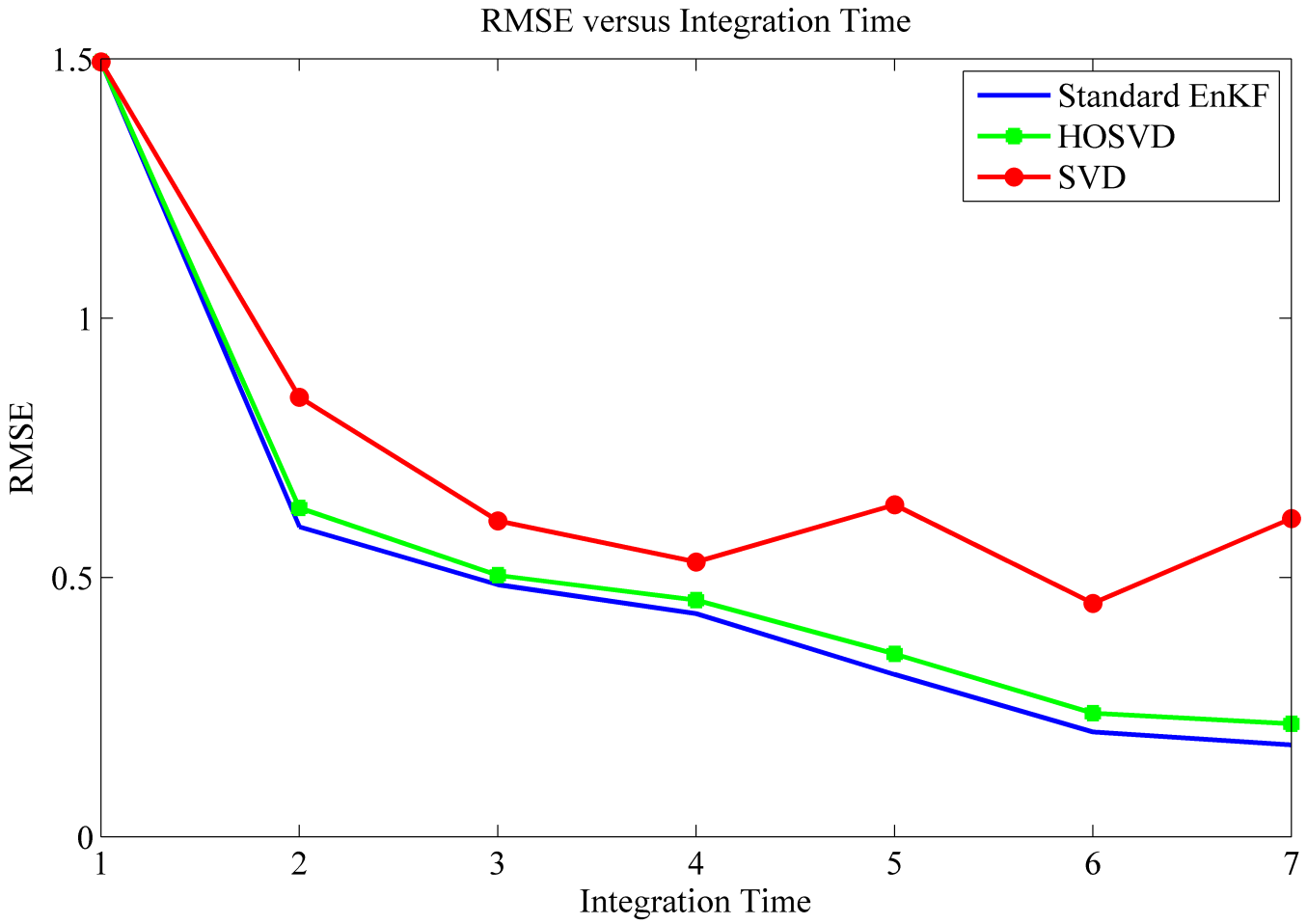

Figure 5.6: RMSE graphs, to compare the performance of standard EnKF and EnKF through HOSVD or SVD parameterization.

6. CONCLUSIONS AND FUTURE WORKS

In this dissertation we addressed the application of higher order singular value decomposition (HOSVD) as a novel parameterization method for inferring reservoir characteristics such as permeability. We also, discussed history matching problem by estimating reservoir parameter distribution inference by the mean of ensemble Kalman filter (EnKF) along with integrated HOSVD-based parameterization. This chapter concludes the present work and provides recommendations for future works.

Reducing the dimensionality of parameter space (like permeability or porosity maps) is of central interest in reservoir simulation specifically when the problem is of very high order (millions of grid blocks). Reduction in size of parameter space decreases the number of unknown geological properties that have to be estimated through the reservoir history matching procedure. Furthermore, a daunting task in reservoir characterization is to choose the principal features of the parameter space, those that conserve most of the energy, in order to improve the estimation. One must note that a powerful parameterization method not only provides better basis but also does so in a time efficient manner. To this end, having a powerful parameterization method is of high importance in reservoir simulation and characterization problems.

We introduced and developed a new parameterization technique using HOSVD method. Employing HOSVD parameterization outperforms the other common existing parameterization algorithms such as classic SVD and KLT in terms of RMSE as well as implementation cost. The results of the present work illuminate the promising power of HOSVD to reparameterize and capture the important geological features of the permeability realizations. Moreover, as a powerful parameterization and compression method, HOSVD regenerates similar petrophysical property estimation, here

permeability, as well as same response of the highly nonlinear and complex reservoir system. In other words, the approach employed in this work can strongly capture all important spatial features and all spatial geological characteristics in an efficient manner, in time and performance perspectives, comparing to SVD which is unable to preserve spatial features due to vectorization. Indeed, HOSVD re-parameterization offers a more geological consistent reduced order version of parameter space as one can observe from the RMSE plots.

In parameterization experiments provided, in order to acquire statistical consistency all examples repeated for two different sets of 1000 permeability samples each. Comparing running time proves that HOSVD overcomes classic SVD in running time as well. One must note that the provided results can easily be reproduced for the case of porosity re-parameterization. To conclude, the present work indicates that HOSVD provides a promising tool for permeability parameterization in reservoir characterization required for history matching processes. Moreover, the central idea of integrating parameterization in the update step of history matching through EnKF is to reduced the dimensionality of the unknown parameter space. This reduces the rank of the original space, consequently, shrinks the number of unknown geological properties that have to be estimated through the reservoir characterization process. In addition, this is not the only reason for reparameterizing parameter or state space within history matching procedure. The most important motivation for doing parameterization is to select the most significant features of the parameter space, those that conserve most energy, in order to improve the estimation.

The results of this dissertation, illustrate the promising power of HOSVD to reparameterize and capture the important geological features of the permeability realizations. Furthermore, as a powerful permeability parameterization and compression method, HOSVD reproduces similar petrophysical property estimation, here perme-

ability, of the highly nonlinear and complex reservoir system. In other words, the approach employed in this work can strongly capture all important spatial features and all spatial geological characteristics in an efficient manner comparing to SVD which is unable to preserve spatial features due to vectorization. Indeed, HOSVD re-parameterization offers a more geological consistent reduced order version of parameter space as one can observe from the RMSE plots. Although, HOSVD outperforms classic SVD method and provides a promising tool for reservoir parameterization in reservoir characterization, a comprehensive investigation need to be done including other parameterization techniques.

In this work, we only addressed 2D problems with relatively small number of gridblocks. Also, comparing to many real reservoir simulation and history match problems, our study models are relatively simple. In actual reservoir simulation and history matching problems, the original reservoir model parameter and state spaces are of orders of millions. The problem of constructing proper training set to obtain space basis for the model reduction and parameterization purposes are very important. Furthermore, the way that we select truncated bases to reduce the dimensionality of original space is another important issue in parameterization of unknown permeability maps. All these issues require further investigation.

Utilizing HOSVD method for the model reduction in developing fast reservoir simulators as well. In fact, one needs to restate the state space equations of reservoir system in a tensor form in order to employ HOSVD analysis and reduce the order of this model. In other words, finding a transformation which transmit existing matrix formulation of reservoir problem to a proper tensor formulation. This also, can be considered as further research studies in regard with HOSVD method. It will also be of great interest to consider the applications of HOSVD method in a production optimization problem as well.

REFERENCES

[1] S. Afra and E. Gildin. Permeability parametrization using higher order singular value decomposition (hosvd). In *12th International Conference on Machine Learning and Applications*, Miami, Florida, USA, December 2013. IEEE.

[2] S. Afra, E. Gildin, and M. Tarrahi. Heterogeneous reservoir characterization using efficient parameterization through higher order svd (hosvd). In *American Control Conference*, Portland, Oregon, USA, June 2014. IEEE.

[3] Inegbenose Aitokhuehi and Louis J. Durlofsky. Optimizing the performance of smart wells in complex reservoirs using continuously updated geological models. *Journal of Petroleum Science and Engineering*, 48(34):254 – 264, 2005.

[4] Maks Aizikovich Akivis and Vladislav Viktorovich Goldberg. *An Introduction to Linear Algebra and Tensors*. Courier Dover Publications, 2012.

[5] A.C. Antoulas. *Approximation of Large-Scale Dynamical Systems*. SIAM, 2005.

[6] T. Arbogast, C. N. Dawson, P. T. Keenan, M. F. Wheeler, and I. Yotov. The application of mixed methods to subsurface simulation. In R. Helmig et al., editors, *Modelling and Computation in Environmental Sciences, Notes on Numerical Fluid Mechanics*, volume 59, pages 1–13. Vieweg Publ., Braunschweig, 1997.

[7] Patricia Astrid. *Reduction of process simulation models: a proper orthogonal decomposition approach*. Technische Universiteit Eindhoven, 2004.

[8] K. Aziz and A. Settari. *Petroleum Reservoir Simulation*. Elsevier Applied Science Publishers, 1986.

[9] Brett W. Bader, Tamara G. Kolda, et al. Matlab tensor toolbox version 2.5. Available online, January 2012.

[10] J. Bear. *Dynamics of Fluids in Porous Media*. Dover, New York, 1972.

[11] F. van Belzen and S. Weiland. Reconstruction and approximation of multidimensional signals described by proper orthogonal decompositions. *IEEE Transactions on Signal Processing*, 2(56).

[12] Andrew F Bennett. *Inverse Methods in Physical Oceanography*. Cambridge University Press, 1992.

[13] G.A. Birnovskii. On optimal control of multiphase porous flow in an oil bed. {*USSR*} *Computational Mathematics and Mathematical Physics*, 28(3):156 – 163, 1988.

[14] Craig H Bishop, Brian J Etherton, and Sharanya J Majumdar. Adaptive sampling with the ensemble transform Kalman filter. part i: Theoretical aspects. *Monthly Weather Review*, 129(3):420–436, 2001.

[15] Ray M Bowen and Chao-Cheng Wang. *Introduction to Vectors and Tensors*, volume 2. Courier Dover Publications, 2008.

[16] F. Brezzi and M. Fortin. *Mixed and Hybrid Finite Element Methods*. Springer-Verlag, New York, 1991.

[17] Jansen J. D. Brouwer, D. R. Dynamic optimization of waterflooding with smart wells using optimal control theory. *SPE Journal*, 9(4):391 – 402, 2004.

[18] D. R. Brouwer. *Dynamic Optimization of Waterflooding With Smart Wells Using Optimal Control Theory*. PhD thesis, Delft University of Technology, 2004.

[19] AT&T Laboratories Cambridge. The database of faces. https://www.cl.cam.ac.uk/research/dtg/attarchive/facedatabase.html, 1994.

[20] Yanhua Cao, Jiang Zhu, Zhendong Luo, and IM Navon. Reduced-order modeling of the upper tropical pacific ocean model using proper orthogonal decomposition. *Computers and Mathematics with Applications*, 52(8-9):1373–1386, 2006.

[21] Jean-François Cardoso. Higher-order narrow-band array processing. In *Proc. Int. Workshop on Higher-Order Stat., Chamrousse, France*, pages 121–130, 1991.

[22] M. A. Cardoso and L. J. Durlofsky. Linearized reduced-order models for subsurface flow simulation. *J. Comput. Phys.*, 229(3):681–700, February 2010.

[23] MA Cardoso and Louis J Durlofsky. Linearized reduced-order models for subsurface flow simulation. *Journal of Computational Physics*, 229(3):681–700, 2010.

[24] M.A. Cardoso and Stanford University. *Development and Application of Reduced-order Modeling Procedures for Reservoir Simulation.* Stanford University, 2009.

[25] Marco Antonio Cardoso, Louis J Durlofsky, et al. Use of reduced-order modeling procedures for production optimization. *SPE Journal*, 15(2):426–435, 2010.

[26] Jess Carrera, Andrs Alcolea, Agustn Medina, Juan Hidalgo, and LuitJ. Slooten. Inverse problem in hydrogeology. *Hydrogeology Journal*, 13(1):206–222, 2005.

[27] Jesus Carrera. State of the art of the inverse problem applied to the flow and solute transport equations. In E. Custodio, A. Gurgui, and J.P.Lobo Ferreira,

editors, *Groundwater Flow and Quality Modelling*, volume 224 of *NATO ASI Series*, pages 549–583. Springer Netherlands, 1988.

[28] Jesus Carrera and Shlomo P Neuman. Estimation of aquifer parameters under transient and steady state conditions: 1. maximum likelihood method incorporating prior information. *Water Resources Research*, 22(2):199–210, 1986.

[29] George Casella and Christian P Robert. Monte carlo statistical methods, 1999.

[30] C.E.Baumann. *An h-p adaptive discontinuous finite element method for computational fluid dynamics*. PhD thesis, The University of Texas at Austin, 1997.

[31] G Chavent, M Dupuy, P Lemmonier, et al. History matching by use of optimal theory. *Society of Petroleum Engineers Journal*, 15(01):74–86, 1975.

[32] G. Chavent and J. Jaffre. *Mathematical Models and Finite Elements for Reservoir Simulation*. North-Holland, Amsterdam, 1986.

[33] WH Chen, GR Gavalas, John H Seinfeld, Mel L Wasserman, et al. A new algorithm for automatic history matching. *Society of Petroleum Engineers Journal*, 14(06):593–608, 1974.

[34] Yan Chen, Dean S Oliver, Dongxiao Zhang, et al. Efficient ensemble-based closed-loop production optimization. *SPE Journal*, 14(04):634–645, 2009.

[35] Yan Chen and Dongxiao Zhang. Data assimilation for transient flow in geologic formations via ensemble Kalman filter. *Advances in Water Resources*, 29(8):1107–1122, 2006.

[36] Z. Chen, G. Huan, and Y. Ma. *Computational methods for multiphase flows in porous media*. SIAM, Philadelphia, PA, 2006.

[37] M.A. Christie and M.J. Blunt. Tenth spe comparative solution project: a comparison of upscaling techniques. spe-72469. *SPEREE*, 4:308–317, 2001.

[38] Pierre Comon and Bernard Mourrain. Decomposition of quantics in sums of powers of linear forms. *Signal Processing*, 53(2):93–107, 1996.

[39] ExxonMobil Corporation. Long-term energy outlook an exxonmobil analysis. *ASPO Third International Workshop on Oil and Gas Depletion, Berlin, Germany*, 2004.

[40] ExxonMobil Corporation. The outlook for energy: A view to 2040. `http://cdn.exxonmobil.com/media/Reports/Outlook%20For20Energy/2014/2014-Outlook-for-Energy.pdf`, Retrieved on 2014.

[41] Lieven De Lathauwer. *Signal Processing based on Multilinear Algebra*. Katholieke Universiteit Leuven, 1997.

[42] Lieven De Lathauwer and Bart De Moor. From matrix to tensor: Multilinear algebra and signal processing. In *Institute of Mathematics and its Applications Conference Series*, volume 67, pages 1–16. Citeseer, 1998.

[43] Lieven De Lathauwer, Bart De Moor, and Joos Vandewalle. A singular value decomposition for higher-order tensors. In *Proc. ATHOS Workshop on System Identification and High-Order Statistics, Nice, France*, 1993.

[44] Lieven De Lathauwer, Bart De Moor, and Joos Vandewalle. The application of higher order singular value decomposition to independent component analysis. *SVD and Signal Processing, III. Algorithms, Applications and Architectures, Elsevier, Amsterdam*, pages 383–390, 1995.

[45] Lieven De Lathauwer, Bart De Moor, and Joos Vandewalle. A multilinear singular value decomposition. *SIAM journal on Matrix Analysis and Applications*,

21(4):1253–1278, 2000.

[46] Lieven De Lathauwer, Bart De Moor, and Joos Vandewalle. On the best rank-1 and rank-(r 1, r 2,..., rn) approximation of higher-order tensors. *SIAM Journal on Matrix Analysis and Applications*, 21(4):1324–1342, 2000.

[47] C. Deutsch and A. Journel. *GSLIB: Geostatistical Software Library and Users Guide*. Oxford University Press, NY, USA, 1998.

[48] John Doherty. Ground water model calibration using pilot points and regularization. *Groundwater*, 41(2):170–177, 2003.

[49] Elisa Portes dos Santos Amorim, Paulo Goldfeld, Flavio Dickstein, Rodrigo Weber dos Santos, and Carolina Ribeiro Xavier. Automatic history matching in petroleum reservoirs using the tsvd method. In *Computational Science and Its Applications–ICCSA 2010*, pages 475–487. Springer, 2010.

[50] Laura Dovera and Ernesto Della Rossa. Multimodal ensemble Kalman filtering using gaussian mixture models. *Computational Geosciences*, 15(2):307–323, 2011.

[51] Y. Efendiev, J. Galvis, and E. Gildin. Local-global multiscale model reduction for flows in high-contrast heterogeneous media. *Journal of Computational Physics.*, 231. doi: http://dx.doi.org/10.1016/j.jcp.2012.07.032(24):8100–8113, 2012.

[52] Yalchin Efendiev, A. Romanovskay, Eduardo Gildin, and Mohammadreza Ghasemi. Nonlinear complexity reduction for fast simulation of flow in heterogeneous porous media. In *SPE Reservoir Simulation Symposium*, The Woodlands, Texas, Feb 2013. Society of Petroleum Engineers. SPE 163618.

[53] Alexandre A Emerick, Albert C Reynolds, et al. Combining the ensemble Kalman filter with markov-chain monte carlo for improved history matching and uncertainty characterization. *SPE Journal*, 17(02):418–440, 2012.

[54] Turgay Ertekin, J.H. Abou-Kassem, and G.R. King. *Basic Applied Reservoir Simulation*. Society of Petroleum Engineers, 2001.

[55] G. Evensen. Squential data assimilation with a non-linear quasigeostrophic model using monte carlo methods to forecast error statistics. *J. Geophys. Res.*, 99(C5):143–162, 1994.

[56] G. Evensen. Data assimilation: The ensemble Kalman filter. *Springer*, 2007.

[57] G. Evensen. The ensemble Kalman filter for combined state and parameter estimation: Monte carlo techniques for data assimilation in large systems. *IEEE Control Syst. Mag.*, 29(3):83–104, 2009.

[58] Geir Evensen. Sequential data assimilation with a nonlinear quasi-geostrophic model using monte carlo methods to forecast error statistics. *Journal of Geophysical Research: Oceans (1978–2012)*, 99(C5):10143–10162, 1994.

[59] Geir Evensen. The ensemble Kalman filter: Theoretical formulation and practical implementation. *Ocean Dynamics*, 53(4):343–367, 2003.

[60] Geir Evensen, Dick P Dee, and Jens Schröter. Parameter estimation in dynamical models. In *Ocean Modeling and Parameterization*, pages 373–398. Springer, 1998.

[61] C.L. Farmer. Upscaling: A review. *Int. J. for Numerical Methods in Fluids*, 40:63–78, 2002.

[62] GR Gavalas, PC Shah, John H Seinfeld, et al. Reservoir history matching by bayesian estimation. *Society of Petroleum Engineers Journal*, 16(06):337–350, 1976.

[63] J.J. Gerbrands. On the Relationships Between SVD, KLT, and PCA. *Pattern Recognition*, 14(1):375–381, 1981.

[64] Mohammadreza Ghasemi, Ibrahim Ashraf, and Eduardo Gildin. Reduced order modeling in reservoir simulation using the bilinear approximation techniques. In *SPE Latin American and Caribbean Petroleum Engineering Conference*, Maracaibo, Venezuela, May 2014. Society of Petroleum Engineers. SPE 169357-MS.

[65] E Gildin and S Afra. Efficient inference of reservoir parameter distribution utilizing higher order svd reparameterization. In *ECMOR XIV-14th European conference on the mathematics of oil recovery*, Sicily, Italy, 2014. European Association of Geoscientists and Engineers.

[66] E. Gildin and M. Ghasemi. A new model reduction technique applied to reservoir simulation. In *ECMOR XIV-14th European conference on the mathematics of oil recovery*, Sicily, Italy.

[67] E. Gildin, M. Ghasemi, A. Protasov, and Y. Efendiev. Nonlinear complexity reduction for fast simulation of flow in heterogeneous porous media. In *In Proceeding of the 2013 SPE Reservoir Simulation Symposium.*, The Woodlands, TX, USA, Feb 18 - 20.

[68] E. Gildin and T. J. Lopez. Closed-loop reservoir management: Do we need complex models ? In *SPE Digital Energy Conference and Exhibition*, The Woodlands, Texas, USA, April 2011.

[69] David Gratton and Karen Willcox. *Reduced-order, trajectory piecewise-linear models for nonlinear computational fluid dynamics*. PhD thesis, Massachusetts Institute of Technology, Department of Aeronautics and Astronautics, 2004.

[70] Johan Håstad. Tensor rank is np-complete. *Journal of Algorithms*, 11(4):644–654, 1990.

[71] R. Henrion. Body diagonalization of core matrices in three-way principal components analysis: Theoretical bounds and simulation. *Chemometrics*, (7):477–494, 1993.

[72] Peter L Houtekamer and Herschel L Mitchell. Data assimilation using an ensemble Kalman filter technique. *Monthly Weather Review*, 126(3):796–811, 1998.

[73] P. Jacquard and C. Jain. Permeability distribution from field pressure data. *Society of Petroleum Engineers Journal*, 5(04):281–294, 1965.

[74] B Jafarpour and Mohammadali Tarrahi. Assessing the performance of the ensemble Kalman filter for subsurface flow data integration under variogram uncertainty. *Water Resources Research*, 47(5), 2011.

[75] Behnam Jafarpour. Sparsity promoting solution of subsurface flow model calibration inverse problems. *Advances in Hydrogeology*, pages 73–94, 2013.

[76] Behnam Jafarpour, Dennis Mclaughlin, et al. Efficient permeability parameterization with the discrete cosine transform. In *SPE Reservoir Simulation Symposium (SPE 106453), Houston*, 2007.

[77] F Jahn, M. Cook, and M. Graham. *Hydrocarbon Exploration and Production) (Developments in Petroleum Science)*. Elsevier, 2008, 2nd. Edition.

[78] H. O. Jahns. A rapid method for obtaining a two-dimensional reservoir description from well pressure response data. *Society of Petroleum Engineers Journal*, 6(04):315–327, 1966.

[79] Anil K Jain. *Fundamentals of Digital Image Processing*. Prentice-Hall, Inc., 1989.

[80] Jan-Dirk Jansen, Okko H. Bosgra, and Paul M.J. Van den Hof. Model-based control of multiphase flow in subsurface oil reservoirs. *Journal of Process Control*, 18(9):846 – 855, 2008.

[81] J.D. Jansen, O.H. Bosgra, and P.M.J. van den Hof. Model-based control of multiphase flow in subsurface oil reservoirs. *Journal of Process Control*, 18(9):846–855, 2008.

[82] A. H. Sayed B. Hassibi Kailath, T. *Linear Estimation*. Prentice Hall, 2000.

[83] Rudolph Emil Kalman. A new approach to linear filtering and prediction problems. *Journal of Fluids Engineering*, 82(1):35–45, 1960.

[84] K. Karhunen. *Über lineare Methoden in der Wahrscheinlichkeitsrechnung*. Annales Academiae scientiarum Fennicae: Mathematica - Physica. Universitat Helsinki, 1947.

[85] David C Kay. *Schaum's Outline of Theory and Problems of Tensor Calculus*. McGraw-Hill, 1988.

[86] Tamara G. Kolda and Brett W. Bader. Tensor decompositions and applications. *SIAM Rev.*, 51(3):455–500, August 2009.

[87] Pieter Kroonenberg and Jan Leeuw. Principal component analysis of three-mode data by means of alternating least squares algorithms. *Psychometrika*, 45(1):69–97, 1980.

[88] Larry W. Lake, Steven L. Bryant, and Aura N. Araque-Martinez. *Geochemistry and fluid flow*. Elsevier Science Ltd, New York, 1st ed. edition, 2002.

[89] S. Lang. *Algebra*. Addison Wesley, 1993.

[90] Lieven De Lathauwer, Bart De Moor, and Joos Vandewalle. A multilinear singular value decomposition. *SIAM J. Matrix Anal. Appl.*, 21(4):1253–1278, March 2000.

[91] Lieven De Lathauwer, Bart De Moor, and Joos Vandewalle. On the best rank-1 and rank-(r1,r2,. . .,rn) approximation of higher-order tensors. *SIAM J. Matrix Anal. Appl.*, 21(4):1324–1342, March 2000.

[92] L Li, H Zhou, HENDRIKUS JOHANNES Hendricks Franssen, and J Jaime Gómez-Hernández. Groundwater flow inverse modeling in non-multigaussian media: performance assessment of the normal-score ensemble Kalman filter. *Hydrology and Earth System Sciences*, 16(2):573–590, 2012.

[93] Yang D. Arhuoma M. A. S. Li, H. Relative permeability estimation from displacement experiments using enkf method. *International Oil and Gas Conference and Exhibition in China, 8-10 June, Beijing, China*, 2010.

[94] Ning Liu and Dean S Oliver. Ensemble Kalman filter for automatic history matching of geologic facies. *Journal of Petroleum Science and Engineering*, 47(3):147–161, 2005.

[95] Ning Liu, Dean S Oliver, et al. Critical evaluation of the ensemble Kalman filter on history matching of geologic facies. *SPE Reservoir Evaluation & Engineering*, 8(06):470–477, 2005.

[96] Michel Loeve. Probability theory. *Graduate Texts in Mathematics*, 45, 1963.

[97] Fjelde K. Fryen J. Lage A. Nvdal G. Vefring E.H. Lorentzen, R.J. Underbalanced drilling: real time data interpretation and decision support. *Presented at the SPE/IADC Drilling Conference, Amsterdam, Netherlands, 27 February1 March 2001*, 2001.

[98] Rolf J Lorentzen, Geir Nævdal, and Antonio CVM Lage. Tuning of parameters in a two-phase flow model using an ensemble Kalman filter. *International Journal of Multiphase Flow*, 29(8):1283–1309, 2003.

[99] Mohammadreza M Khaninezhad, Behnam Jafarpour, et al. Hybrid parameterization for robust history matching. *SPE Journal*, (Preprint), 2013.

[100] G. De Marsily, G. Lavedau, M. Boucher, and G. Fasanino. Interpretation of interference test in a well field using geostatistical techniques to fit the permeability distribution in a reservoir model. In G. Verly, M. David, A. G. Journel, and A. Marechal, editors, *Geostatistics for Natural Resources Characterization, Proceedings of the NATO Advanced Study Institute*. Dordrecht, Holland, 1984.

[101] Marc Moonen and Bart De Moor. *SVD and Signal Processing, III: Algorithms, Architectures and Applications*. Elsevier, 1995.

[102] Trivedi J. J. & Leung J. Y. W. Nejadi, S. Estimation of geological facies boundaries using categorical indicators with p-field simulation and ensemble Kalman filter (enkf). *SPE Latin America and Caribbean Petroleum Engineering Conference, 16-18 April, Mexico City, Mexico*, 2012.

[103] R.A. Nelson. *Geologic Analysis of Naturally Fractured Reservoirs*. Gulf Publishing Company, 2nd Edition, 2001.

[104] D. Oliver, A. Reynolds, and N. Liu. *Inverse Theory for Petroleum Reservoir Characterization and History Matching*. Combridge Press, 2008.

[105] Dean S Oliver, Albert C Reynolds, and Ning Liu. *Inverse Theory for Petroleum Reservoir Characterization and History Matching*, volume 1. 2008.

[106] L. E. Payne and B. Straughan. Analysis of the boundary condition at the interface between a viscous fluid and a porous medium and related modelling questions. *J. Math. Pures Appl. (9)*, 77(4):317–354, 1998.

[107] D. W. Peaceman and Jr. H. H. Rachford. The numerical solution of parabolic and elliptic differential equations. *Society for Industrial and Applied Mathematics*, 3(1):28–41, 1955.

[108] M. Peszynska, Q. Lu, and M. F. Wheeler. Coupling different numerical algorithms for two phase fluid flow. In J. R. Whiteman, editor, *MAFELAP Proceedings of Mathematics of Finite Elements and Applications*, pages 205–214, Uxbridge, U.K., 1999. Brunel University.

[109] Zu-Qing Qu. *Model Order Reduction Techniques with Applications in Finite Element Analysis*. Springer, 2004.

[110] W. Fred Ramirez. *Application of Optimal Control Theory to Enhanced Oil Recovery*. Elsevier Science, 1987.

[111] Albert C Reynolds, Nanqun He, Lifu Chu, and Dean S Oliver. Reparameterization techniques for generating reservoir descriptions conditioned to variograms and well-test pressure data. In *Society of Petroleum Engineers. Annual technical conference*, pages 609–624, 1995.

[112] B. Rivière. *Discontinuous Galerkin finite element methods for solving the miscible displacement problem in porous media*. PhD thesis, The University of Texas at Austin, 2000.

[113] C.W. Rowley. Model reduction for fluids, using balanced proper orthogonal decomposition. *International Journal of Bifurcation and Chaos*, 15, 2005.

[114] D. Oliver A. Reynolds S. Aanonsen, G. Naevdal and B. Valles. The ensemble Kalman filter in reservoir engineering–a review. *SPE J*, 14(3):393–412, 2009.

[115] F. S. Samaria, F. S. Samaria *t, A.C. Harter, and Old Addenbrooke's Site. Parameterisation of a stochastic model for human face identification. 1994.

[116] Malcolm Sambridge and Klaus Mosegaard. Monte carlo methods in geophysical inverse problems. *Reviews of Geophysics*, 40(3):3–1, 2002.

[117] Hanan Samet. *The design and analysis of spatial data structures*, volume 85. Addison-Wesley Reading, MA, 1990.

[118] P. Sarma and Stanford University. *Efficient Closed-loop Optimal Control of Petroleum Reservoirs Under Uncertainty*. Stanford University, 2006.

[119] Pallav Sarma, Louis J Durlofsky, Khalid Aziz, and Wen H Chen. Efficient real-time reservoir management using adjoint-based optimal control and model updating. *Computational Geosciences*, 10(1):3–36, 2006.

[120] Schlumberger Technology Corporation. *Eclipse-100, Technical Description*, 1998.

[121] M Schmutz. Optimal and suboptimal separable expansions for 3d-signal processing. *Pattern recognition letters*, 8(4):217–220, 1988.

[122] Ch. Schwab. *p- and hp- finite element methods, theory and applications in solid and fluid mechanics*. Oxford science publications, 1998.

[123] Laurent Sorber, Marc Van Barel, and Lieven De Lathauwer. Tensorlab v1.0. `http://www.tensorlab.net/`, Retrieved on 2013.

[124] RM Srivastava et al. Reservoir characterization with probability field simulation. In *SPE Annual Technical Conference and Exhibition*. Society of Petroleum Engineers, 1992.

[125] Eka Suwartadi. *Gradient-based Methods for Production Optimization of Oil Reservoirs*. PhD thesis, Norwegian University of Science and Technology, 2012.

[126] L. R. Tucker. The extension of factor analysis to three-dimensional matrices. In H. Gulliksen and N. Frederiksen, editors, *Contributions to mathematical psychology.*, pages 110–127. Holt, Rinehart and Winston, New York, 1964.

[127] Ledyard R Tucker. Some mathematical notes on three-mode factor analysis. *Psychometrika*, 31(3):279–311, 1966.

[128] Paul M. J. Van Den Hof, Jan-Dirk Jansen, Gijs Van Essen, and Okko H. Bosgra. Model-based control and optimization of large scale physical systems: Challenges in reservoir engineering. In *Proceedings of the 21st Annual International Conference on Chinese Control and Decision Conference*, CCDC'09, pages 42–51, Piscataway, NJ, USA, 2009. IEEE Press.

[129] Jorn FM van Doren, Renato Markovinović, and Jan-Dirk Jansen. Reduced-order optimal control of water flooding using proper orthogonal decomposition. *Computational Geosciences*, 10(1):137–158, 2006.

[130] Nick Vannieuwenhoven, Raf Vandebril, and Karl Meerbergen. A new truncation strategy for the higher-order singular value decomposition. *SIAM J. Scientific Computing*, 34(2), 2012.

[131] M. A. O. Vasilescu and Demetri Terzopoulos. Multilinear analysis of image ensembles: Tensorfaces. In *Proceedings of the 7th European Conference on*

Computer Vision-Part I, ECCV '02, pages 447–460, London, UK, UK, 2002. Springer-Verlag.

[132] S. Volkwein and M. Hinze. Proper orthogonal decomposition surrogate models for nonlinear dynamical systems: error estimates and suboptimal control. In *Reduction of Large-Scale Systems, P. Benner, V. Mehrmann, D. C. Sorensen (eds.), Lecture Notes in Computational Science and Engineering*, volume 45, pages 261–306. Edited by: Dafermos and Pokorny, Elsevier, 2005.

[133] D. Weber, F.T Edgar, L.W. Lake, L.S. Larson, and K. Sawas. Improvements of the capacitance resistive modeling and optmization of large scale reservoirs. In *SPE Western Regional Meeting*, San Jose, California, March 2009. SPE 121299.

[134] Zhan Wu, Akhil Datta-Gupta, et al. Rapid history matching using a generalized travel-time inversion method. *SPE Journal*, 7(02):113–122, 2002.

[135] Fengjun Zhang, Jan-Arild Skjervheim, Albert C Reynolds, Dean S Oliver, et al. Automatic history matching in a bayesian framework example applications. *SPE Reservoir Evaluation & Engineering*, 8(03):214–223, 2005.